Politecnico di Torino
Dipartimento di Ingegneria Meccanica e Aerospaziale

Master's Degree in Biomedical Engineering

Master's Degree Thesis

Dynamics of cortical activation during task-switching paradigm through MEG analysis: An extensive study.

Supervisors

Lucia M. Vaina, MD PhD (Boston University)

Sheraz Khan, PhD (Harvard Medical School)

Gabriella Olmo, MD PhD (Politecnico di Torino)

Candidate

Samuele Morello

Turin, October 2021

Abstract

The overall aim of this thesis is a better understanding of the main brain mechanisms through different magnetoencephalography (MEG) analysis methods, during a task-switching experiment. MEG is a non-invasive functional neuroimaging technique that relies on the measurement – outside of the head – of the magnetic field produced by neuronal activity. Because of its high temporal and spatial resolution yet complex and expensive system, MEG is still considered today a cutting-edge technology whose use is still mainly for research purposes and not a widely established diagnosis method like fMRI or EEG. This work has the objective to localize and investigate in space, time and frequency, the origin and propagation of the cortical signal, implementing specific functions provided mostly by the MNE-Python package. MNE-Python is the most known and up-to-date tool containing a set of algorithms that address and solve the mathematical challenges that MEG imaging is characterized by. The first part of this work focuses on introducing the main concepts of MEG and the linked challenges that need to be tackled to accurately estimate patients' cortical activation. Later in the dissertation, the most important concepts about cognitive learning are broadly described and a precise illustration of the held task-switching experiment is provided. The last two chapters of this thesis gaze on different approaches to investigate the dynamics of cortical activations over time by looking directly at the spatiotemporal source estimates. Particularly, analyses have been carried on exploring different aspects of the signals: from a straightforward cortical source estimate to a more advanced machine learning regression. This project was done in collaboration with the Athinoula A. Martinos Center for Biomedical Imaging (Boston) and the Brain & Vision Research Laboratory (Biomedical Engineering Department - Boston University).

Acknowledgments

I would like to express my most sincere gratitude to Professor Lucia Maria Vaina, who made all this work possible and boldly helped me in Boston. Her guidance and contribution to this thesis have been fundamental, and I cannot thank her enough for the profound belief in my capabilities that she demonstrated day by day. I am also deeply thankful to Sheraz Khan for his relentless support and assistance during the whole time. He never let me down and always tried to help me with all the technical issues and doubts I had. The contribute of Dr. Vaina and Dr. Khan has been precious, and my debt goes beyond this thesis.
I would also like to thank Seppo Ahlfors, Dimitrios Pantazis, and Kunjan Rana for reviewing my job and make important suggestions to improve it. Many thanks to my friend and colleague Abhishek Samal, with whom I enjoyed sharing 'Brain & Vision Research Laboratory'.

I gratefully acknowledge the important assistance of Professor Gabriella Olmo, who remotely followed this work with her substantial guidance and support.
I cannot leave Polytechnic of Turin without mentioning Giuliana Monachino and Alberto Tironi, who have been my closest friends during this journey of personal growth and encouraged me to keep doing my best.

This thesis would have not been possible without the full support of my whole family. My most sincere gratitude goes to my parents Luisella and Silvano, my grandparents Adriana, Pasqualina, Ferruccio and Mario, and my brother Mattia. Also, a heartfelt thanks to Stefania, who always believed in me.

Finally, I cannot express how deeply I am thankful to my best friends, with whom who I shared a lifetime and every day keep reminding me how rich life can be with the right persons beside you. Thanks to Michela Lanza, Luca Costabello, Paolo Martiradonna, Fabio Maurino and Fabio Rostan.

To my brother, Mattia.

Contents

Chapter 1

THEORETICAL OVERVIEW

To provide a better understanding of the following thesis, this first chapter gaze on the main aspects and phenomena behind magnetoencephalography (MEG), focusing both on the biological and functional aspects of the human brain as well as the main software and tools to process the collected data.

Contents

1.1 PRINCIPAL BRAIN STRUCTURES

1.1.1 An anatomical and functional overview

The human brain is the most complex structure in the known universe and – along with the spinal cord – it is the largest part of our central nervous system (CNS). It is composed of a lower part, the brainstem, and an upper part, the prosencephalon – a.k.a. the forebrain –. The brainstem is composed by the mesencephalon, the medulla, and the pons, while the forebrain by the telencephalon and diencephalon (see *Figure1.1*). The diencephalon is located in the midline of the brain and contains the thalamus and the hypothalamus. The most superior structure, the telencephalon – a.k.a. cerebrum – includes the lateral ventricles, the basal ganglia and the cerebral cortex. (*Figure 1.1*)

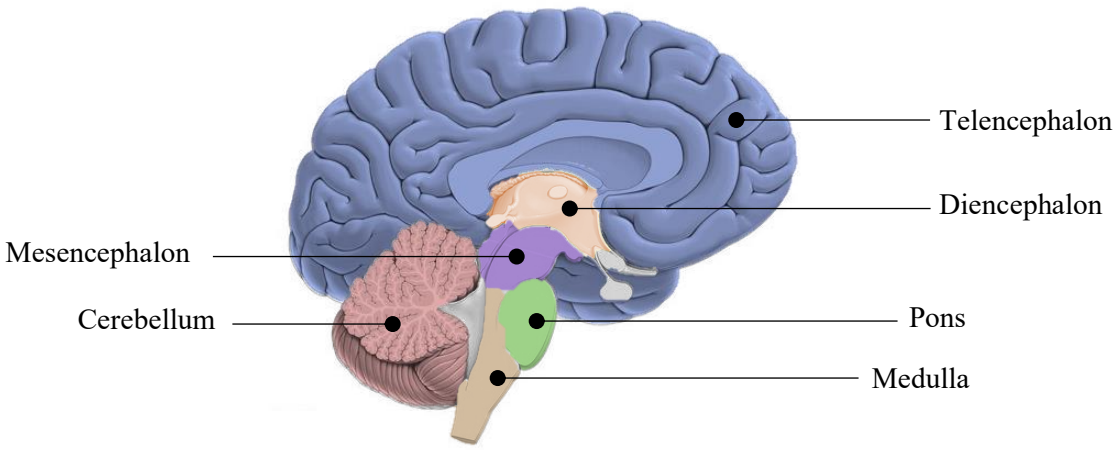

Figure 1.1. Main anatomical structures of the human brain.

Considering a coronal slice of the telencephalon (see *Figure 1.2*), we can notice two main structures: the white matter and the grey matter. The grey matter is the outer layer and forms the cerebral cortex, while the inner part identifies the white matter. The latter one is composed mainly by myelinated axons, which are responsible for the different color.

Cerebral cortex plays a fundamental role in higher-order brain functions by more fully evolved animals (such as humans, primates, dolphins etc.) and is divided into a left and a right hemisphere.

Each of them is further divided into 4 lobes as represented in *Figure 1.3*, roughly related with the following functions:

- Frontal lobe: involved in voluntary muscle movement, memory, thinking, decision-making and planning.
- Parietal lobe: responsible for receiving and processing sensory information, orientation, and recognition.
- Occipital lobe: responsible for receiving and processing visual information from the retina.
- Temporal lobe: organized sensory input and aid in auditory perception, memory information, and language and speech production.

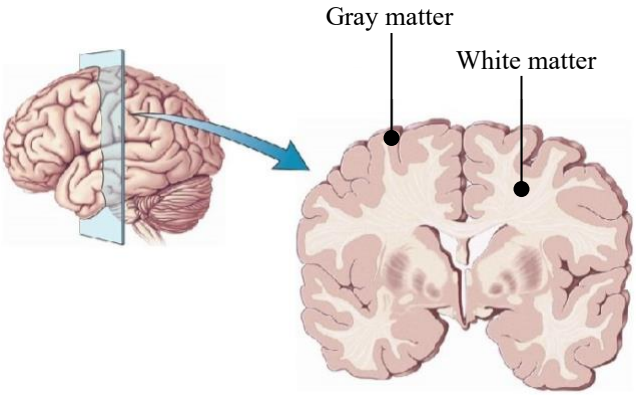

Figure 1.2. Coronal slide of the human brain.

Lobes are separated by major fissures that are present in all individuals. This makes the identification of the different lobes on a particular subject possible by simple visual inspection. For example, the parietal and frontal lobes are separated by the central fissure, a.k.a. the central sulcus, and the temporal lobe is separated from the parietal and frontal ones by the Sylvian fissure. Fissures are also commonly called sulci.

The counterpart of the cortical fissures are the gyri. Gyri are the structures between fissures. Some of the gyri contain brain regions with known cognitive functions, like the post-central gyrus that includes the primary somatosensory cortex (S1).

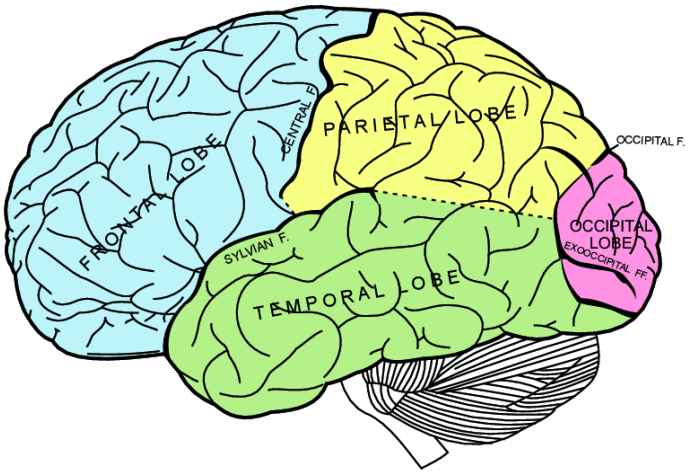

Figure 1.3. Lobes of the human brain.

Such a knowledge on the localization of some brain functions and processing pathways is fundamental to achieve validation over brain imaging recordings associated with different tasks.

Structural properties of grey matter vary across different regions of the brain, like the number of layers, the cell composition, the thickness and organization. These properties, called by neuroanatomists cytoarchitectonic properties, are not the same over the whole surface of the cortex. Their differences led, in 1909, the neuroanatomist Korbinian Brodmann to divide the cortex into 52 regions called Brodmann areas (see *Figure 1.4*) whose historical characteristics were homogeneous (Brodmann, 1909). Some functions were then assigned to some of these areas, however their utility in brain functional imaging is usually limited labelling areas like "posterior part of the post-central gyrus" as Brodmann area 5 (BA5).

Looking at a section of the cortex, we can observe six different layers of neurons: from layer I at the cortex's surface to layer VI, close to the white matter. For humans, the cortical thickness varies from 3 to 6 mm. It has been observed not only a neuronal laminar organization but they also communicate moving perpendicularly to the cortex. Forming a cortical column, they respond to precise stimulations with similar activities throughout the layers. This columnar organization was discovered by Mountcastle with a pioneering experiment in 1957 (Mountcastle, 1957), showing that a similar cortical activities is recorded inside column of 300 to 500 µm of diameter. A schematic representation is displayed in *Figure 1.5*.

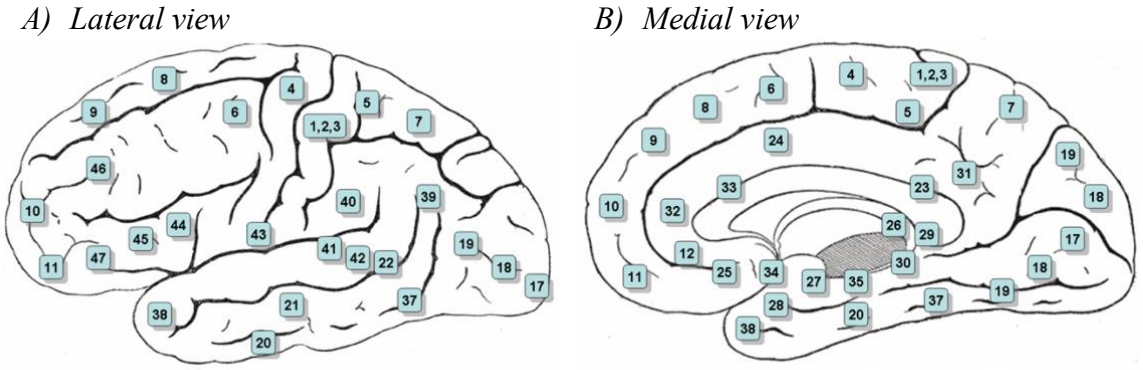

Figure 1.4. Representation of the Brodmann areas.

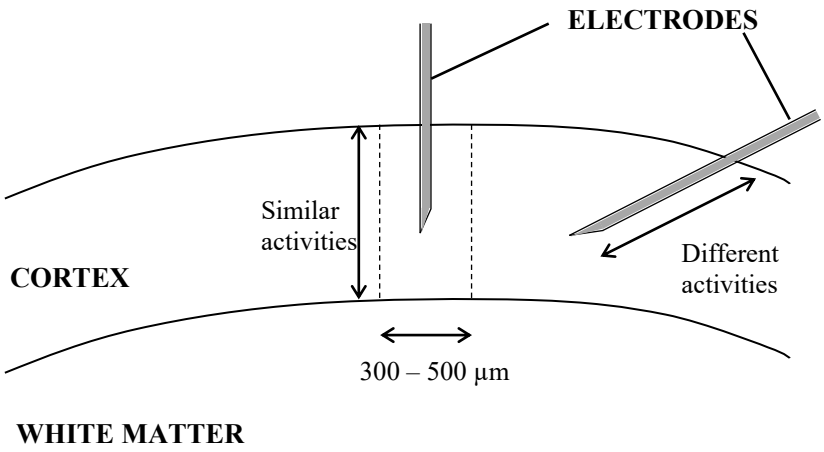

Figure 1.5. Schematic representation of Mountcastle's experiment.

1.1.2 How neurons generate electromagnetic field

The human brain contains around 100 billion neurons (10^{11}), linked together reaching up to 10'000 connections. Every single neuron receives, processes, and transmits a signal. Neuron's main structures are the dendrites - where the signal is received –, the soma – that process the signal – and the axon – where the signal is carried along towards other neurons. During this process, neurons produce an electromagnetic field that can be detected by various neuroimaging techniques (e.g. MEG, EEG, etc.).

The signals produced can be divided into 2 types: post-synaptic potentials (PSP) and action potential (AP).

Post-synaptic potentials are signals produced in dendrites, and allow communication between different neurons through junctions called synapses. It can be a direct electrical junction, but synapses are mostly chemical: when an action potential reaches the end of an axon terminal, it leads to the release of neurotransmitters, which affect membrane permeability so that Na+ and K+ ions migrate inside the membrane increasing the resting state potentials of about 10mV for a 10ms period. This is called post-synaptic potentials (PSP).

If many PSP sum up, soma's membrane potential can locally reach a threshold which causes a neuron's spike. If that happens, some voltage-sensitive channels open and positive ions are able to flow inside the cell, causing a rapid potential increase that lasts 1 ms before coming back to its resting state. Due to this peak, also the neighbor regions of the neuron reach the threshold, therefore the AP will propagate along the axon, as shown schematically in *Figure 1.6*.

Due to the tiny amplitude of the electromagnetic field produced by a single neuron, a lot of them need to sum up to be directly measured outside of the head with M/EEG. However, action potentials have a temporal duration close to the millisecond, making them hard to synchronize and sum up. On the other hand, PSPs have a temporal duration around 10 ms, which makes them more likely to produce a signal measurable outside the head. Moreover, electrical current is a vector quantity and has both an amplitude and a direction. In order to sum up, the currents produced by the neurons must have a common direction and therefore it is necessary to add the contribute of at least ten thousand (10^4) neurons with a common direction to produce a clear and detectable signal from outside of the head.

Indeed, some of the brain cells which have dendrites in many directions (e.g. stellate cells) will not produce a consistent and measurable electromagnetic field, while others - like pyramidal neurons - thanks to their particular shape and structure will.

Pyramidal neurons represent 70-80% of the neocortex and have a dense and regular geometric organization, with a current that flows through their axons (see *Figure 1.7*). Nowadays, due to the progress of brain imaging devices like MRI, this organization can be observed non-invasively. Activity of pyramidal neurons is theoretically detectable over an area of around 1 mm^2, however

an experimental study involving magnetoencephalography showed that the minimal detectable activity spreads over an area of around 100 mm^2 (Hämäläinen et al., 1993).

As we are going to discuss in the following paragraphs, the orientation of pyramidal neurons and their current flow have an influence on the magnetic and electric fields measurable by each type of sensor. In MEG, for example, radial current flows – considering the human brain roughly as a sphere – won't be detected.

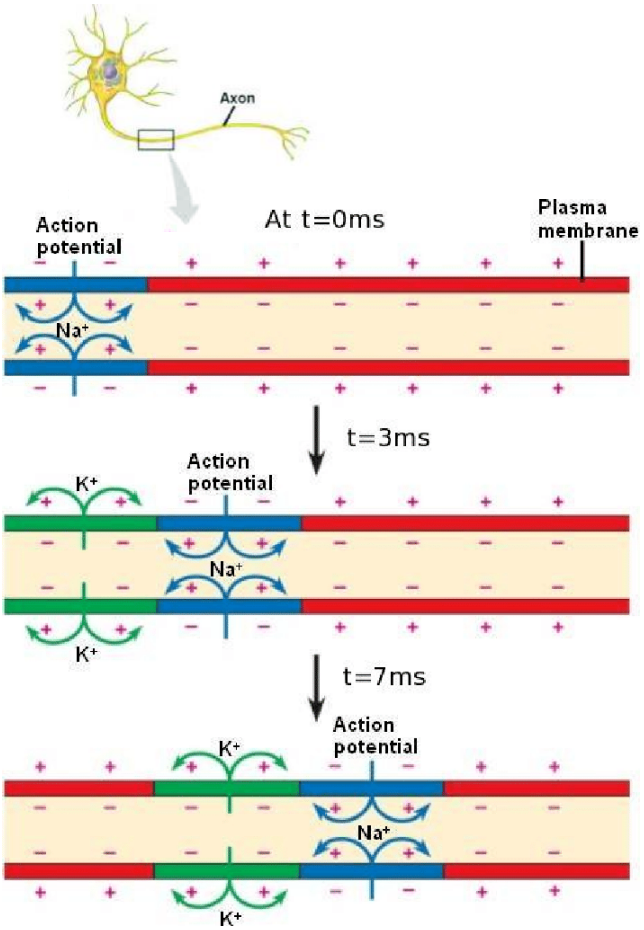

Figure 1.6. Propagation of an action potential.

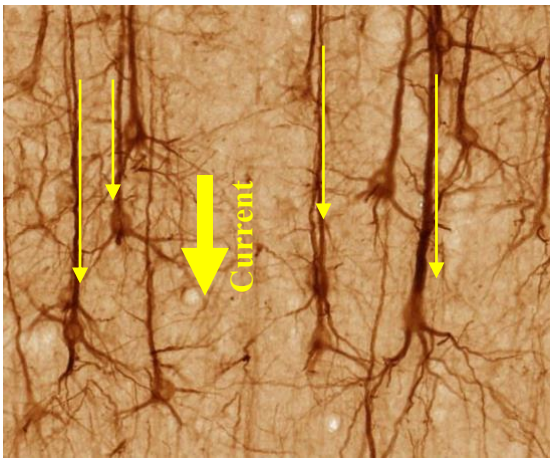

Figure 1.7. Pyramidal neurons.

1.2 BRAIN FUNCTIONAL PATHWAYS

1.2.1 Visual pathways

The human visual system plays a key role in identifying motion and perception, specifically with two distinct pathways: the parvocellular (P-pathway) and the magnocellular (M-pathway). These are characterized by two different types of nerve cells, which is the fundamental principle of a well-known insight in neuroscience known as the two-stream hypothesis. In 1992 David Milner and Melvyn A. Goodale proposed this hypothesis, arguing that humans possess two different visual systems. The M-cells carry visual information along the upper, dorsal stream, while the P-cells carry visual information along ventral areas (see *Figure 1.8*).

Concerning motion processing, dorsal stream is proposed to be involved in visually guided behavior and recognizing where objects are in space. It is responsible to project the signal from the retina to the primary visual cortex (V1), starting exclusively with visual functions in the occipital lobe before addressing questions about spatial awareness moving to parietal lobe. Indeed, the parietal lobe is essential for the interpretation of spatial relationships, and it is therefore so-called the "where" stream.

On the other hand, ventral stream is mainly associated with object recognition and form representation. It develops through the medial temporal lobe – responsible for long-term memory – and involves the limbic system, responsible for controls of emotions. The main differences between the dorsal and ventral pathway rely on the different type of decoding that these streams provide: dorsal pathway merely provide an understanding of the spatial characteristics of an object, while ventral pathway is seen to be significant in attention, working memory, stimulus salience, and providing information about the significance of an object. Indeed, damages concerning the main areas of the ventral stream lead to the inability to decode and understand facial characteristics or expressions. The ventral stream is therefore also so-called the "what" stream.

However, motion perception – which is one of the main aspects in the experiment described in this dissertation – has been seen to be clearly dissociated from other visual abilities like object recognizing. The area of the brain responsible for motion perception is the middle temporal (MT^+) cortical area, where neurons are selective for global motion direction and perception of motion.

Also, it is important to point out that external motion is processed differently than biological motion. Indeed, biological motion (with the few exceptions of eye and organs movements that do not evoke a motion perception) is processed by superior temporal sulcus (STS) areas, while external motion involves the middle temporal (MT^+) area.

A famous example concerning external motion perception is the well-known "patient LM", a 43-years old female that in 1978 has been observed suffering from akinetopsia (a.k.a. motion

blindness). Akinetopsia is a particular neuropsychological disorder developed after brain lesions, strokes, Alzheimer's disease and transcranial magnetic stimulation (TMS) which is characterized by the loss of motion perception. Although the patient could clearly see static objects and had perfect memory – due to her bilateral lesions of MT^+ area – she couldn't see car moving or liquids flowing. In *Figure 1.8* we can observe an approximative position of middle temporal area.

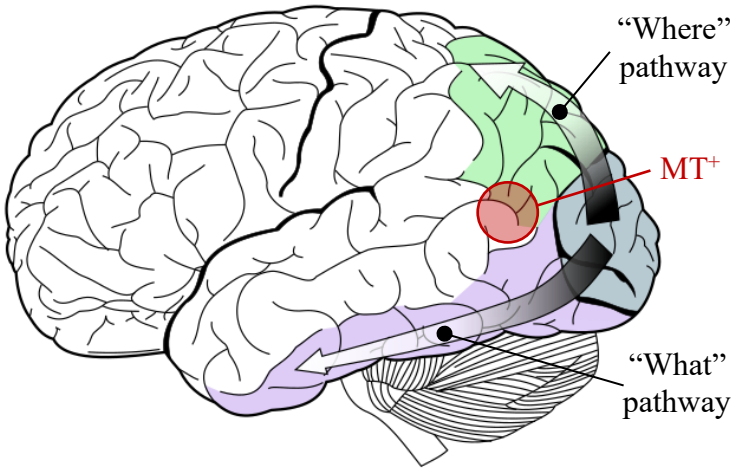

Figure 1.8. Dorsal (green) and ventral (purple) streams. Both pathways originate from the occipital lobe (V1, V2). In red is indicated the middle temporal area (MT^+), strongly involved in motion perception.

1.2.2 Cognitive functional networks

The human brain of an adult is intrinsically organized into about twenty independent functional networks, involved in cognitive functions and tasks. The most important networks during the development are the frontoparietal network (a.k.a. central executive network – CEN), the salience network (SN), and the default mode network (DMN). The CEN is anchored in the dorsolateral prefrontal cortex and posterior parietal cortex, while the SN in the anterior insula and anterior cingulate cortex, and finally the DMN is anchored in the posterior cingulate cortex and medial prefrontal cortex. Each one of them plays an important functional role.

The CEN is involved in the actively maintaining and manipulating of the information in working memory, for judgment and decision making (Petrides M. et al., 2005, Koechlin E. et al., 2007), the SN is critical in orienting attention to salient stimuli and facilitating goal-directed behavior (Sridharan D. et al., 2008), while the DMN has been seen to play an important role in self-referential mental activity and autobiographical memory (Kim H., 2012).

The anterior insula is fundamental in saliency detection by switching between other large-scale networks to facilitate access to attention and working memory when a salient event occurs.

Moreover, the insula is connected through strong functional connections with the anterior cingulate cortex, allowing its access to the motor system. Also, the interaction of the anterior and posterior insula facilitates physiological reactivity to salient stimuli.

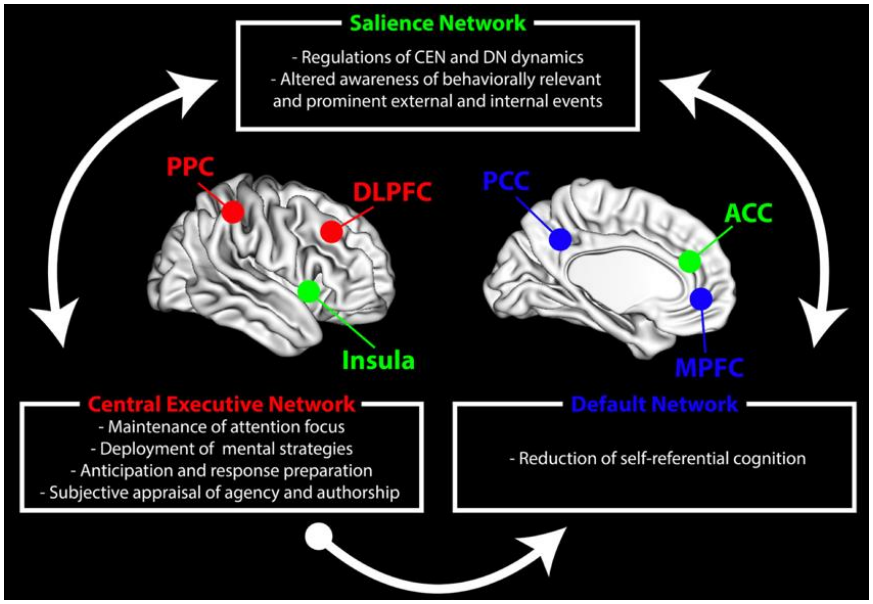

Figure 1.9 Schematic representation of the Central Executive Network (CEN), Salience Network (SN) and Default Mode Network (DMN). Source: M. Landry, M. Lifshitz, A. Raz. Brain correlates of hypnosis: A systematic review and meta-analytic exploration. *Neuroscience and Biobehavioral Reviews* 81: 75-98 (2017).

1.3 MEG: PRINCIPLES AND METHODS

1.3.1 Basics of MEG

Magnetoencephalography (MEG) is a noninvasive functional technique for recording and mapping brain activity from the head surface, detecting directly the magnetic flux associated with intracranial electrical currents. The magnetic field associated with this imaging technique is ranged between a few hundred femto-tesla (fT, 10^{-15} T) to few pico-tesla (pT, 10^{-12} T), providing a very high temporal resolution and spatial resolution. Considering that Earth's magnetic field is between 10^{-4} T and 10^{-5} T, MEG sensors need to be incredibly accurate and sensitive.

MEG is usually combined with magnetic resonance imaging (MRI) to estimate the sources of signals inside the brain. The combination of MEG and MRI is called magnetic source imaging (MSI). Although they are referring to different concepts, the terms MEG and MSI are often used interchangeably.

MEG recordings are nowadays used in two different ways. On the one hand, it is used for clinical purposes similarly to conventional electroencephalogram (EEG) and evoked potentials (EPs). In these cases, the aim is to detect abnormalities in spontaneous brain activity or in evoked-response activity. For example, MEG recordings might highlight a cerebral activity associated with epilepsy or mental disorders that can lead to low or delayed brain response. On the other hand, MEG is used for estimating the locations and time courses of sources of either spontaneous or evoked events of interest (MSI). This second use is particularly relevant in neuroscientific research because it allows to map the brain activity in pseudo-controlled conditions.

In principle, the measurement of the magnetic field is straightforward: we can easily observe changes in a magnetic field by putting a wire loop into it – so that an electric current will be induced to flow within the wire – and, measuring the voltage difference between the two ends of it, we will easily assess the magnetic field variation.

In 1963, for the first time in history, Baule and McFee (Department of Electrical Engineering at Syracuse University, New York) achieved to measure the magnetic field fluctuations associated with the heart cycle with an induction-coil magnetometer. Their magnetometer contained about 2 million turns of copper wire rolled up on a ferrite core. Placing two of such solenoids over the chest of the subject, they observed the first magnetocardiogram (MCG).

MEG is considered the magnetic counterpart of EEG but, due to its higher technical complexity, the first MEG recording is dated 40 years later than EEG. Indeed, MEG was measured for the first time in 1968 by the physicist David Cohen at the University of Illinois, using a copper induction coil as detector in a magnetically shielded room. Due to the promising results of his first

experiment, he decided to build a much better shielded room (see *Figure 1.10*) at the Massachusetts Institute of Technology, in Boston, using the first SQUID sensor developed by James E. Zimmerman. This time the signals were almost as clear as those of EEG (see *Figure 1.11*). This discovery broke the ground and stimulated the interest of physicists, neuroscientists, and engineers all over the world. Since then, magnetoencephalography became one of the most technical challenging neuroimaging techniques in the whole biomedical engineering community.

Figure 1.10. Dr. Cohen's shielded room at MIT.

Figure 1.11. First MEG (alpha rhythm) measured with SQUID sensors in Dr. Cohen room at MIT – *Science* 1972.

1.3.2 SQUID Sensors

As already mentioned in the last paragraph, in 1969, after 4 years of studies and perfectioning at Ford Motor Co., Zimmerman and colleagues developed the first SQUID sensor, which was used for the first time in neuroscience in 1972 by David Cohen.

Superconductive quantum interference device (SQUID) is the only sensor with enough sensitivity for high-quality biomagnetic measurements, because it relies on the conducting tunneling principle. This physical principle has been observed for the first time in 1962 by Brian Josephson and brought him the Nobel Prize in physics in 1973.

After Cohen's first experiment, many questions about possible improvements for SQUIDs arose and, in two decades, first led to the development of multichannel devices and finally in 1992 to the first helmet-shaped neuromagnetometer covering the whole scalp with 122 channels (Ahonen et al., 1993), and soon followed by systems with over 300 sensors.

Firstly, most of the studies were based on RF-SQUID sensors because they were simpler and cheaper, but in the last decades – due to decreasing of the manufacturing price – they have been substituted by more precise and low-noise DC-SQUIDs.

Currently, the most sensitive MEG sensors are SQUIDs, which are made of superconductive material organized in loops containing Josephson junctions: two or more superconductors coupled by a weak link that allows current flowing continuously without any voltage applied.

Figure 1.12 shows a schematic representation of SQUID circuit, in which two different coils are noticeable: a pickup coil – a.k.a. flux transformer – where the brain's magnetic field (B_{ext}) flows inducing a current that flows to the input coil, generating another magnetic field ($B_{coupled}$) whose intensity is sensed by the SQUID sensor itself due to its Josephson junctions. Thanks to these few-atoms-width junctions made by superconductive material, the magnetic flux (F) that will thread them will be quantized in magnetic-flux quanta (F_0):

$F_0 = h/(2e) \approx 2.068 \times 10^{-15}$ Wb

Where h is Planck's constant $6.62607004 \times 10^{-34}$ m^2kg/s, and e is the electron charge $1.60217662 \times 10^{-19}$ C. Note that Wb stands for *weber* – the unit for magnetic flux – and Wb = T m^2.

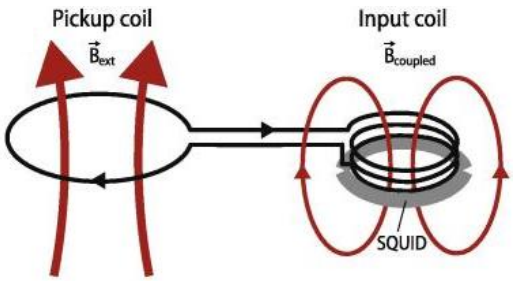

Figure 1.12. Schematic representation of SQUID circuit. Source: Hari R, Baillet S, Barnes G, et al. IFCN-endorsed practical guidelines for clinical magnetoencephalography (MEG). *Clinical Neurophysiology: Official Journal of the International Federation of Clinical Neurophysiology* 129(8):1720-1747 (2018).

With a proper tuning of construction parameters, the sensitivity of the SQUID system can be increased, allowing a tiny brain's magnetic field to be detected. Indeed, sensitivity can be augmented by adding more loops to the input coil – and therefore generating a higher flux coupled to the SQUID detector – or by increasing the area of the pickup coil. However, a too wide area will decrease spatial resolution of the MEG device.

SQUID sensors, due to their challenging operating conditions, suffers from low frequency noise (usually called 1/f noise or pink noise) generated by biological systems. It is typically lower than 1 Hz, depending on the properties of the SQUID. The traditional superconducting materials for SQUIDs are pure niobium or a lead alloy with 10% of indium or gold. Sensors are maintained at a temperature around absolute zero by a cooling system employing liquid helium close to 4 K.

Niobium – a.k.a columbium – is a ductile transition metal that becomes superconductive under 9.2 K, therefore on a working condition of around 4 K the thermal noise is low and the SNR of the SQUID is excellent. Indeed, in terms of thermal noise, our body generates about 0.1 fT/$\sqrt{Hz}$ which corresponds to the lower limit of SQUID sensitivity, but nowadays we can produce SQUIDs with a noise between 2 and 4 fT/$\sqrt{Hz}$, which is a huge improvement from the 40-50 fT/$\sqrt{Hz}$ we were able to reach years ago.

Flux transformers (pickup coils) can be shaped in multiple ways, called magnetometers and gradiometers. Magnetometers are simple loops that pick up the magnetic flux both close and far from the scalp but are also very sensitive to artifacts. On the other hand, gradiometers are designed with multiple loops that make the current flowing in an opposite sense. Therefore, they work as differential amplifiers and are sensitive to the difference between the two opposite currents flowing to the input coil, which is proportional to the respective magnetic flux flowing through the loops. Thus, they are sensitive to the nearby signals and reject the ones coming from deeper areas that induce a similar current in both pickup coils.

In other words, magnetometers would better distinguish between surface or inner brain magnetic signals while gradiometers between different signals on the surface.

There are two types of gradiometers: axial and planar gradiometers. In the axial ones, the coils are along the same axis and, according to the number of loops, are classified as "first-order" (two coils), "second-order" (three coils), etc. The higher the gradiometer order, the less sensitive to distant homogeneous fields (artifacts), but the more it dampens brain signals of interest.

The distance between gradiometer's coils is defined as *baseline*, and it is typically between 4 to 14 cm. If the baseline is higher, the sensor would act as a magnetometer.

Planar gradiometers are designed as two loops wound up in the same plane, whose current flows in two opposite senses, and pick up the largest signal above the source.

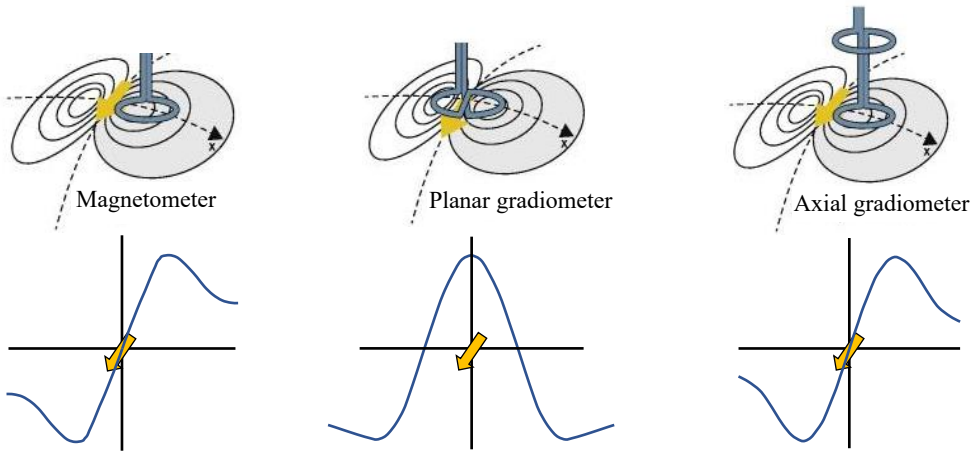

Figure 1.13. Different flux transformers in MEG. At the top of the picture is shown a magnetometer (left), a planar (middle) and an axial (right) gradiometer. Respectively, at the bottom is represented the signal strength, plotted along a line above the source, perpendicularly to the direction of the current dipole.
Source: Hari R, Baillet S, Barnes G, et al. IFCN-endorsed practical guidelines for clinical magnetoencephalography (MEG). *Clinical Neurophysiology: Official Journal of the International Federation of Clinical Neurophysiology* 129(8):1720-1747 (2018).

1.3.3 MEG device setup

During the MEG recording (shown in *Figure 1.14*), the subject is sitting with the head inside a helmet-shaped vacuum flask ("dewar") that houses from 200 up to 306 sensors, depending on the device. The name of this vacuum-insulated flask was named after its inventor, James Dewar (1842-1923), and it is fundamental to maintain quasi-absolute zero working conditions for SQUID sensors.

Moreover, to eliminate external disturbances and noises, the measurements are performed within a magnetically shielded room. These rooms are made of three nested layers, which are composed by aluminum and mu-metals (high-permeability ferromagnetic layers), to respectively filter out high-frequency and low-frequency noise. Magnetically shielded room (MSR) is carefully assembled with insulating washers between the screws and the panel, to electrically isolate each layer and eliminate radio frequency radiation that would degrade SQUIDs performances. Conductivity of aluminum is also enhanced by electroplating the junctions of the inner layer with gold or silver. Moreover, an active shielding system is provided for three-dimensional noise cancellation.

During MEG recordings, eye movement and blinks, which cause major artifacts, are monitored by an infrared camera placed in front of the subject or with an electro-oculogram. Although, they can also be detected and filtered out in the processing of the data, using frontal MEG channels.

Performing the experiment, the subject must keep the head as still as possible and moderately speak or perform little hands or eye movements. To suppress facial movements artifacts, also facial and bodily actions can be recorded with a video and monitored with accelerometers and surface electromyogram (sEMG). Everything in the MSR must be compatible and not create unwanted noise.

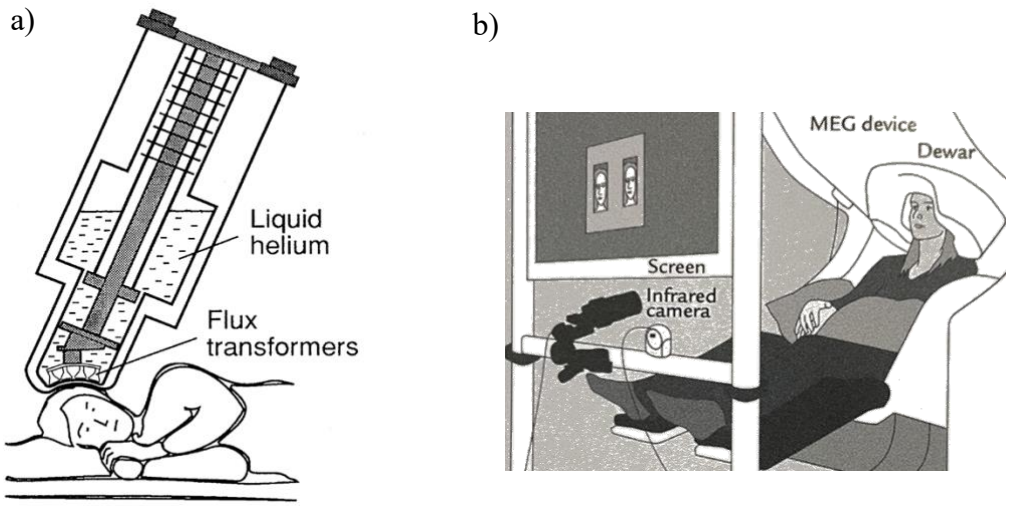

Figure 1.14. a) Section of MEG equipment. Source: M. Haimalainen et al. Magnetoencephalography. theory, instrumentation, and applications to noninvasive studies of the working human brain. *Reviews of Modern Physics* 65(2) 413-497 (1993). b) Typical position and setup for MEG experiments. Source: Hari R, On brain 's magnetic responses to sensory stimuli, *J Clin Neurophysiol* 8(2): 157-69 (1991).

1.3.4 MEG and EEG: characteristics and differences

MEG and EEG have rather different historical trajectories. EEG has been used for clinical diagnoses since early 1930s in patients who were thought to have mental disorders. A real leap in EEG occurred in 1960s and 1970s, when the first computers became accessible and allowed to average EEG signals, thereby significantly increasing the signal-to-noise ratio (SNR).

On the contrary, MEG technique underwent an opposite development: the first recordings were made in research laboratories by physicist, and they were averaging a very high number of single trials to lower the noise. It took several years to develop an MEG equipment able to analyze single trials with acceptable SNR. Only with recent technical development, MEG became popular in clinical environments, notwithstanding the fact that it is still not widespread in hospitals due to the high cost of the system. Moreover, MEG analyzing software are state-of-the-art technologies that are considered less reliable than EEG or fMRI ones for some purposes.

The area covered by a neuron assembly is very small with respect to the distance from the M/EEG sensors. Therefore, the electromagnetic field produced by an active neuron assembly at the sensor level is similar to the fields produced by a current dipole.

The summation of the neural currents produced by elementary generators can be approximated by an equivalent current dipole (ECD), and the fields produced by this ECD are strong enough to be measured outside the head.

Due to the bivalent electrical and magnetical nature of this signal, EEG and MEG are closely related and measure a similar neuron assembly activity. When neuron assembly spikes, they generate both a magnetic field and an electric potential that can be sensed by MEG sensors and EEG sensors, respectively. There are 3 types of dipoles: current dipole, electric dipole, and magnetic dipole (see *Figure 1.15*).

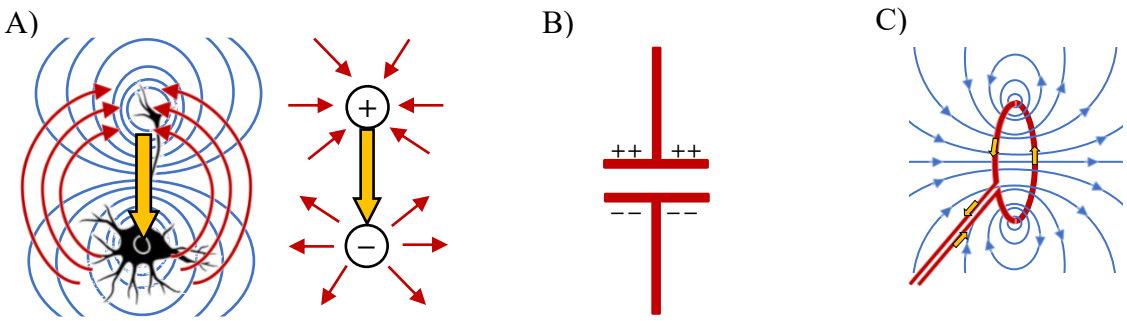

Figure 1.15. A) Current dipole. B) Electric dipole. C) Magnetic dipole

The current dipole represents the intracellular “primary current” due to net flow of ions within soma and dendrites of the activated neurons. Since the current loop must be closed, primary current

is always associated with a return current, a.k.a. volume current. Current dipoles are commonly used as source models for MEG and EEG signals, as we will describe later in the introduction with the forward and inverse problems.

A magnetic dipole, instead, is a current loop that, in the ideal case, does not produce any electric potential but just a magnetic field around it, as shown in *Figure 1.15*.

Considering the brain as a sphere, can be assumed that radial primary currents generated inside the sphere are symmetrical and therefore do not produce any magnetic fields (Hamalainen et al.,1993). However, tangential current dipoles are associated with volume currents that are not symmetrical and therefore produce a net magnetic field outside the sphere. *Figure 1.16-A* shows different orientations of current dipoles in a spherical head model.

The higher sensitivity and selectivity of MEG with respect to EEG to tangential currents result in a more precise measurement of MEG activity, recorded in the walls of cortical fissures (*Figure 1.16-B*). Considering that about two-thirds of the cerebral cortex is located within fissures (including all primary sensory cortices), this MEG characteristic becomes very useful and allows recording signals hardly detectable even with intracranial imaging methods (e.g. stereoelectroencephalography - sEEG)

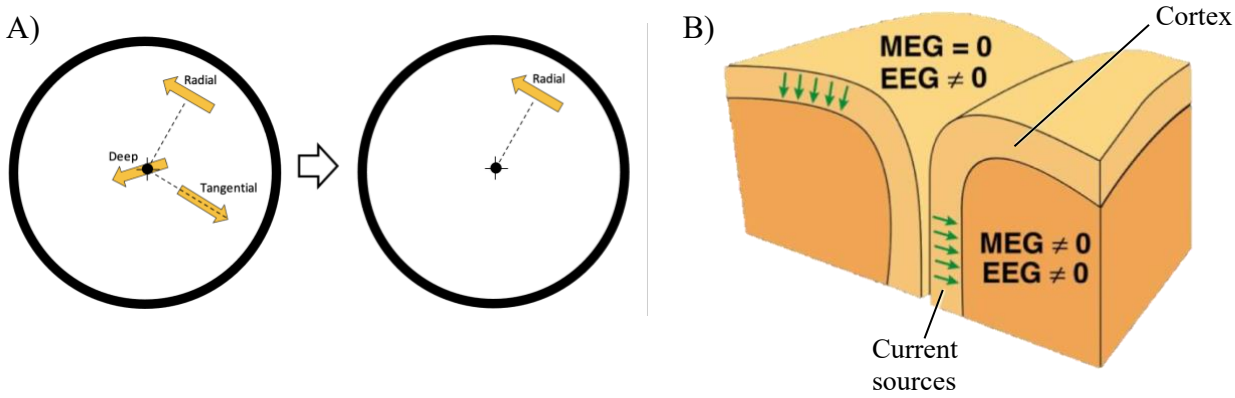

Figure 1.16. A) Dipole orientation in a spherical head model. In the first sphere, three different orientation are represented. However, in MEG recordings only radial dipoles are influent in the measurements. B) Current sources in human cortex for EEG and MEG recordings.

Another important characteristic about magnetic field is that it is detectable even if the sphere is composed of concentric shells with different conductivity. Conductivity is in fact a function of the radius only, thus MEG sees directly the signal inside the brain without distortion by the spinal fluid, the skull etc. Also, the pattern of the magnetic field follows the right-thumb rule.

On the contrary, in EEG measurements all the currents of different orientations and depth contribute to the generation of EEG potentials on the surface of the sphere. Moreover, the electric inhomogeneities, represented for example by the skull and scalp, dampen and smear potential distribution, resulting in a widespread signal source estimation. In *Figure 1.17* an example of the recorded signal and their projections on the head model is provided, underlining the transparency of MEG to radially oriented dipoles.

Another major difference between MEG and EEG is that EEG recordings measure voltage difference between two recording sites, whereas MEG recordings provide information on magnetic flux and gradient exactly at the measurement site.

EEG and MEG are optimal and complementary methods with their own strengths and weaknesses, allowing us to see brain activation from different perspectives. A table to sum up all the main differences between EEG and MEG is provided below (*Table 1*). Also, due to the strict correlation with functional magnetic resonance imaging to investigate brain activity, in *Table 2* is shown a comparison between M/EEG and fMRI.

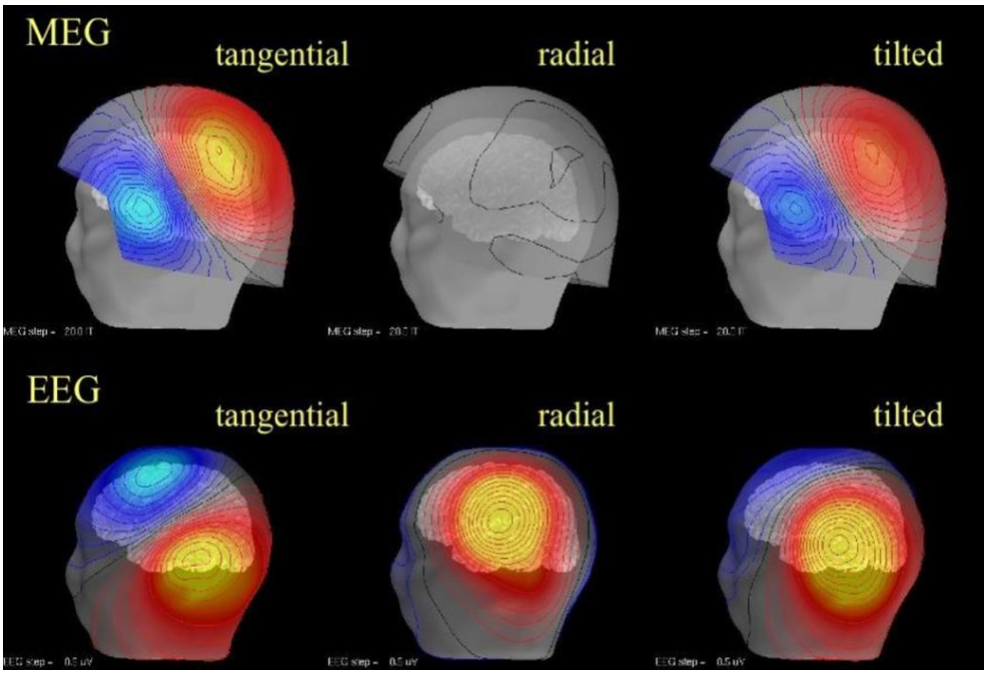

Figure 1.17. Mapping of neural activity sources in MEG and EEG, based on the dipoles orientations.

	EEG	MEG
Signal amplitude	10 mV	10 fT
Measurement	Secondary currents	Primary currents
Signal attenuation	Skull and scalp attenuation	Quasi non-attenuation by the skull and scalp
Temporal resolution	~ 1 ms	~ 1 ms
Spatial resolution	~ 1 cm	< 1 cm
Movement artifacts	Subjects can move a little wearing the helmet.	Subjects must remain as still as possible.
Dipole orientation	Radial and tangential	Only tangential
System complexity	Easy, cheap and portable	Expensive and technically challenging

Table 1. EEG and MEG differences.

	M/EEG	fMRI
Measurement	Primary/secondary currents (Direct)	Blood flow (Indirect)
Temporal resolution	~ 1 ms	~ 1 s
Spatial resolution	< 1 cm	< 1 mm
Signal reconstruction	Forward and inverse problems (Ill-posed)	Deconvolution
Depth	~ 4 cm	Whole brain
Signal orientation detected	Tangential (and radial)	All

Table 2. M/EEG and fMRI differences.

1.4 THE FORWARD AND INVERSE PROBLEMS

1.4.1 The forward problem

M/EEG captures the electrical activity of structured assemblies of neurons. For the last four decades, neuroscientists have built models of neuron assemblies based on the knowledge of neuronal dynamics, but these dynamics are far from being fully understood.

For one assembly, the EEG and MEG measurements reflect its average activity, but usually the intrinsic dynamics of the group of neurons is unknown. Recently, scientists struggled to find the best model to estimate signal sources inside human brain. To do so, they introduced the "forward problem" – which consists in modeling the head in order to compute the electrical potential and the magnetic field that is supposed to be produced by a given configuration of generators – and the "inverse problem" – represented by the mathematical model that describes how a certain distribution of neural generators might have produced the measurements –.

The solution of the forward problem is the first step in the M/EEG data processing pipeline, and to solve this problem we start from Maxwell's equations, making some realistic assumptions and finally derive realistic head models.

We are denoting by E the electric field, B the magnetic field, J the current density and ρ the charge density. Also, bold characters represent vectors. Maxwell equations are a set of four differential equations, that relate the electromagnetic field to the current and charge density:

$$\begin{cases} \nabla \cdot \boldsymbol{E} = \dfrac{\rho}{\varepsilon} & (1) \\ \nabla \times \boldsymbol{E} = -\dfrac{\partial \boldsymbol{B}}{\partial t} & (2) \\ \nabla \cdot \boldsymbol{B} = 0 & (3) \\ \nabla \times \boldsymbol{B} = \mu\left(\boldsymbol{J} + \varepsilon \dfrac{\partial \boldsymbol{E}}{\partial t}\right) & (4) \end{cases} \tag{1.4.1}$$

where ε and μ are respectively the electrical permittivity and the magnetic permeability of the medium. In physics, medium is defined as a substance that transfer any form of energy from one place to another.

For human tissues, magnetic permeability is the same as in vacuum, therefore $\mu = \mu_0$, whereas the relative electrical permittivity depends on the considered tissues: $\varepsilon_r = \frac{\varepsilon}{\varepsilon_0}$. For instance, when

the frequency is around 100 Hz, ε_r is 4×10^6 for grey matter, 5×10^5 for fat and 6×10^3 for compact bone (Gabriel et al., 1996).

As we already mentioned in the previous paragraphs, post-synaptic potentials last around 10 ms. Therefore, it is typically accepted that the frequency of the observed electromagnetic field – despite rare exceptions – cannot exceed 100 Hz. Within these conditions, we can accept a quasi-static approximation, according to which the time derivates of Maxwell's equations can be neglected (Hamalainen et al., 1993).

Consequently, the curl of electric field in 1.4.1(2) is zero and therefore $\boldsymbol{E} = -\nabla V$.

In order to derive the electric potential equation, it is important to understand that in a medium with current generators, the total current can be decomposed in a primary current flow J^P related to the generators, and a volume current flow J^V – a.k.a. ohmic current flow – related to the electric field in the volume. Considering Ohm's law ($\boldsymbol{J}^V = \sigma \boldsymbol{E}$):

$$\boldsymbol{J} = \boldsymbol{J}^P + \boldsymbol{J}^V = \boldsymbol{J}^P + \sigma \boldsymbol{E} = \boldsymbol{J}^P - \sigma \nabla V.$$

Considering now 1.4.1(4),

$$\nabla \times \boldsymbol{B} = \mu \left(\boldsymbol{J} + \varepsilon \frac{\partial \boldsymbol{E}}{\partial t} \right) \quad \text{(QUASI-STATIC APPROXIMATION} \Longrightarrow 0\text{)}$$

$$\Rightarrow \quad \nabla \times \boldsymbol{B} = \mu \boldsymbol{J}$$

$$\Rightarrow \quad \nabla \cdot (\nabla \times \boldsymbol{B}) = \nabla \cdot (\mu \boldsymbol{J})$$

$$\Rightarrow \quad 0 = \nabla \cdot (\mu \boldsymbol{J})$$

$$\Rightarrow \quad 0 = \nabla \cdot \boldsymbol{J}$$

Which leads to

$$\nabla \cdot \boldsymbol{J} = \nabla \cdot (\boldsymbol{J}^P - \sigma \nabla V) = 0$$

And finally to the electric potential equation:

$$\nabla \cdot (\sigma \nabla V) = \nabla \cdot \boldsymbol{J}^P. \qquad (1.4.2)$$

Furthermore, considering Biot-Savart law:

$$\boldsymbol{B}(\boldsymbol{r}) = \frac{\mu_0}{4\pi}\int_{\mathbb{R}^3} \boldsymbol{J}(\boldsymbol{r}') \times \frac{\boldsymbol{r}-\boldsymbol{r}'}{\|\boldsymbol{r}-\boldsymbol{r}'\|^3}\, d\boldsymbol{r}'.$$

Because the current can be written as $\boldsymbol{J} = \boldsymbol{J}^P - \sigma\nabla V$, Biot-Savart law becomes:

$$\boldsymbol{B}(\boldsymbol{r}) = \boldsymbol{B}_0(\boldsymbol{r}) - \frac{\mu_0}{4\pi}\int_{\mathbb{R}^3} \sigma\nabla V(\boldsymbol{r}') \times \frac{\boldsymbol{r}-\boldsymbol{r}'}{\|\boldsymbol{r}-\boldsymbol{r}'\|^3}\, d\boldsymbol{r}', \tag{1.4.3}$$

with

$$\boldsymbol{B}_0(\boldsymbol{r}) = \frac{\mu_0}{4\pi}\int_{\mathbb{R}^3} \boldsymbol{J}^P(\boldsymbol{r}') \times \frac{\boldsymbol{r}-\boldsymbol{r}'}{\|\boldsymbol{r}-\boldsymbol{r}'\|^3}\, d\boldsymbol{r}'.$$

$\boldsymbol{B}_0(\boldsymbol{r})$ is called *primary* magnetic field, while the second term is called *secondary* magnetic field. It is important to notice that the primary magnetic field does not depend on the medium considered – which in our case is represented by the head – and therefore its conductivity.

Additionally, if we consider a homogeneous conductor in its whole volume, with a constant conductivity σ, we can write the general solution of the Poisson equation with the following expression:

$$V(\boldsymbol{r}) = \frac{1}{4\pi\sigma}\int_{\mathbb{R}^3} \boldsymbol{J}^P(\boldsymbol{r}') \cdot \frac{\boldsymbol{r}-\boldsymbol{r}'}{\|\boldsymbol{r}-\boldsymbol{r}'\|^3}\, d\boldsymbol{r}'. \tag{1.4.4}$$

Considering 1.4.3 – since σ is supposed constant and V vanished at infinity due to 1.4.4 – we can simplify the integral, obtaining:

$$\boldsymbol{B}(\boldsymbol{r}) = \boldsymbol{B}_0(\boldsymbol{r}) = \frac{\mu_0}{4\pi}\int_{\mathbb{R}^3} \boldsymbol{J}^P(\boldsymbol{r}') \times \frac{\boldsymbol{r}-\boldsymbol{r}'}{\|\boldsymbol{r}-\boldsymbol{r}'\|^3}\, d\boldsymbol{r}'.$$

However, human head cannot be considered an infinite homogeneous conductor due to two main aspects: there is no electric current flow outside head boundaries (except at the neck) and the electrical conductivity σ is not constant. For instance, skull is 20 to 100 times less conductive than the grey and white matter.

In order to take into consideration these aspects, a more accurate approximation of human head can be obtained modeling the head as a series of nested concentric spheres. Considering that the average scalp thickness is 6.9 ±3.6 mm, while the average skull thickness is 6.0 ±1.9 mm (G. E. Strangman et al., 2014), *Figure 1.18* shows a proportional spherical model of the human head. Although, to improve forward calculation, anatomical brain data usually derives from MRI scan

– which results in a more precise view of soft tissues – or from a CT scan to highlight hard structures like the skull (see *Figure 1.19*).

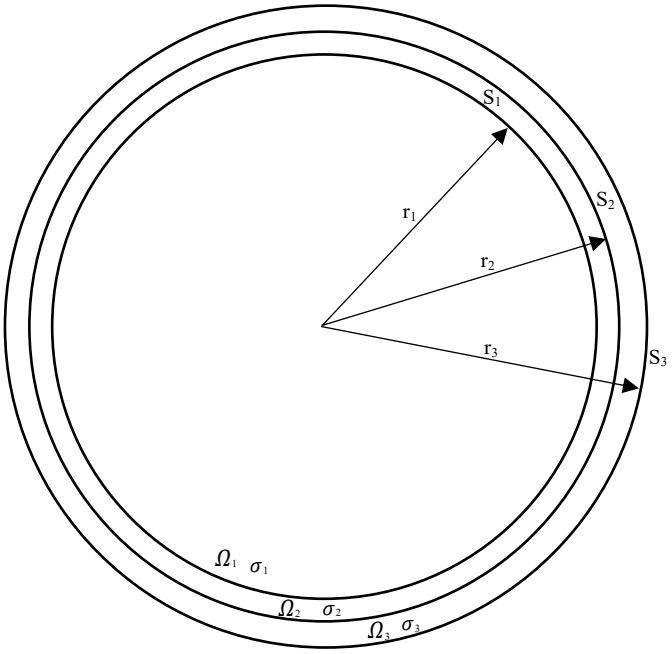

Figure 1.18. Proportional spherical model of the head with three layers. The inner, middle, and outer layers are respectively the brain, the skull, and the scalp.

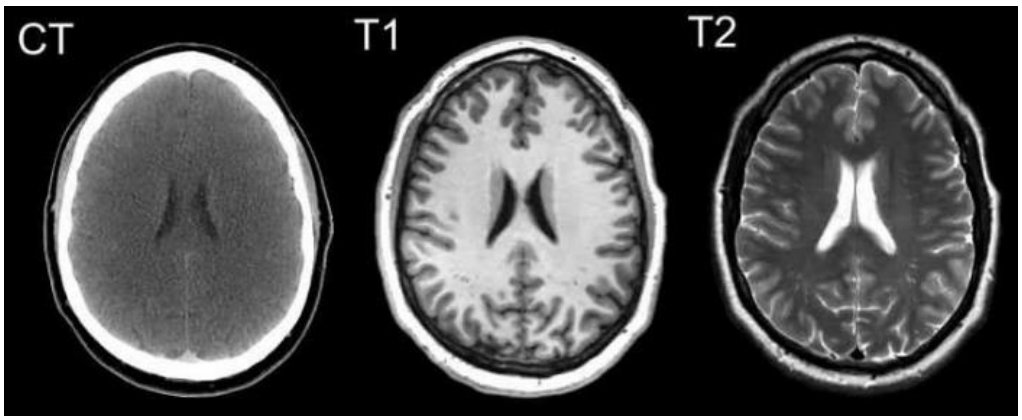

Figure 1.19. Axial view of CT and MRI brain scans. On the left, an axial view of a CT brain image. On the middle and right, the same slice obtained with T1 MRI and T2 MRI. T1 and T2 refers to different relaxation times of hydrogen atoms during MRI scan.

Nowadays, different approaches and algorithms are implemented to solve the forward problem, but the most famous are the Finite Difference Method (FDM), the Finite Element Method (FEM) and the Boundary Element Method (BEM).

The Boundary Element Method (BEM) is a numerical method aimed to solve linear differential equations transformed to integral equations, defining them into separate boundaries (e.g. white matter, grey matter, etc.). As we can see in *Figure 1.19*, from a MRI scan is easy to extract different brain structures. In a first approximation, we can consider a homogeneous conductivity within each of these structures (see *Figure 1.20*) in order to apply the boundary element method.

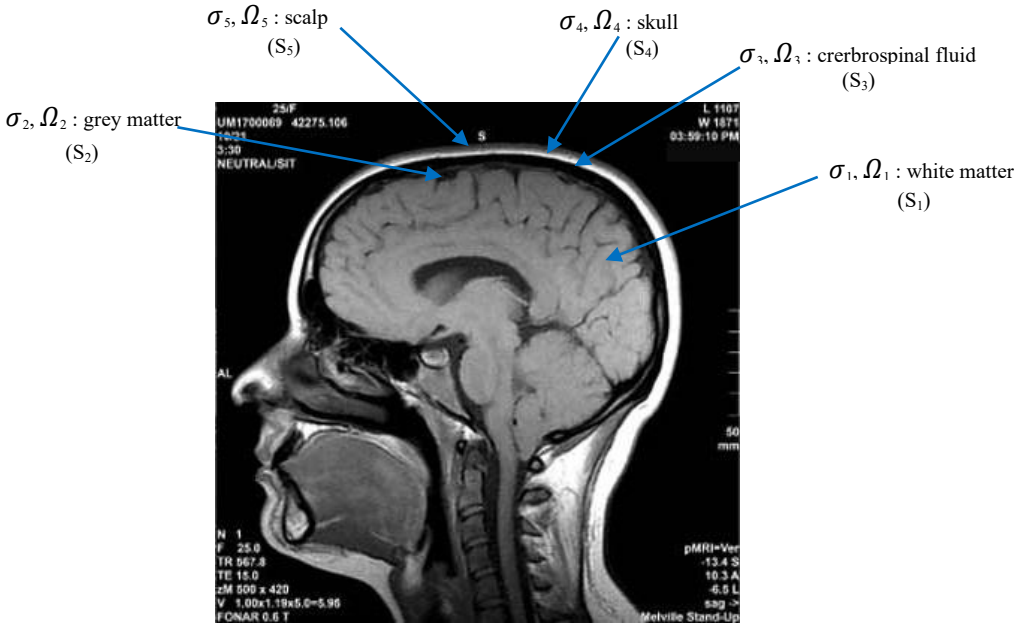

Figure 1.20. Example of a homogeneous division of a head model.

Applying this approximation, we will model the head as a domain Ω composed of several regions Ω_k separated by surfaces S_k. Each region has a homogeneous conductivity σ_k and $\sigma = 0$ outside the domain Ω.

Under these premises, Biot-Savart (1.4.3) and electric potential (1.4.2) expressions can be written as integral equations:

$$\frac{\sigma_k+\sigma_{k+1}}{2} V(\boldsymbol{r}) = V_0(\boldsymbol{r}) - \frac{1}{4\pi}\sum_l (\sigma_l - \sigma_{l+1}) \int_{S_l} V(\boldsymbol{r}') \frac{\boldsymbol{r}-\boldsymbol{r}'}{\|\boldsymbol{r}-\boldsymbol{r}'\|^3} \cdot \boldsymbol{n}_l(\boldsymbol{r}') ds', \quad (1)$$

$$\boldsymbol{B}(\boldsymbol{r}) = \boldsymbol{B}_0(\boldsymbol{r}) - \frac{\mu_0}{4\pi}\sum_l (\sigma_l - \sigma_{l+1}) \int_{S_l} V(\boldsymbol{r}') \frac{\boldsymbol{r}-\boldsymbol{r}'}{\|\boldsymbol{r}-\boldsymbol{r}'\|^3} \cdot \boldsymbol{n}_l(\boldsymbol{r}') ds', \quad (2) \quad (1.4.5)$$

where $\boldsymbol{r} \in S_k, V_0$ and $\boldsymbol{B}_0$ are the electric potential and magnetic field generated by the primary current flow $\boldsymbol{J}^P$ in a homogeneous domain. These formulas are derived from (Geselowitz, 1967; Geselowitz, 1970).

Now, assuming a division of the surfaces S_k as *n* triangles $\{T_i \mid i \in [1,\ldots,n]\}$ so that the solution will be approximated in a subspace of finite dimension. Indicating with E_h the approximation subspace, where h stands for the index of the largest triangle's size.

For each triangle, we will find $V \in E_h$ such that:

$$\forall i, T_i \in S_k, \ \frac{\sigma_k+\sigma_{k+1}}{2} V_i = V_0(\boldsymbol{r}_i) - \frac{1}{4\pi}\sum_l(\sigma_l - \sigma_{l+1}) \sum_{T_j \in S_l} V_j \int_{T_j} \Phi_j(\boldsymbol{r}') \frac{\boldsymbol{r}_i - \boldsymbol{r}'}{\|\boldsymbol{r}_i - \boldsymbol{r}'\|^3} \cdot \boldsymbol{n}_j ds' ,$$

Where $\mathbf{r}_i$ is the center of the triangle T_i and $\mathbf{n}_j$ is the constant normal to triangle T_j. So, this last equation can be written as:

$$V_i = b_i + \sum_j a_{ij} V_j ,$$

Where b_i and a_{ij} are constant coefficients that can be calculated. In conclusion, the problem will become once again a linear system:

$$\boldsymbol{A}\,[V_i] = b .$$

All the V_i values of V will be derived by the resolution of this linear system.

Once we calculated this electric potential, an approximate solution of the magnetic field generated by the same source can be drawn using the equation 1.4.5(2) (Ferguson et al., 1994). Doing that, the tiny electromagnetic fields produced by the neural activity can be modeled to approximate what is measured by MEG device.

1.4.2 The inverse problem

The inverse problem of M/EEG processing is considered the counterpart of the forward problem and consists of retrieving the neural generators distribution that produced the observed and measured electromagnetic field.

There are three main approaches to solve the inverse problem:

- The dipole fitting approaches (parametric models);
- The beamforming or scanning techniques;
- The image-based methods with distributed source models.

The dipole fitting approach is based on the assumption that the measured data have been produced by a small number of active regions and each of them can be modeled as a single dipole (equivalent current dipole – ECD). Also, the number of dipoles and therefore the active regions are a priori fixed. That represents a huge limit to this approach and these models are commonly used when one or few dipoles are present. However, when this technique is combined for example with fMRI, the position of dipoles can be supposed as known.

Another important way to approach the inverse solution is represented by the beamforming method. It is a scanning technique in which a certain region of interest – typically the gray matter in the cortical mantle – is filtered with spatial filtering or using signal classification indices to estimate the contribution of each source location. The better the spatial filter is, the better the estimation will get. A well-designed spatial filter is one that filters out sources that do not come from a small volume around a chosen radius. There are different spatial filters employed in these problems. The simplest one is called “matched filter”, but more complex ones have been designed to reach a higher precision avoiding crosstalk from other areas. For example, Linearly Constrained Minimum Variance (LCMV) beamformer or Synthetic Aperture Magnetometry (SAM) are two of the most common spatial filters.

Beamforming methods do not require any information about the number or nature of the sources, though they made the strong assumption that the activations of the different sources are uncorrelated.

The last method is represented by the image-based approaches. In this case, source models are distributed over a certain source space. The surface is typically the cortical mantle, modeled as a triangular mesh. Therefore, instead of dealing with scalar values over a 2D or 3D complex grid, the space is defined with vertices of triangles over a brain surface. Once the dipoles are estimated with their orientation, software that implements and handles this image-based method (e.g. Freesurfer, BrainVisa, etc.) proceeds to inflate the cortical surface in order to derive a nicer brain view with their highlighted active regions. By doing so, oriented activities detected in the gyri are represented in an inflated cortical mesh, as shown in *Figure 1.21*.

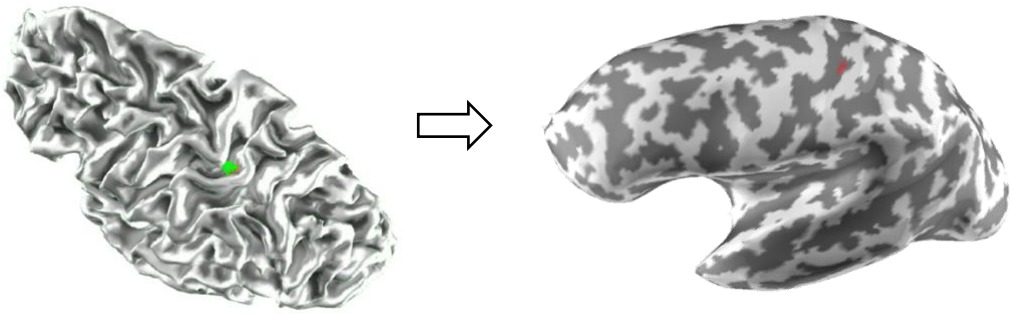

Figure 1.21 Dipolar sources distributed over a brain surface.

When orientations of dipoles are fixed and only the amplitude of distributed sources needs to be estimated, the problem to solve can be simplified into the following.

$$\underset{①}{M} = \underset{②③}{G}\underset{④}{X} + E$$

M = MEG data (measurements)
G = Gain matrix
X = Source amplitudes (unknown)
E = Additive noise

① MEG data matrix (M)

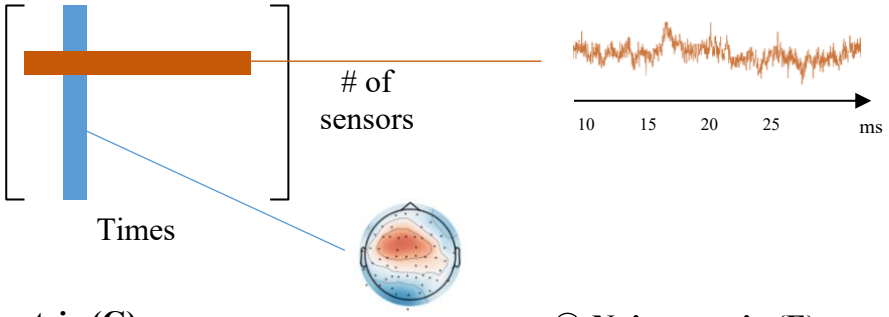

② Gain matrix (G)

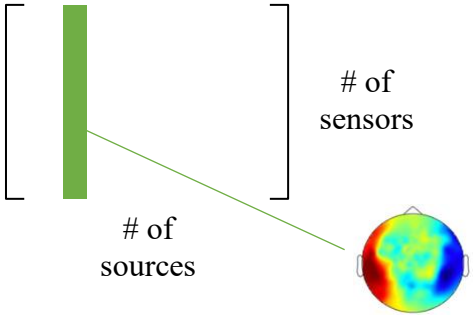

④ Noise matrix (E)

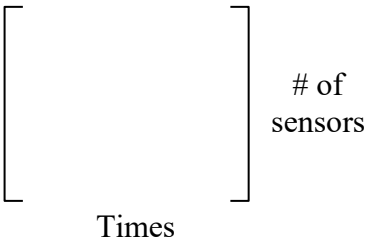

③ Source amplitude matrix (X)

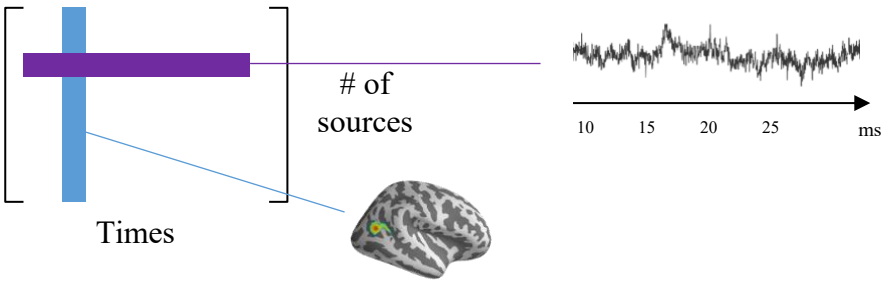

Due to the higher number of sources with respect to the number of MEG measurements (sensors), the problem is undetermined and what we do is find the best solution using an optimization method. These optimizing methods based on ℓ_2 penalization will compute the minimum norm solution of:

$$X^* = \arg\min \|M - GX\|^2 + \lambda \|X\|^2$$

Some alternative methods are the weighted minimum-norm (WMN), the dynamic statistical parametric mapping (dSPM) and the standardized low-resolution brain electromagnetic tomography (sLORETA).

1.5 SOFTWARE AND TOOLS

1.5.1 MNE-Python

As we went through the forward and inverse problem in the last paragraphs, it is clear now that localizing the neural currents in M/EEG is very complex and requires approximations. Thus, in order to achieve a good result, a group of scientists and engineers at the Martinos Center for Biomedical Imaging (Massachusetts General Hospital, Boston, MA) have developed the MNE software suite. It contains many command line functions written in C and compiled in Linux and MacOSX, interactive tools for reviewing the recordings and the source estimates, and the Matlab and Python code to interact with a wide variety of other environments (source Biomedical Image Group, USC).

MNE-Python provides a set of algorithms (Gramfort et al., 2014) that allow to plot and analyze the data recorded by the MEG device, and it has been used in this dissertation to analyze and plot the results (see Chapter 4). MNE-Python is only one of several packages that has been created in the last two decades. Other examples are Brainstorm (University of Southern California and MIT, 2011), FieldTrip (Donders Institute for Brain, Cognition and Behaviour, Radbound University Nijmegen, 2011) and NutMeg (University of California San Francisco, 2004). They are all implemented in Matlab.

MNE-Python is currently the state-of-the-art package for the Python community. Nevertheless, due to its NeuroMag FIF file format, it interacts with other MNE suite components. MNE-Python provides many features to analyze every aspect of the MEG/EEG signals, such as time-frequency analysis, brain connectivity, independent component analysis, but also multivariate pattern

analysis and machine learning algorithms. With MNE-Python is easy to address every aspect of the analysis pipeline: from preprocessing, through source estimation and plotting, to machine learning predictions.

As per its own structure, MNE-Python has been built on a scientific Python environment that integrates its main libraries: NumPy, to manage n-dimensional data structures, SciPy which contains modules of linear algebra and signal/image processing, Matplotlib, used for 2D graphics, PyVista or Mayavi for the 3D graphics, Pandas to handle data frames and Scikit-Learn that implements machine learning algorithms.

In the previous paragraph, we saw that the forward problem refers to the correspondence between neural currents and M/EEG sensor measurements, while the inverse problem resolves the cortical sources that produce a specific set of M/EEG recordings. In MNE-Python, both problems can be solved in different methods, from simple spherical head models to boundary or finite element for the forward problem, to depth-weighted minimum L2 norm estimator of cortical current density for the inverse one. Furthermore, some normalization techniques can be implemented using MNE-Python (dSPM, sLORETA, etc.).

In order to make it run – once a version of Python 3.x is installed on the computer – we need to create a virtual environment on the Python integrated development environment (IDE). The whole virtual environment that allows 3D plotting capabilities and source analysis is available on GitHub and to download it just a few lines of code are required:

Linux

```
$ curl --remote-name https://raw.githubusercontent.com/mne-tools/mne-python/main/environment.yml
$ conda env update --file environment.yml
```

MacOS

```
$ conda install --name base nb_conda_kernels "spyder>=4.2.1"
$ curl --remote-name https://raw.githubusercontent.com/mne-tools/mne-python/main/environment.yml
$ conda env update --file environment.yml
```

Windows

```
- Download the environment file at: https://raw.githubusercontent.com/mne-tools/mne-python/main/environment.yml
- Open on Anaconda command prompt
- Run conda install --name base nb_conda_kernels "spyder>=4.2.1"
- cd to the directory where you downloaded the file
- Run conda env update --file environment.yml
```

The virtual environment will be saved by default as ‘mne’ on the machine. Finally, you need to start a new project from the Python-IDE and select ‘mne’ as interpreter.

A.

```
import mne
# Load data
raw = mne.fiff.Raw('raw.fif',preload=True)
raw.info['bads'] = ['MEG 2443', 'EEG 053'] # mark bad channels
# Low-pass filter data
raw.filter(l_freq=None, h_freq=40.0)
# Extract epochs and save them
picks = mne.fiff.pick_types(raw.info, meg=True, eeg=True, eog=True,
                            exclude='bads')
events = mne.find_events(raw)
reject_criteria = dict(mag=4000e-15,     # 4000 fT
                       grad=4000e-13,    # 4000 fT/cm
                       eeg=150e-6,       # 150 µV
                       eog=250e-6)       # 250 µV
epochs = mne.Epochs(raw, events, event_id=1, tmin=-0.2, tmax=0.5,
                    reject=reject_criteria, picks=picks, preload=True,
# Compute noise covariance
cov = mne.compute_covariance(epochs, tmax=0)
# Compute inverse operator
fwd_fname = 'sample_audvis-meg-eeg-oct-6-fwd.fif'
fwd = mne.read_forward_solution(fwd_fname,surf_ori=True)
inv = mne.minimum_norm.make_inverse_operator(raw.info, fwd, cov, loose=0.2)
# Compute inverse solution
stc = mne.minimum_norm.apply_inverse(evoked, inv, lambda2=1./9., method='dSPM')
# Morph it to average brain for group study and plot it
stc_avg = mne.morph_data('sample', 'fsaverage', stc, 5, smooth=5)
```

B.

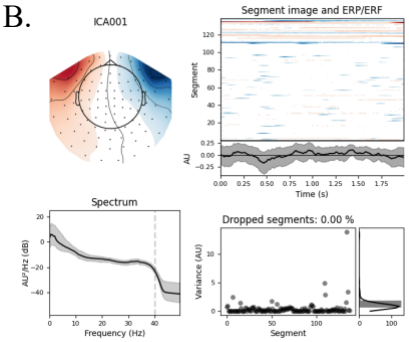

C.

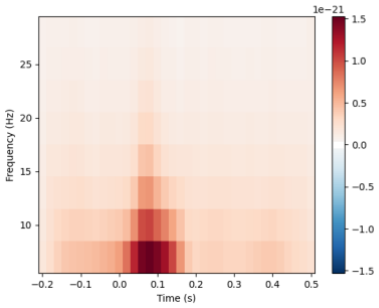

D.

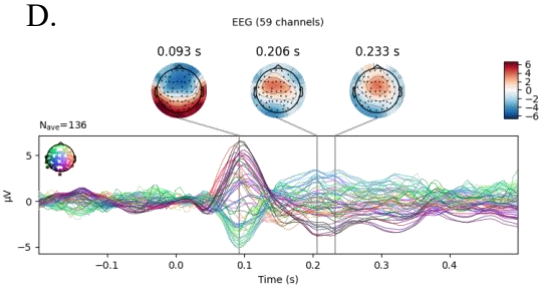

E.

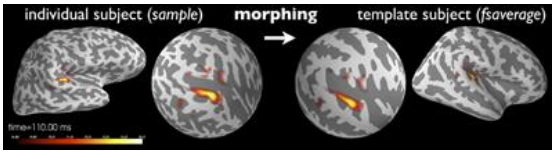

Figure 1.22. A. Example of Python code pipeline to preprocess the data, compute the inverse operator and morph the data into another source space (fsaverage); B. Plot of the independent component analysis (ICA) properties; C. Example of a time-frequency analysis plot; D. Example of an evoked response EEG plot; E. Morphing and normalization of source estimates to another cortical surface.
Source: [B, C, D] MNE-Python (v0.24.0.dev0) Tutorial – Overview of MEG/EEG analysis with MNE-Python; [A, E] Gramfort A.,Luessi M.,Larson E.,Engemann D.,Strohmeier D.,Brodbeck C., et al.(2013a).MNE software for processing MEG and EEG data

1.5.2 BraviShell and Psychtoolbox-3

Psychtoolbox-3 is a free package of functions and instructions for Matlab and GNU Octave, used in vision and neuroscience research. It allows to easy synthesize visual and auditory stimuli, interacting with the computer hardware to facilitate the collection of observer responses.

Even though the experiment relies on Psychtoolbox-3 during its implementation in Matlab, the whole code has been written in BraviShell. BraviShell is a software package developed in the Brain and Vision Research Laboratory (Biomedical Engineering Department, Boston University, Boston, MA, 2005-2014) that provides the main resources to easily design and code new experiments using Matlab. Due to its custom and goal-oriented development, it is designed to interact with the main brain research infrastructures in Boston: Brain and Vision Laboratory (Boston University), Athinoula A. Martinos Center for Biomedical Imaging (Harvard Medical School, Massachusetts General Hospital), and McGovern Institute for Brain Research (Massachusetts Institute of Technology).

BraviShell installer is hosted on GitHub and access to the installer is allowed only to trusted collaborators. If the installation is completed without any errors, moving to the BraviShell directory from the command prompt will allow to call Matlab with the command 'ptb3-matlab' and successfully access to the experiment folder typing 'BraviShell + name_of_experiment' in the Matlab command prompt. *Figure 1.23* shows a view of the interface just described.

A)

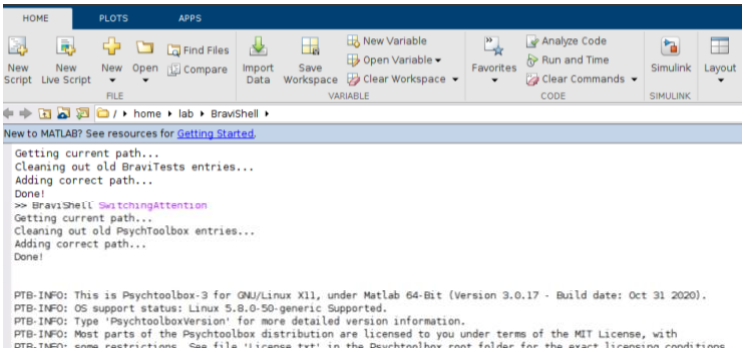

B)

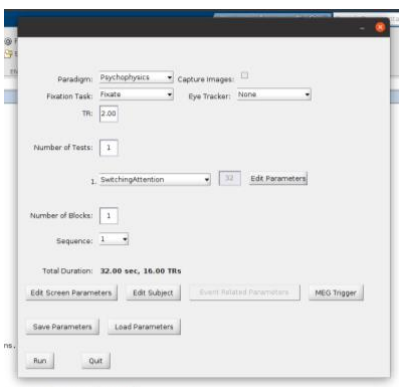

Figure 1.23. A) Call to BraviShell platform from Matlab environment. B) An example of the main menu for the 'SwitchingAttention' experiment.

References

Ahonen, A. I., Hämäläinen, M. S., Kajola, M. J., Knuutila, J. E. T., Laine, P. P., Lounasmaa, O. V. Parkkonen, L. T., Simola J. T., Tesche, C. D. 122-channel squid instrument for investigating the magnetic signals from the human brain. *Physica Scripta* T49: 198–205 (1993).

Brodmann, K. Vergleichende Lokalisationslehre der Grobhirnrinde. *J.A.Barth, Leipzig* (1909).

Ferguson, A., Zhang, X., Stroink, G. A complete linear discretization for calculating the magnetic field using the boundary element method. *IEEE Transitions on Biomedical Engineering* 41(5):455–459 (1994).

Gabriel, S., Lau, R.W., Gabriel, C. The dielectric properties of biological tissues II: measurements in the frequency range 10 Hz to 20 GHz. *Physics in Medicine and Biology*, 41:2251–2269 (1996).

Geselowitz, D. On bioelectric potentials in an homogeneous volume conductor. *Biophysics Journal* 7:1–11 (1967).

Geselowitz, D. On the magnetic field generated outside an inhomogeneous volume conductor by internal volume currents. *IEEE Transactions on Magnetics* 6:346–347 (1970).

Gramfort, A., Luessi, M., Larson, E., Engemann, D., Strohmeier, D., Brodbeck, C., Parkkonen, L., Hamalainen, M. MNE software for processing MEG and EEG data. *Neuroimage* 86: 446–460 (2014).

Hämäläinen, M., Hari, R., Ilmoniemi, R., Knuutila, J., Lounasmaa, O.V. Magnetoencephalography:
theory, instrumentation, and applications to noninvasive studies of the working human brain. *Reviews of Modern Physics* 65(2):413–497 (1993).

Kim, H. A dual-subsystem model of the brain's default network: self-referential processing, memory retrieval processes, and autobiographical memory retrieval. *Neuroimage* 61: 966–977 (2012).

Koechlin, E., Summerfield C. An information theoretical approach to prefrontal executive function. Trends in Cognitive Sciences 11: 229–235 (2007).

Landry, M., Lifshitz, M., Raz, A. Brain correlates of hypnosis: A systematic review and meta-analytic exploration. *Neuroscience and Biobehavioral Reviews* 81: 75–98 (2017).

Mountcastle, V.B. Modality and topographic properties of single neurons of cat's somatosensory cortex. *Journal of Neurophysiology* 20:408–434 (1957).

Petrides, M. Lateral prefrontal cortex: architectonic and functional organization. *Philosophical Transactions of the Royal Society B: Biological Sciences* 360: 781–795 (2005).

Sridharan, D. et al. A critical role for the right fronto-insular cortex in switching between central-executive and default-mode networks. *Proceedings of the National Academy of Sciences of the U.S.A.* 105: 12569–12574 (2008).

Strangman, G. E., Zhang, Q., Li, Z. Scalp and skull influence on near infrared photon propagation in the Colin27 brain template. *Neuroimage* 15(85):136–49 (2014).

Chapter 2

EXPERIMENTAL BACKGROUND

In this chapter, a brief discussion about cognitive science's main theories is carried along. Hence, I am going to review previous studies regarding cognitive learning, task switching hypothesis and switching brain asymmetries, inhibition mechanisms, brain pathways, and the role of cerebral cortices during goal-oriented tasks.

In the discussion, several papers will be cited along with the point they tried to make. References will be found at the end of the chapter for the reader to deepen.

Contents

2.1 PREVIOUS STUDIES

2.1.1 A brief discussion on cognitive science

Cognitive psychology is defined as the scientific study of mental processes such as attention, language use, memory, perception, problem solving, creativity, and reasoning.
The origin of cognitive psychology occurred in the 1960s, to face the lack of empirical science in the understanding of internal brain processes. Along with cognitive psychology, different branches that focused on different aspects of the brain developed. One of these is cognitive learning theory (CLT), which is a wide topic approached both from a psychological and physiological point of view. The first – a.k.a. behaviorists approach – concerns external observable behavior and held as the main study approach from the 1920s to 1950s, while psychological studies – a.k.a. cognitive approach – investigate internal brain processes that lead to learning. There is a huge literature aimed to understand how the brain is capable of actively understanding and learning a particular task, defining the role of the different brain cortices and their internal communication pathways. We will focus on them later in the dissertation.

One of the major research topics in cognitive psychology is task switching, and its study has become one of the major research tools to understand the dynamic and flexible control of task sets. A task set is typically assumed to include a task goal, a set of task-relevant stimuli, and a set of possible responses. A task goal is usually represented by performing a classification between two different possibilities (letters, numbers, shapes, colors, etc.), a task-relevant stimulus aims to indicate the subject which task to perform between different possibilities, and finally during a task set the subject can respond to the task in different ways, such as speaking, moving eyes or pressing a key. In typical task-switching studies, participants switch between two tasks.
The typical phenomenon in task switching is called switch cost (e.g., Rogers & Monsell, 1995) and is likely observed with a drop in performance (higher reaction times and error rates) in task switching rather than in task repetition (e.g. Allport et al. 1994). In the study of Allport et al. 1994, switch cost was explained with a task set inertia (TSI) hypothesis, stating that high switching costs were due to persisting activation of the task that was relevant prior to the switch. When subjects moved from Task A to Task B – according to the TSI hypothesis – the activation pathways associated with Task A remained high for some time after the switch to Task B. Thus, conflicts between Task A and Task B pathways resulted in a high switching cost and drop in performances. Another valid hypothesis that tried to explain this phenomenon was proposed by Monsell in 1996 and called the 'task-set reconfiguration hypothesis' (TSR), according to which, switch cost never disappears entirely – contrarily at the TSI hypothesis where inertia was present only at the

beginning of the task due to sudden switch (Allport et al. 1994, Meiran, Chorev, & Sapir, 2000; Milán et al., 2005) – and is sustained by two components: an 'endogenous' component under subjects' voluntary control and an involuntary 'exogenous' one . Respectively, the first component can be actively eliminated before the upcoming new task, but the latter one holds until the stimulus was actually presented, and it is often identified as "residual switch cost".

In a typical task-switching paradigm, important studies have also demonstrated the existence of switch-cost asymmetries related to subjects' stronger and weaker tasks (Allport et al. 1994). Allport et al. (1994) observed a higher switch cost when participants switched to the stronger task – the one in which they performed better and were more confident – rather than when they were asked to switch to the weaker one. Asymmetries have been observed in many types of tasks, which involved different sensory areas. However, the most interesting results have been drawn from color-naming task sets (e.g. Arbuthnott, 2008; Koch, Prinz & Allport, 2005; Monsell, Yeung & Azuma, 2000) and in language-related paradigm. These latter studies, for example, reported greater switch cost when subjects had to move to their first language rather than when they moved to their second language (e.g. Campbell, 2005; Costa & Santesetban, 2004, Philipp, Gade & Koch, 2007). A reason for this asymmetry can be found in the previously discussed TSI hypothesis, according to which a strong brain signal persists after our dominant task and its inhibition requires a higher cost and therefore a performance drop.

Although, even if the TSI hypothesis could be a reasonable explanation of this phenomena, different hypotheses have been proposed by scientists.

For example, Monsell et al. (2000) argued that switch-cost asymmetry could be explained without taking into consideration inhibitory processes but by introducing a "task priming" concept, which relies on the idea that a higher brain activation baseline (related with the dominant task) has a greater aftereffect on the other – non-dominant – task. Importantly, task priming is asymmetrical because the tasks have different activation baselines that indicate which is the strongest one. Furthermore, Yeung & Monsell (2003) modeled the switch-cost asymmetry as a priming-based modulation of task-repetition benefits, based on the concept that task interference is higher when switching to the weaker task because of strong priming, and this interference is modulated and reduced in task repetition.

However, the aforementioned studies focused only on asymmetrical activation related to switch-cost and didn't assess the role of inhibition mechanisms. Hence, Mayr and Keele in a paper published in 2000 tried to answer the question of whether or not brain inhibition mechanisms are fundamental during a task-switching paradigm. They found inhibition mechanisms triggered by "top-down" processes and that cue-encoding processes themselves are not an inhibition target. By "top-down" processes they meant the ones based on specific cues that reveal the identity of the upcoming task, while with "bottom-up" processes they identify those where the information is provided in the actual stimulus display itself (e.g. Hubner, Dreisbach, Haider & Kluwe, 2003;

Mayr & Kelee, 2000). However, it is still not clear whether task-unspecific cues do or do not lead to task inhibition, and further examinations need to be done before stronger conclusions can be drawn.

From the neuropsychological perspective, cognitive neuroscience has to address multiple challenges related to spatial brain activation during task switching in everyday life. It has been already proven the fundamental role of the prefrontal cortex in situations that require flexible adjustment to different task demands (Owen et al., 1993; Milner, 1963), but the neuroimaging literature is still studying the cognitive control processes involved in such problem. Specifically, we refer to cognitive control as the ability to flexibly adjust behaviors and thoughts to reach a specific goal (Miller & Cohen, 2001).

Neuroimaging studies have already shown a sustained activity in the frontal and parietal cortices during cognitive control, raising questions about the specific contribution of prefrontal and parietal brain regions to achieve an end. Early invasive experiments on monkeys (Miller & Cohen, 2001; Tomita, Ohbayashi, Nakahara, Hasegawa & Mijashita, 1999) tried to assess the contribution of the prefrontal cortex, finding its role as a bias for the posterior brain processing. Therefore, it is likely to consider true what was shown by Brass et al. (2005), who tried to observe a prior activation in the prefrontal cortex, which modulates – in a task-switching paradigm – the parietal cortex activity. This experiment was conducted considering both fMRI imaging – for its high spatial resolution – and ERP data –for their higher temporal resolution –.

However, within a brain structure as large and complex as the prefrontal cortex, a lot of scientists argued about different regional specialization of function, finding out ambiguous behaviors. On one hand, some studies have demonstrated specific properties of single neurons in the prefrontal cortex during particular tasks, which underline a high specialization. Considering for example a specifically-driven task regarding spatial working memory, the region of the principal sulcus is shown to be majorly involved in the localization processes (Funahashi et al., 1989). On the other hand, some studies suggested that neurons distributed through the lateral frontal cortex might adapt their properties and activation depending on the task demand (Rao et al., 1997).

Even anatomical data of the frontal cortex could be misunderstood because, even though it is true that subregions of the frontal cortex have a different function and local structure (Petrides & Pandya, 1994), connectivity pathways in these regions are very complex. Indeed, experiments on monkeys explained how even a small region of the frontal cortex is connected not only with the immediately surrounding areas but also with a widely spread network involving the whole frontal lobe (Pucak et al., 1996). One method to address this challenge about brain connectivity is called Granger causality – a.k.a “G-causality” –. This concept was first proposed in 1969 by the econometrician Sir Clive William John Granger (1934-2009), whose work to determine whether one-time series is useful for forecasting another in terms of causality has been used in many disciplines in the last decades. Also, it has been proven to represent a consistent statistical analysis

method in neuroscience research (Bressler et al., 2011). Despite the long-held belief about high task-specificity of brain regions may hold true, in recent years brain connectivity has become a flourishing topic because scientists – applying Granger causality concepts – have tried to look at the brain in a network-centric approach to describe the information flow inside the brain.

Brain functions are now thought to be associated with complex neural networks rather than simple brain regions. In other terms, scientists are investigating brain functions focusing on the information flow between areas rather than the areas themselves (Knight, 2007). The dynamics of these networks are governed by stochastic processes evolving through time, which led to the conclusion that by giving the brain the same input stimulus multiple times, the output of the brain network will be slightly different every time. Granger causality analysis – in neuroscience – is based on the idea of how to best predict the future of a neuron or a small group of them considering first an entire ensemble of neurons and then the same ensemble without one certain target neuron. If the prediction is worse by excluding that neuron, then it will be considered "g-causal" with respect to the ensemble.

Moreover, it is interesting to focus on the imaging literature where different imaging methods have been used to establish a more specific overview of the main brain networks.

For example, functional magnetic resonance imaging (fMRI) studies found sustained activity of the cingulo-opercular network (CON) and frontoparietal network (FPN) during the performance of many cognitive activities and maintenance of alertness state (Sheffield et al., 2015; Sepideh, D'Esposito, 2015). These networks (see *Figure 2.1*) involve different regions of the frontal and parietal cortex. The CON spreads through anterior cingulate, anterior prefrontal, and anterior insula/frontal regions, while the FPN includes regions from dorsolateral and ventrolateral prefrontal cortices, motor areas, inferior and superior parietal lobes, and intraparietal sulci (Braver et al.,2003; Dosenbach et al.,2006; Dosenbach et al., 2007, Dosenbach et al.2008). In task-switching paradigms, these networks have been observed to increase their activity when the subject underwent a switch of tasks (Braver et al.,2003; Dove et al.,2000; Sohn et al.,2000; Derrfuss et al.,2005; Crone et al.,2006; Guard et al.,2002; Yeung et al.,2006; Rushworth et al.,2002). Moreover, prefrontal and posterior parietal regions have been found to modulate their activities accordingly to the behavioral cost associated with task switching: the higher the cost, the higher the activation.

As previously mentioned, several studies reflect frontal-lobe activation to be associated with different cognitive demands, such as spatial attention, decision making, and task switching (Dove et al., 2000). In general, goal-directed behaviors rely on the prefrontal cortex (Diamond, 2013; Miller & Cohen, 2001), which – due to multiple factors – can undergo cognitive fatigue, associated with a drop in performance. This is known as cognitive fatigability and affects principal brain processes such as information processing, working memory, planning, sustained attention, ignoring irrelevant cues, etc. (Kurzban, Duckworth, Kable & Myers, 2013; Boksem & Tops,

2008). In recent years, functional imaging studies tried to better understand this phenomenon using network analyses on fMRI and EEG data. They suggested a brain response to cognitive fatigability consisting in the alteration of the long-range connectivity to a lower-range one, and a right-left hemisphere asymmetrical connectivity between the beginning and the end of the task (Sun, Lim, Kwok & Bezerianos, 2014; Sun et al., 2017, Verweij et al., 2014).
Cognitive fatigue related to task switching has been shown to have different effects whether the subject had to rely on working memory or on a self-explanatory external cue (Gajewski, Kleinsorge & Falkeinstein, 2010; Wolff, Roessner & Beste, 2016). Hence, it is likely to suppose that – during a task-switching paradigm involving working memory – fatigue is enhanced by the prefrontal cortex's need to maintain multiple processes (Petruo, Mückschel & Beste, 2018).

During our everyday life, working memory is one of the most important mnemonic operations we are dealing with. It includes online maintenance of information, coming from internal or external stimuli, and is extremely important for the performance of a large number of tasks.. Remembering addresses, directions, names, or perform a calculation are only a few of them.
The name ‘working memory’ was coined by Miller, Galanter, and Pribram in 1960 in their book called ‘Plans and the Structure of Behaviour’ and – during the ‘60s – became of major interest because of its implications with the new era of information processing and digital computers.
We already mentioned the role of the prefrontal cortex (PFC) during goal-oriented tasks, but research in the somatosensory domain provided evidence that neurons in PFC increase or decrease their firing rate to encode working memory content (Brody et al., 2003).

2.1.2 Neural oscillations in cognitive processes

Brain activity is characterized by neural oscillations – a.k.a. brainwaves – which are rhythmic patterns generated by the central nervous system at different frequencies. Since their discovery in 1924 by Hans Berger, neural oscillations became one of the main aspects to focus on in neuroscience. Nowadays, brain signals throughout different frequencies are still considered extremely significant to figure out communication between different areas of the brain and between inner and outer parts of the cortex.
There is a wide literature referring to EEG and fMRI imaging that shows alpha oscillations to be related to switching cost. In particular, a strong decrease in the alpha band has been observed for switch trials with respect to repeat trials during the preparatory period and reactive period for both cued and non-cued task-switching paradigms (Sauseng et al.,2006; Wu et al.,2015; Cunillera et al.,2012; Cooper et al.,2016; Foxe et al.,2014; Rapela et al.,2012; Poljac & Yeung, 2014; Murphy et al.,2016). Other studies have also found evidence for alpha activity decrease in the frontal and parieto-occipital electrodes (Foxe et al.,2014; Murphy et al.,2016; Verstraeten & Cluydts,2002),

while beta band decrease has been observed in paradigms that involved task-switching in a certain and predictable block, allowing the subject to predict and anticipate the switching. In these experiments, a sharp decrease in beta band has been observed anticipating the upcoming task switching (Cunillera et al.,2012, Gladwin et al,2006).

In the last few years, one of the main challenges in neuroscience has been reaching a good anatomical specificity, capable of precisely locate brain activity during task-switching paradigms. One of the first insightful results – thanks to the advance of technology and better mathematical models – has been achieved by Oh et al. in 2014. They assess the alpha-rhythm contribute in the right inferior parietal and left superior frontal regions, while found the beta oscillations in the right frontal and inferior parietal cortices. Both activities were modulated in magnitude by a task-switching paradigm between multiple sets of rules.

Along with a better signal source localization, in the last decade, a technological improvement on brain imaging systems (i.e. MEG) led the way to a more meaningful and precise frequency analysis of brain signals. Indeed, even frequency components that – due to the low amplitude – were thought to carry low information have been analyzed during the task-switching paradigm. For example, gamma band – which has always been considered too noisy to be significant and hard to handle by common EEG recordings – has been studied thanks to the temporal sensitivity reached by MEG. Since – in terms of cognitive processes – gamma-band proved to be very significant (Jensen et al.,2007; Wilson et al.,2016), a recent study conducted by Proskovec et al. (2019) linked gamma oscillations with task switching, showing an increase of gamma activity in CON and FPN related with the switching cost. Also, they showed a strict interaction and modulation between alpha and beta decreasing of activity within right prefrontal and inferior parietal cortices that led to an increase of gamma activity within the anterior cingulate and right temporoparietal regions during switch trials.

Basing on the task the subjects are asked to perform, alpha oscillations have been seen to be related to spatial attention as an inhibitory attentional mechanism. In 2006, Kelly et al. (2006) tried to demonstrate this hypothesis by performing a task that required ignoring a specific location. When it happened, subjects have shown an enhanced alpha amplitude involved in the suppression of distracting inputs. Expanding on the Kelly et al. findings, other studies linked lateralized changes in alpha amplitude with spatial attention and saw alpha to modulate attention (Sauseng et al., 2005; Thut et al.,2006; Bacigalupo & Luck, 2019) and even anticipating visual distractors, suppressing known distractor locations only when they were known in advance (Worden et al., 2000; Noonan et al.,2016). Recently, scientists questioned these assumptions due to the presumably weak reliability of the correlation between visual distractors and alpha amplitudes. Indeed, most of the studies that focused on attention modulation did not filter only alpha activity, and when they did, very little neuronal information about distractors was collected. Therefore, assuming a link between alpha oscillations and visual distractors suppression has eventually been considered likely

to be wrong or – at least – a long shot. With these premises, Antonov et al. (2020) – modifying Kelly et al. (2006) paradigm to record both alpha amplitudes and neuronal mechanisms during spatial attention – concluded that alpha band effects are too small and delayed to be related with an actual active suppression strategy. On the contrary, the alpha rhythm is thought to be a consequence of attentional selection rather than preceding it and therefore underlining a suppression mechanism.

More invasive studies have been carried out on monkeys to investigate the directionality of different frequency cortical pathways related to major cognitive activities. Recording data directly on the brain surface (ECoG), Bastos and colleagues (2015) tested a new hypothesis regarding the functions of beta rhythms in the visual cortex, by having monkeys perform tasks that involved both bottom-up and top-down processing. By using Granger causality analysis, they identified two different flows of information, coded in frequency, through the visual areas: gamma rhythm was seen to flow in a feedforward (bottom-up) direction, while beta rhythm proceeds top-down across the visual areas (see *Figure 2.2*).

Also, low and high gamma frequency – respectively about 30-70 Hz and 70-100 Hz – have been reported to carry information in separate channels in the hippocampal network (Colgin et al.,2009) (see *Figure 2.3*).

Furthermore, an enhanced gamma activity has been shown to indicate active working memory processes, whereas prefrontal beta oscillations encode and maintain quantitative information (Spitzer et al., 2014).

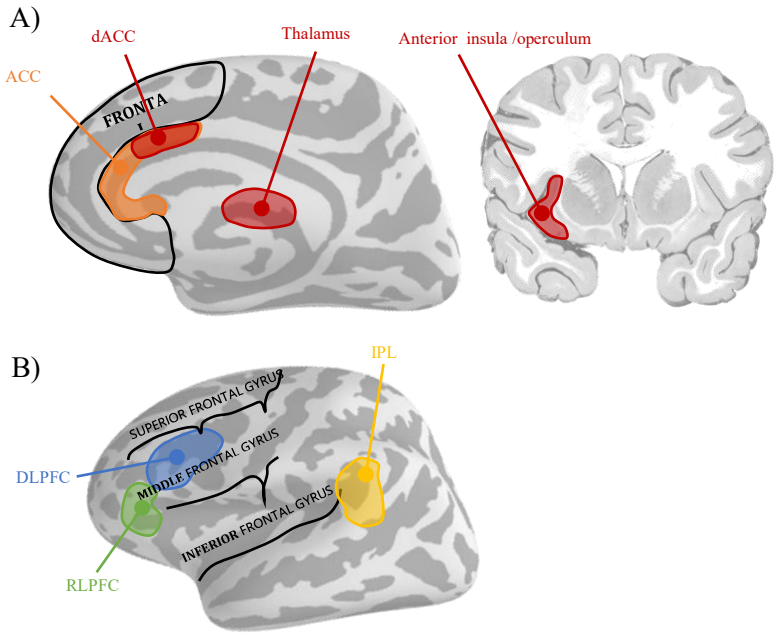

Figure 2.1. A) Cingulo-opercular network (CON) is composed of anterior insula/operculum, dorsal anterior cingulate cortex (dACC), and thalamus. B) Frontoparietal network (FPN), also known as central executive network, it is primarily composed of the rostral lateral and dorsolateral prefrontal cortex (RLPFC, DLPFC) and the anterior inferior parietal lobule (IPL).

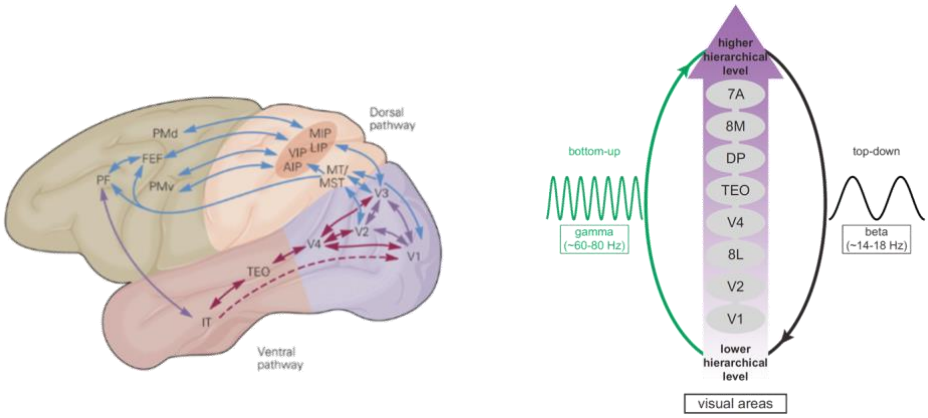

Figure 2.2. (Left) Visual brain pathway in a macaque monkey. (Right) Representation of the different directions and frequencies in the information flow through visual network. Gamma rhythm promotes feedforward processes (from lower to higher visual areas), while beta is related to feedback processes.

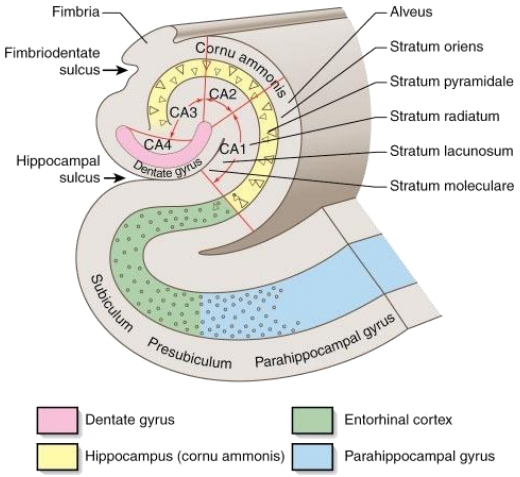

Figure 2.3 Schematic illustration of the main structures within the hippocampus. The hippocampal network is principally uni-directional, with the input from the Entorhinal Cortex (EC), flowing to the Dentate Gyrus (DG) and CA3 pyramidal neurons via the Perforant Path (PP) (Kesner et al., 2013).

References

Allport, A., Styles, E. A., Hsieh, S. Shifting intentional set: Exploring the dynamic control of tasks. *In C. Umiltà & M. Moscovitch (Eds.), Attention and performance 15: Conscious and nonconscious information processing. The MIT Press.* 421–452 (1994).

Antonov, P. A., Chakravarthi, R., Andersen, S. K. Too little, too late, and in the wrong place: Alpha band activity does not reflect an active mechanism of selective attention. *NeuroImage* 219, 117006 (2020).

Arbuthnott, K. Asymmetric switch costs and backward inhibition: Carryover activation and inhibition in switching between tasks of unequal difficulty. *Canadian Journal of Experimental Psychology* 62, 91–100 (2008).

Bacigalupo, F., Luck, S. J. Lateralized suppression of alpha-band EEG activity as a mechanism of target processing. *Journal of Neuroscience* 39, 900–917 (2019).

Bastos, A.M., et al. Visual Areas Exert Feedforward and Feedback Influences through Distinct Frequency Channels. *Neuron* 85, 2, 390–401 (2015).

Boksem, M. A. S. & Tops, M. Mental fatigue: Costs and benefits. *Brain Research Review* 59, 125–139 (2008).

Brass, M., Ullsperger, M., Knoesche, T. R., von Cramon, D. Y., Phillips, N. A. Who Comes First? The Role of the Prefrontal and Parietal Cortex in Cognitive Control. *Journal of Cognitive Neuroscience* 17, 1367–1375 (2005).

Braver, T.S., Reynolds, J.R., Donaldson, D.I. Neural mechanisms of transient and sustained cognitive control during task switching. *Neuron* 39, 713–726 (2003).

Bressler, L. S., Anil, K. S. Wiener–Granger Causality: A well established methodology. *NeuroImage* 58, 323–329 (2011).

Brody, C. D., Hernández, A., Zainos, A., and Romo, R. Timing and neural encoding of somatosensory parametric working memory in macaque prefrontal cortex. *Cerebral Cortex* 13, 1196–1207 (2003).

Campbell, J. I. D. Asymmetrical language switching costs in Chinese–English bilinguals' number naming and simple arithmetic. *Bilingualism: Language & Cognition* 8, 85–91 (2005).

Colgin, L. L., Denninger, T., Fyhn, M., Hafting, T., Bonnevie, T., Jensen, O., Moser, M. B. & Moser, E. I. Frequency of gamma oscillations routes flow of information in the hippocampus. *Nature* 462, 353–357.

Costa, A., & Santesteban, M. Lexical access in bilingual speech production: Evidence from language switching in highly proficient bilinguals and L2 learners. *Journal of Memory & Language* 50, 491–511 (2004).

Crone, E.A., Wendelken, C., Donohue, S.E., Bunge, S.A. Neural evidence for dissociable components of task-switching. *Cerebral Cortex* 16, 475–486 (2006).

Cunillera, T., et al. Brain oscillatory activity associated with task switching and feedback processing. *Cognitive, Affective, & Behavioral Neuroscience* 12, 16–33 (2012).

Derrfuss, J., Brass, M., Neumann, J., von Cramon, D. Y. Involvement of the inferior frontal junction in cognitive control: meta-analyses of switching and Stroop studies. *Human Brain Mapping* 25, 22–34 (2005).

Diamond, A. Executive functions. *Annual Review of Psychology* 64, 135–168 (2013).

Dosenbach, N. U., et al. A core system for the implementation of task sets. *Neuron* 50, 799–812 (2006).

Dosenbach, N. U., et al. Distinct brain networks for adaptive and stable task control in humans. *Proceedings of the National Academy of Sciences of the United States of America* 104, 11073–11078 (2007).

Dosenbach, N. U., Fair, D. A., Cohen, A. L., Schlaggar, B. L., Petersen, S. E. A dual-networks architecture of top-down control. *Trends in Cognitve Sciences* 12, 99–105 (2008).

Dove, A., Pollmann, S., Schubert, T., Wiggins, C. J., von Cramon, D. Y. Prefrontal cortex activation in task switching: an event-related fMRI study. *Brain Research. Cognitive Brain Research* 9, 103–109 (2000).

Foxe, J. J., Murphy, J. W., De Sanctis, P. Throwing out the rules: anticipatory alpha-band oscillatory attention mechanisms during task-set reconfigurations. *The European Journal of Neuroscience* 39, 1960–1972 (2014).

Funahashi, S. et al. Mnemonic coding of visual space in the monkey's dorsolateral prefrontal cortex. *Journal of Neurophysiology* 61, 331–349 (1989).

Gajewski, P. D., Kleinsorge, T. & Falkenstein, M. Electrophysiological correlates of residual switch costs. *Cortex* 46, 1138–1148 (2010).

Gladwin, T. E., Lindsen, J. P., de Jong, R. Pre-stimulus EEG effects related to response speed, task switching and upcoming response hand. *Biological Psychology* 72, 15–34 (2006).

Gurd, J. M., et al. Posterior parietal cortex is implicated in continuous switching between verbal fluency tasks: an fMRI study with clinical implications. *Brain* 125, 1024–1038 (2002).

Hübner, M., Dreisbach, G., Haider, H., & Kluwe, R. H. Backward inhibition as a means of sequential task-set control: Evidence for reduction of task competition. *Journal of Experimental Psychology: Learning, Memory, & Cognition* 29, 289–297 (2003).

Jensen, O., Kaiser, J., Lachaux, J. P. Human gamma-frequency oscillations associated with attention and memory. *Trends in Neurosciences* 30, 317–324 (2007).

Kelly, S. P., Lalor, E. C., Reill, R. B., Foxe, J. Increases in alpha oscillatory power reflect an active retinotopic mechanism for distracter suppression during sustained visuospatial attention. *Journal of Neurophysiology* 95, 3844–3851 (2006).

Kesner, R., Neurobiological foundations of an attribute model of memory. *Comparative Cognition & Behavior Reviews* 8, 29–59 (2013).

Knight, R. T. Neural networks debunk phrenology. Science 316, 1578-1579 (2007).

Koch, I., Prinz, W., & Allport, A. Involuntary retrieval in alphabet-arithmetic tasks: Task-mixing and task-switching costs. *Psychological Research* 69, 252–261 (2005).

Kurzban, R., Duckworth, A., Kable, J. W. & Myers, J. An opportunity cost model of subjective effort and task performance. *Behavioral and Brain Sciences* 36, 661–679 (2013).

Mayr, U., & Keele, S. W. Changing internal constraints on action: The role of backward inhibition. *Journal of Experimental Psychology: General* 129, 4–26 (2000).

Meiran, N., Chorev, Z., Sapir, A. Component processes in task switching. *Cognitive Psychology* 41, 211–253 (2000).

Milan, E. G., Sanabria, D., Tornay, F., González A. A more complete task-set reconfiguration in random than in predictable task switch. *Acta psicologica* 118, 319–331 (2005).

Miller, E. K., & Cohen, J. D. An integrative theory of prefrontal cortex function. *Annual Review of Neuroscience* 24, 167–202 (2001).

Milner, B. Effects of different brain lesions on card sorting. *Archives of Neurology* 9, 90–100 (1963).

Monsell, S. Control of mental processes. *In V. Bruce (Ed.), Unsolved mysteries of the mind: Tutorial essays in cognition. Hove, U.K.: Erlbaum, Taylor & Francis,* 93–148 (1996).

Monsell, S., Yeung, N., Azuma, R. Reconfiguration of task-set: Is it easier to switch to the weaker task? *Psychological Research* 63, 250–264 (2000).

Murphy, J. W., Foxe, J. J., Molholm, S. Neuro-oscillatory mechanisms of intersensory selective attention and task switching in school-aged children, adolescents and young adults. *Developmental Science* 19, 469–487 (2016).

Noonan, M. P., Adamian, N., Pike, A., Printzlau, F., Crittenen, B. M., Stokes, M. G. Distinct mechanisms for distractor suppression and target facilitation. *Journal of Neuroscience* 36, 1797–1807 (2016).

Oh, A., Vidal, J., Taylor, M. J., Pang, E. W. Neuromagnetic correlates of intra- and extra-dimensional set-shifting. *Brain* 86, 90–97 (2014).

Owen, A. M., Roberts, A. C., Hodges, J. R., Summers, B. A., Polkey, C. E., & Robbins, T. W. Contrasting mechanisms of impaired attentional set-shifting in patients with frontal lobe damage or Parkinson's disease. *Brain* 116, 1159–1175 (1993).

Petrides, M. and Pandya, D. N. Comparative architectonic analysis of the human and the macaque frontal cortex. *Handbook of Neuropsychology* 9, 17–58 (1994).

Petruo, V.A., Mückschel, M. & Beste, C. On the role of the prefrontal cortex in fatigue effects on cognitive flexibility - a system neurophysiological approach. *Scientific Reports* 8, 6395 (2018).

Philipp, A. M., Gade, M., Koch, I. Inhibitory processes in language switching? Evidence from switching language-defined response sets. *The European Journal of Cognitive Psychology* 19, 395–416 (2007).

Poline, J. B., Worsley, K. J., Holmes, A. P., Frackowiak, R. S., Friston, K. J. Estimating smoothness in statistical parametric maps: variability of p values. *Journal of Computer Assisted Tomography* 19, 788–796 (1995).

Proskovec, A. L., Wiesman, A. I., Wilson, T. W. The strength of alpha and gamma oscillations predicts behavioral switch costs. *NeuroImage* 188, 274–281 (2019).

Pucak, M. L. et al. Patterns of intrinsic and associational circuitry in monkey prefrontal cortex. *The Journal of Comparative Neurology* 376, 614–630 (1996).

Rao, S. R. et al. Integration of what and where in the primate prefrontal cortex. *Science* 276, 821–824 (1997).

Rapela, J., Gramann, K., Westerfield, M., Townsend, J., Makeig, S. Brain oscillations in switching vs. focusing audio-visual attention. *Conference: Engineering in Medicine and Biology Society (IEEE)*, 352–355 (2012).

Rogers, R. D., & Monsell, S. Costs of a predictable switch between simple cognitive tasks. *Journal of Experimental Psychology: General* 124, 207–231 (1995).

Rushworth, M. F., Hadland, K. A., Paus, T., Sipila, P. K. Role of the human medial frontal cortex in task switching: a combined fMRI and TMS study. *Journal of Neurophysiology* 87, 2577–2592 (2002).

Sadaghiani, S., D'Esposito, M. Functional characterization of the cingulo-opercular network in the maintenance of tonic alertness, *Cerebral Cortex* 25, 2763–2773 (2015).

Sauseng, P., Klimesch, W., Stadler, W., Schabus, M., Doppelmayr, M., Hanslmayr, S., et al. A shift of visual spatial attention is selectively associated with human EEG alpha activity. *The European Journal of Neuroscience* 22, 2917–2926 (2005).

Sauseng, P., et al. Relevance of EEG alpha and theta oscillations during task switching. *Experimental Brain Research* 170, 295–301 (2006).

Sheffield, J. M., et al. Fronto-parietal and cingulo-opercular network integrity and cognition in health and schizophrenia. *Neuropsychologia* 73, 82–93 (2015).

Sohn, M. H., Ursu, S., Anderson, J. R., Stenger, V. A., Carter, C. S. The role of prefrontal cortex and posterior parietal cortex in task switching. *Proceedings of the National Academy of Sciences of the United States of America* 97, 13448–13453 (2000).

Spitzer, B., Gloel, M., Schmidt, T. T., and Blankenburg, F. Working memory coding of analog stimulus properties in the human prefrontal cortex. *Cerebral Cortex* 24, 2229–2236 (2014).

Sun, Y., Lim, J., Kwok, K., & Bezerianos, A. Functional cortical connectivity analysis of mental fatigue unmasks hemispheric asymmetry and changes in small-world networks. *Brain and Cognition* 85, 220–230 (2014).

Sun, Y et. al. The effects of a mid-task break on the brain connectome in healthy participants: A resting-state functional MRI study. *NeuroImage* 152, 19–30 (2017).

Thut, G., Nietzel, A., Brandt, S.A., Pascual-Leone, A. α-Band electroencephalographic activity over occipital cortex indexes visuospatial attention bias and predicts visual target detection. *Journal of Neuroscience* 26, 9494–9502 (2006).

Tomita, H., Ohbayashi, M., Nakahara, K., Hasegawa, I., & Mijashita, Y. Top-down signals from prefrontal cortex in executive control of memory. *Nature* 401, 699–703 (1999).

Verstraeten, E., Cluydts, R. Attentional switching-related human EEG alpha oscillations. *Neuroreport* 13, 681–684 (2002).

Verweij, I. M., et al. Sleep deprivation leads to a loss of functional connectivity in frontal brain regions. *BMC Neuroscience* 15, 88 (2014).

Wilson, T. W., Heinrichs-Graham, E., Proskovec, A. L., McDermott, T. J. Neuroimaging with magnetoencephalography: a dynamic view of brain pathophysiology. *Translational Research* 175, 17–36 (2016).

Wolff, N., Roessner, V. & Beste, C. Behavioral and neurophysiological evidence for increased cognitive flexibility in late childhood. *Scientific Reports* 6, 28954 (2016).

Worden, M.S., Foxe, J.J., Wang, N., Simpson, G.V. Anticipatory biasing of visuospatial attention indexed by retinotopically specific alpha-band electroencephalography increases over occipital cortex. *Journal of Neuroscience* 20, RC63 (2000).

Wu, S., et al. The neural dynamic mechanisms of asymmetric switch costs in a combined Stroop-task-switching paradigm. *Scientific Reports* 5, 10240 (2015).

Yeung, N., & Monsell, S. Switching between tasks of un-equal familiarity: The role of stimulus-attribute and response-set se-lection. *Journal of Experimental Psychology: Human Perception & Performance* 29, 455–469 (2003).

Yeung, N., Nystrom, L. E., Aronson, J. A., Cohen, J. D. Between-task competition and cognitive control in task switching. *Journal of Neuroscience* 26, 1429–1438 (2006).

Chapter 3

EXPERIMENTAL PROCEDURE AND METHODS

In this chapter, I am going to describe in detail all the aspects concerning the experimental procedure, starting from the subjects involved in this research, moving to the description of the experimental paradigm, and finally focusing on the data acquisition with MEG and MRI.

Contents

3.1 RESEARCH PARTICIPANTS

3.1.1 Subjects

Five healthy volunteers (mean age: 24 years, SD: 2.67, range: 22-29; 3 of them female) participated in this study. Subjects were recruited from the Boston University community, and they were students or postdoctoral researchers. Exclusion criteria included any medical illness affecting central nervous system functions, neurological or psychiatric disorders, history of head trauma, current substance abuse, and ferromagnetic implants. None of the subjects were excluded from the study and all of them were naïve as to the purpose of the study. Also, they reported to be right-handed as confirmed by the Edinburgh Inventory of handedness (Oldfield, 1971) and had normal or corrected-to-normal vision.

Four subjects underwent two different sessions of the experiment (about one week apart from one another), maintaining the same experimental procedure. From now on in the dissertation, we will refer to 'N_01' and 'N_01b' respectively for the first and the second session of the first subject, and this logic is maintained for all subjects.

After providing a complete description of the experiment and the measurements we were going to record, they underwent a quick training session aimed to shun differences between volunteers. The training consisted of performing the experiment until the subject became confident with the paradigm. It took around 1-2 minutes per subject.

Written informed consent was obtained from all participants in accordance with the Declaration of Helsinki (World Medical Association, 2013), and all the procedures were approved by the local Ethics Committee of Human Resources at Boston University and "Athinoula A. Martinos Center for Biomedical Imaging" at Massachusetts General Hospital (MGH).

3.2 EXPERIMENTAL PROCEDURE

3.2.1 Stimuli

The stimuli presented to the subjects consisted of a cue and an imperative stimulus. The cue was a 1000 ms random-dot kinematogram (RDK) within a circular aperture of 15 degrees of visual angle as outer diameter. RDK was either an expansion or contraction dot motion. Dots had the following characteristics: density = 2 dots/(degree^2), speed = 3 deg/s, diameter = 4 mm, and 90%

of radial motion coherence. An example of RDK with different coherence can be seen in *Figure 3.1*.

When the cue was an expansion RDK, subjects were instructed to perform the number task in the forthcoming imperative stimulus; vice versa, when the cue was a contraction RDK, they performed the letter task. Cues changed pseudo-randomly across trials, but the number of different trials was equalized within each experimental block (see *Figure 3.2*).

The imperative stimulus (800 ms duration) was a pair of two letters and two numbers (white, 80-point, Times New Roman, 150 m/cd^2 luminance) displayed on a grey background (Red=NaN, Green=NaN, Blue=NaN, Grey=247.373). Letters and numbers were presented on opposite sides of a screen-centered fixation cross. The side of letters and numbers, with respect to the fixation cross, randomly changed across trials.

Moreover, between the cue and the imperative stimulus, a cue-target interval (CTI) was presented. The CTI varied randomly between 300 ms, 800 ms, and 1300 ms. Along with the dissertation, the CTI period is often referred to as the 'delay' or 'delay period'.

In the imperative stimulus, letters and numbers were randomly drawn from a set containing [C, N, V, S] as consonants, [A, E, O, U] as vowels, [2, 4, 6, 8] as even numbers and [1, 3, 5, 7] as odd numbers.

After the imperative stimulus, a blank period – similar to the CTI – was displayed for 1700 ms. In this period, the screen had a grey background (Red=NaN, Green=NaN, Blue=NaN, Grey=247.373) with a centered white fixation cross.

Subjects were asked to respond to the task during the imperative stimulus or the following blank period. If they didn't answer on time, the trial was considered "out of time" and therefore excluded in the data analysis. *Figure 3.3* shows a schematic representation of the experiment stimuli just described.

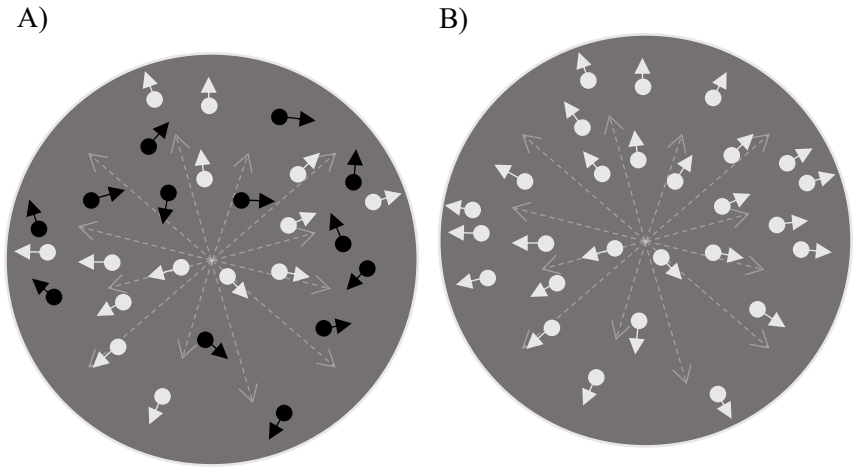

Figure 3.1. Radial random-dot kinematogram (RDK) with different coherences. A) RDK with 50% of coherence. B) RDK with 100% of coherence.

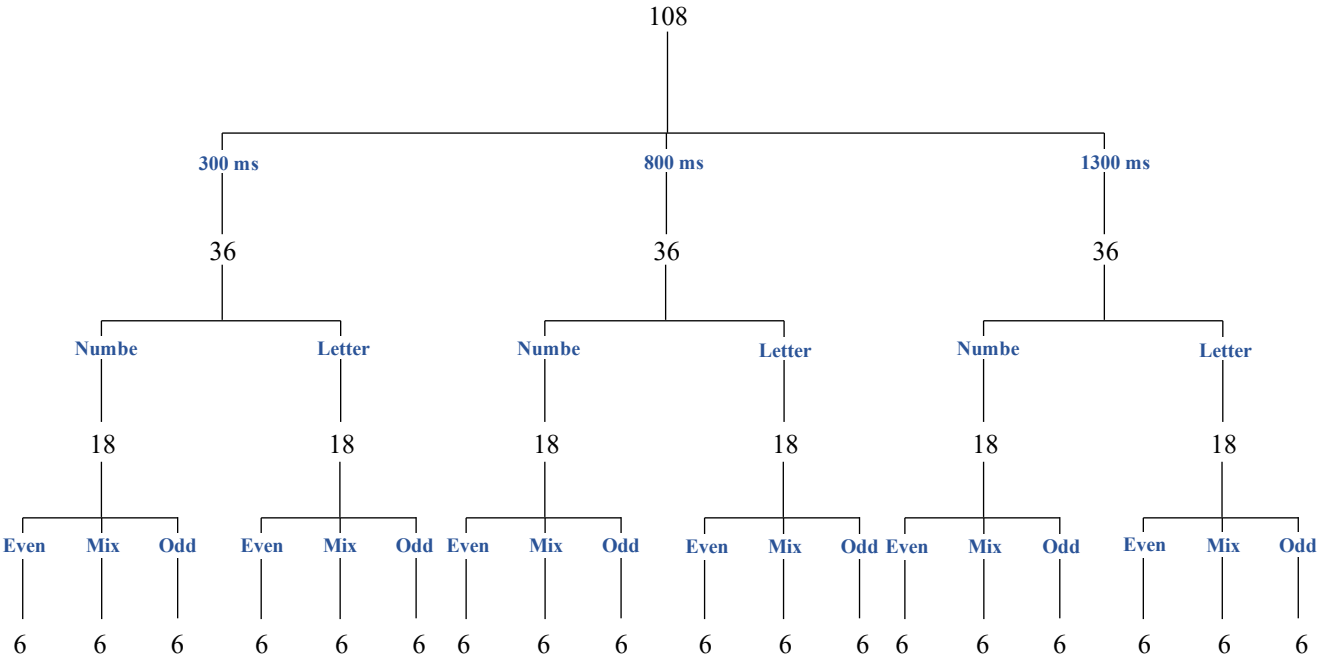

Figure 3.2. Schematic representation of one experimental block (108 trials).

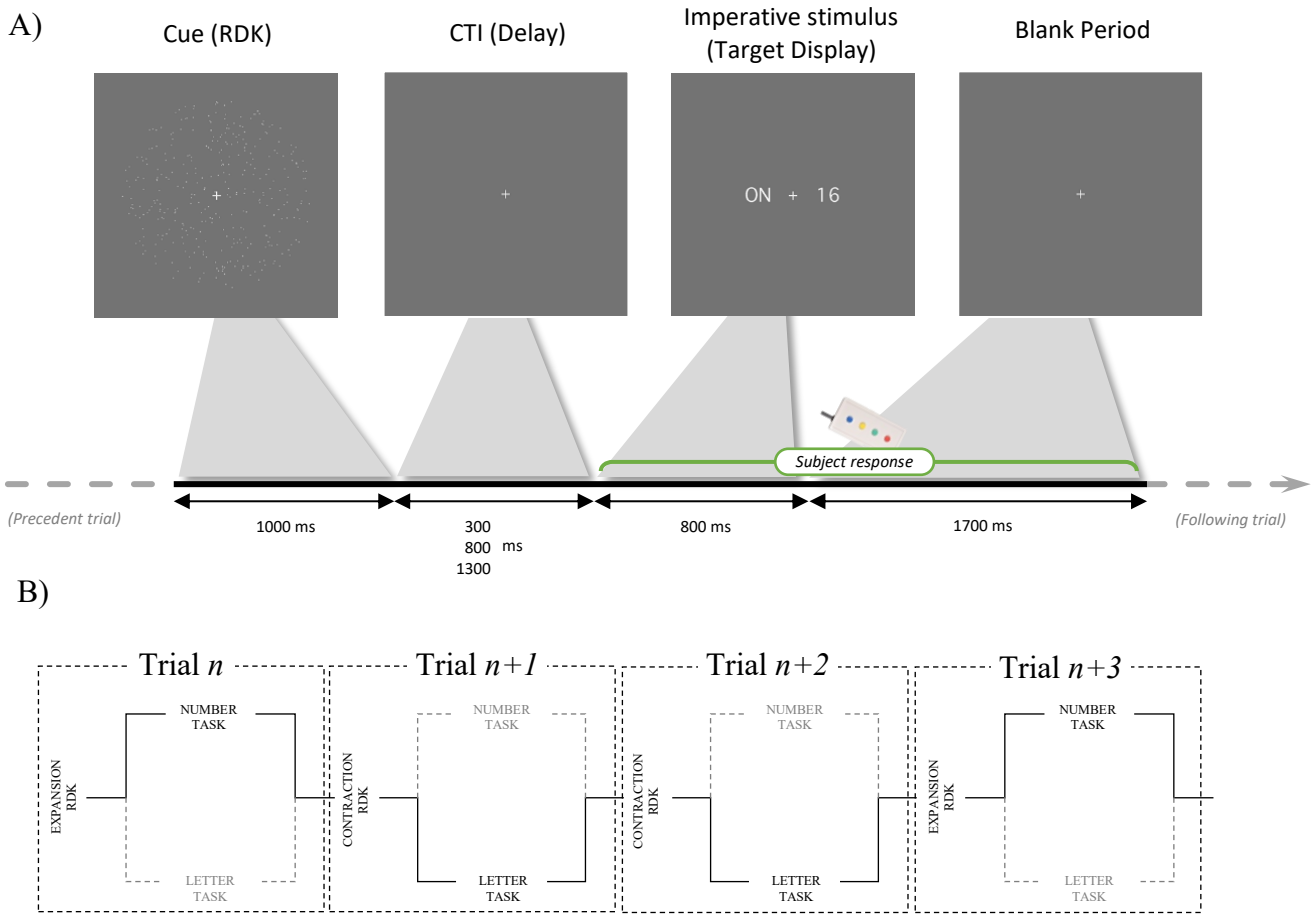

Figure 3.3. A) Depiction of the events' sequence during one trial. B) Example of 4 subsequent cued trials.

3.2.2 Experimental paradigm

Subjects were asked to perform the experiment in 3 blocks, and each of them contained 108 cued trials. The target to attend – which could be either 'number' or 'letter' – was not *a priori* known by the subject, therefore participants were forced to remember the rule associated with the cue but not a specific pattern between trials' targets.

If the subjects were cued to perform a letter task (with a contraction RDK), they had to categorize the pair of letters displayed on the screen according to whether they were both consonants, both vowels, or one of each. Using a fiber-optic response device provided in the MEG room, participants had to press the first button if the letters were both consonants, the second one if they were both vowels, and the third otherwise.

On the contrary, if the cue was an expansion RDK motion, subjects had to perform the 'number task' and therefore press the first button if the numbers were both odd, the second one if they were both even, and the third otherwise.

Between the end of the cue and the imperative stimulus, subjects were forced to withhold the response for a delay period not known in advance. As previously mentioned, it could be either 300 ms, 800 ms, or 1300 ms, and it is a key point in the experimental paradigm for further analysis. Participants were asked to maintain central fixation throughout all the 108 trials and to take short breaks between the blocks to prevent fatigue and concentration lapses.

3.3 RECORDINGS AND DATA ACQUISITION

3.3.1 MEG Data Acquisition

The MEG data were acquired at Athinoula A. Martinos Center for Biomedical Imaging, Massachusetts General Hospital. The acquisition system was housed in a three-layers magnetically-shielded, sound attenuated, and dimly lit room (Imedco AG, Switzerland), and participants were seated in a non-magnetic chair performing the task-switching experiment described in the previous paragraphs. They were sat in the upright position at a distance of 138 cm from a 44" back-projection screen, and the stimuli were projected through an aperture in the MEG chamber using a Panasonic LP350 DLP with a resolution of 1024x768 pixels and a 75 Hz refresh rate.

Data were recorded with a 306-channel Neuromag Vectorview whole-head system (Elekta-Neuromag, Finland), comprising 102 pairs of planar gradiometers and 102 magnetometers.
Also, on the day of MEG scanning, a two-minutes empty room recording was acquired for computing the noise covariance matrix of the sensors. To avoid any electromagnetic influences, participants were asked to not place their heads under the dewar during these recordings.
MEG sessions were aligned to a common head position through the Maxfilter software, Maxmove. Sensor data was spatially filtered via simulated head translation and rotation to represent signal measurements onto the realigned space.
To measure the participants' head position inside the MEG, five head-position indicator (HPI) coils were fixed on the scalp. Then, participants' head shape and the HPI coil locations were digitized with a 3D Fastrak digitizer (Polhemus Inc., Colchester, VT) integrated with the VectorView system. HPI coil locations were used to localize the head position and orientation with respect to the sensors at the beginning of each trial.
To align the coordinate systems between MEG recordings and MRI scans, at least 80 points have been sampled on the scalp during subjects' preparation. Also, before entering the MEG room, participants were asked to change their clothes and wore a standard surgical gown.

3.3.2 MRI Data Acquisition

A high resolution T1-weighted Magnetic Resonance Imaging (MRI) was acquired on a 3-T MRI scanner (Siemens-Trio, Erlagen, Gernamy) with an 8-channel phase array head coil.
MRI recordings were acquired with the following parameters: distance factor = 50%, slices per slab = 128, FOV = 256 mm, FOV phase = 100 degrees, slice thickness = 1.33 mm, TR = 2530 ms, TE = 3.39 ms. Then, Freesurfer software was used for cortical reconstruction and volumetric segmentation of the T1 weighted whole brain images for each volunteer. The individual brain scans were motion corrected, spatially co-registered by morphing into the Freesurfer average brin through spherical surface mapping and spatially smoothed with a 5mm FWHM (full width at half maximum) kernel.

References

Oldfield R.C. The assessment and analysis of handedness: The Edinburgh inventory. *Neuropsychologia* 9, 97–113 (1971).

World Medical Association. World medical association declaration of Helsinki: ethical principles for medical research involving human subjects. *JAMA* 310, 2191–2194 (2013).

Chapter 4

DATA ANALYSIS

Contents

4.1 PREPROCESSING

After the MEG and MRI recordings – as described in Chapter 3 – Dr. Ahlfors Seppo (Associate professor at Harvard Medical School, Massachusetts General Hospital) and its colleagues firstly preprocessed the data by identifying EOG and ECG artifacts, removing 60 Hz line noise, and creating an event file from the one produced by the MEG trigger.

Specifically, Dr. Seppo & colleagues created EOG signal space projectors (see paragraph 4.1.2) related with eye blinks choosing the data from -500 ms to +500 ms with respect to the peak of each blink artefact and selecting the principal component of these data as SSP. Then, they removed line noise with a notch filtering centered around 60 Hz and its harmonics, and finally they read the event file produced by the MEG trigger, which was steer by the Matlab experimental script. Indeed, while the experiment was running, at each trial it was sending coded signals to the MEG trigger in order to timing each event inside the trial. Thus, when the cue started a 'code = 1 'signal was sent to the MEG trigger, and the same for the start of CTI (code = 2) and the start of imperative stimulus (code = 4). At the end of the experiment, a file containing all trials timing was written.

A representation of the files produced during the processing and used afterward for the analyses is shown in *Figure 4.1*.

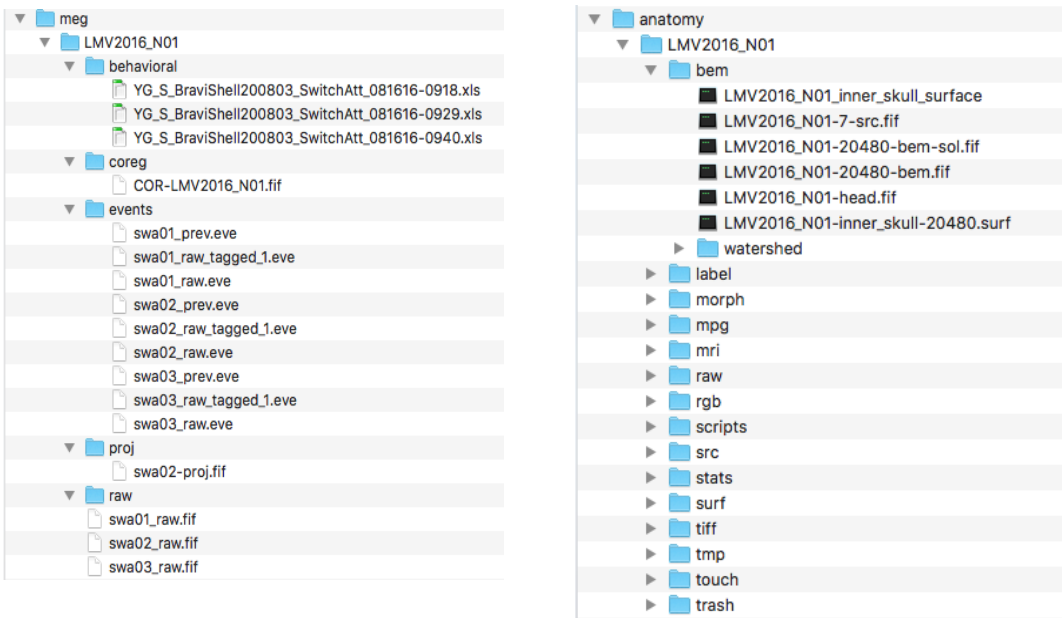

Figure 4.1. (Left) MEG directory of the first subject 'N01'. Behavioral folder contains the results of the three session's experimental blocks. Coreg folder contains the coregistration (transformation file) in order to align MRI and MEG coordinate systems. Events folder contains all the events and their timing, retrieved from the trigger file. Proj and Raw folders contain respectively the EOG projectors and the MEG data preprocessed by Dr. Seppo. (Right) Anatomy directory of the first subject 'N01'. Most of the data, except the bem solutions, have been obtained from Freesurfer software and are standard MRI data.

4.1.1 Data pre-inspection

As one of the first steps in order to understand the quality and organization of data, a data inspection is fundamental. Therefore, the first step I did was to represent raw data, observe their characteristics, and then apply SSPs to project out the EOG artifacts.

Also, a frequency-domain check has been held to verify the line noise removal and cut the signal between the frequencies we were interested in (~ 0.1 Hz – 110 Hz).

For instance, looking closely at the MEG raw data for the first block of the first subject 'N01', we can draw some considerations. In *Figure 4.2*, in fact, we can notice that in the power spectral density of the data, the line noise has been correctly removed. Furthermore, comparing the independent component analysis (ICA) of the signals before and after applying the SSPs (*Figure 4.*3 and *Figure 4.4*), we can observe the EOG-related artifacts as the first component ('ICA000 ' in *Figure 4.3*).

After applying the preprocessing, both ECG and EOG artifacts have been projected out and the signal appears cleaner. An example of 5 sensors 'MEG recordings before and after the preprocessing is shown in *Figure 4.5*.

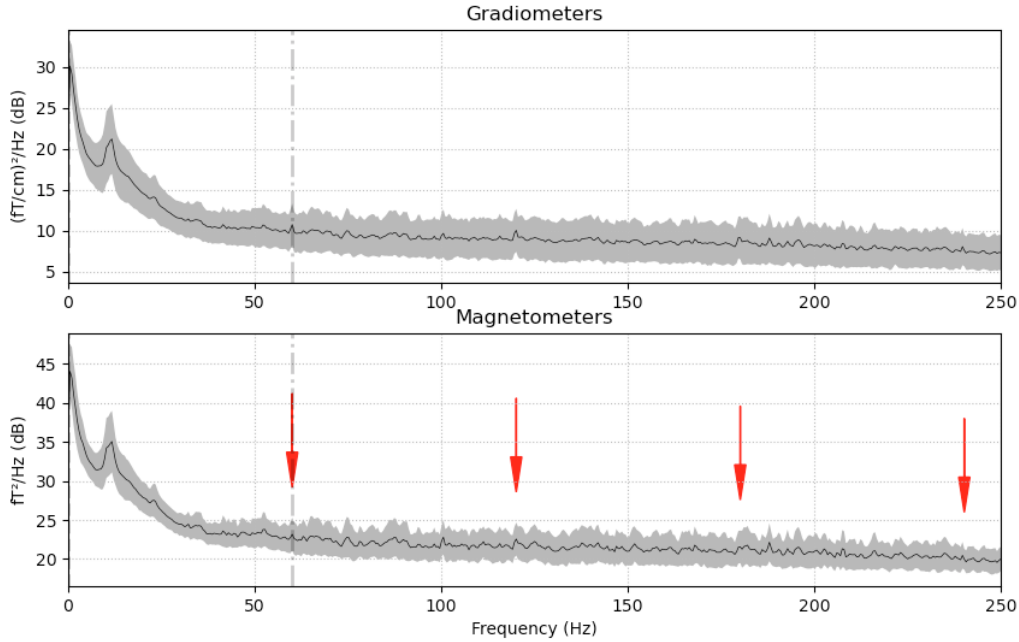

Figure 4.2. Example of power spectral density (PSD) computed on one of the first subject's signals (see in Figure 1 'swa01_raw.fif'). Red arrows are centered in 60 Hz line noise and its harmonics.

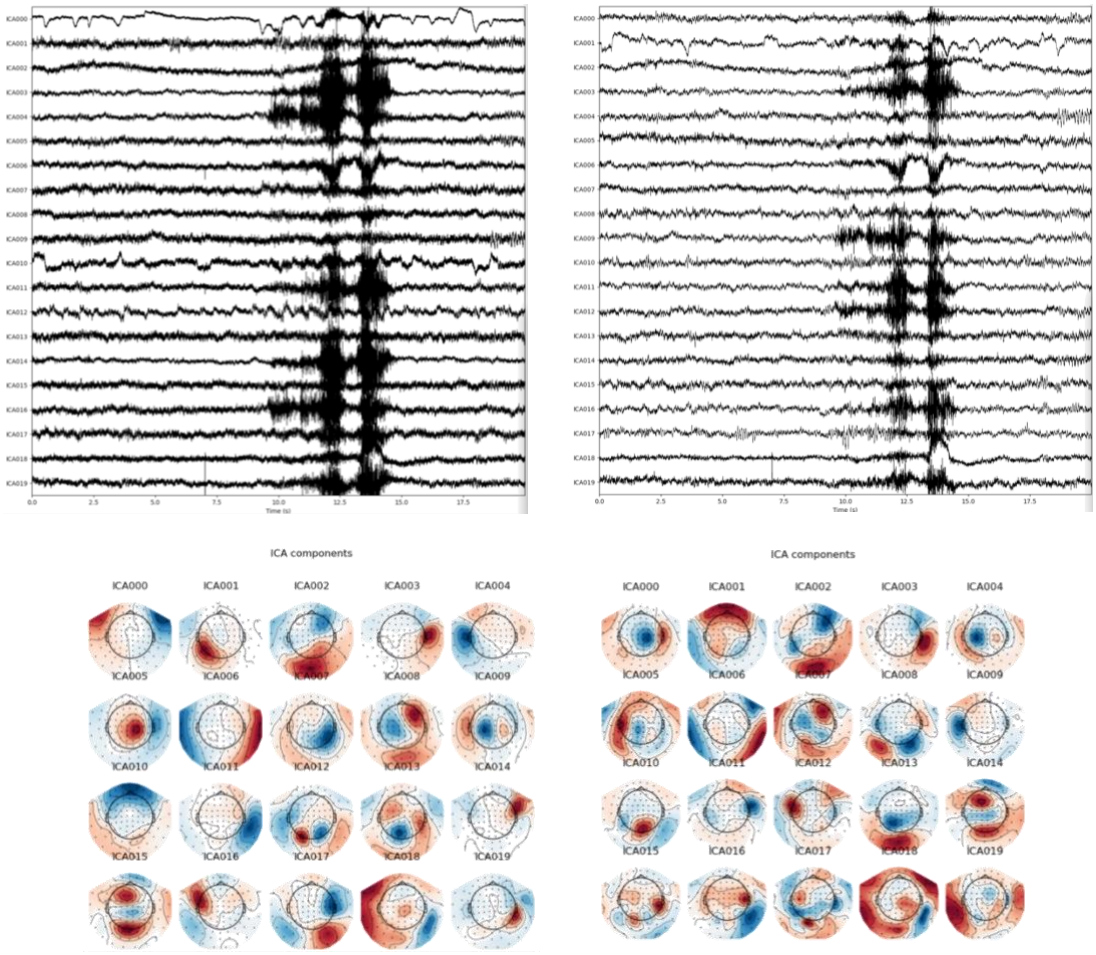

Figure 4.3. Independent component analysis (ICA) applied on the subject 'N01'. An ICA before the preprocessing and artifacts removal has been performed on the left, while on the right the same analysis has been held after projecting out EOG and ECG-related components. At the bottom, the 20 ICA components are shown on the brain as an average over time, and at the top the same components are shown as signals over a 20 second window.

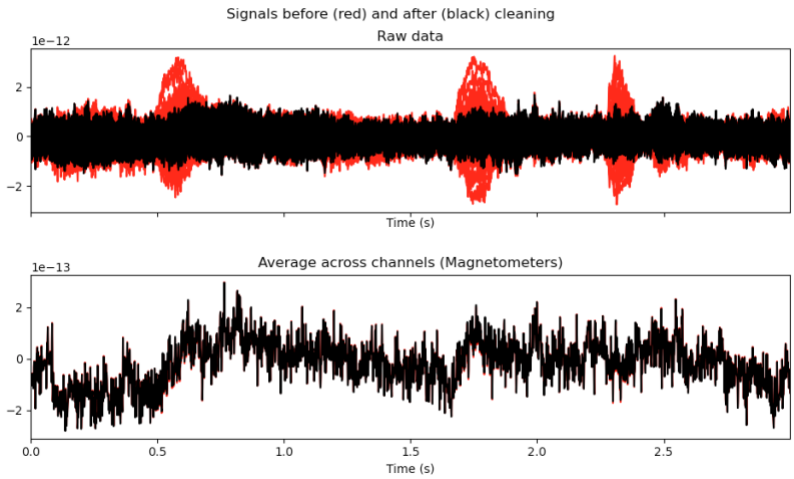

Figure 4.4. MEG signals before and after preprocessing. In the first plot, red and black lines represent the signal before and after artifacts removal.

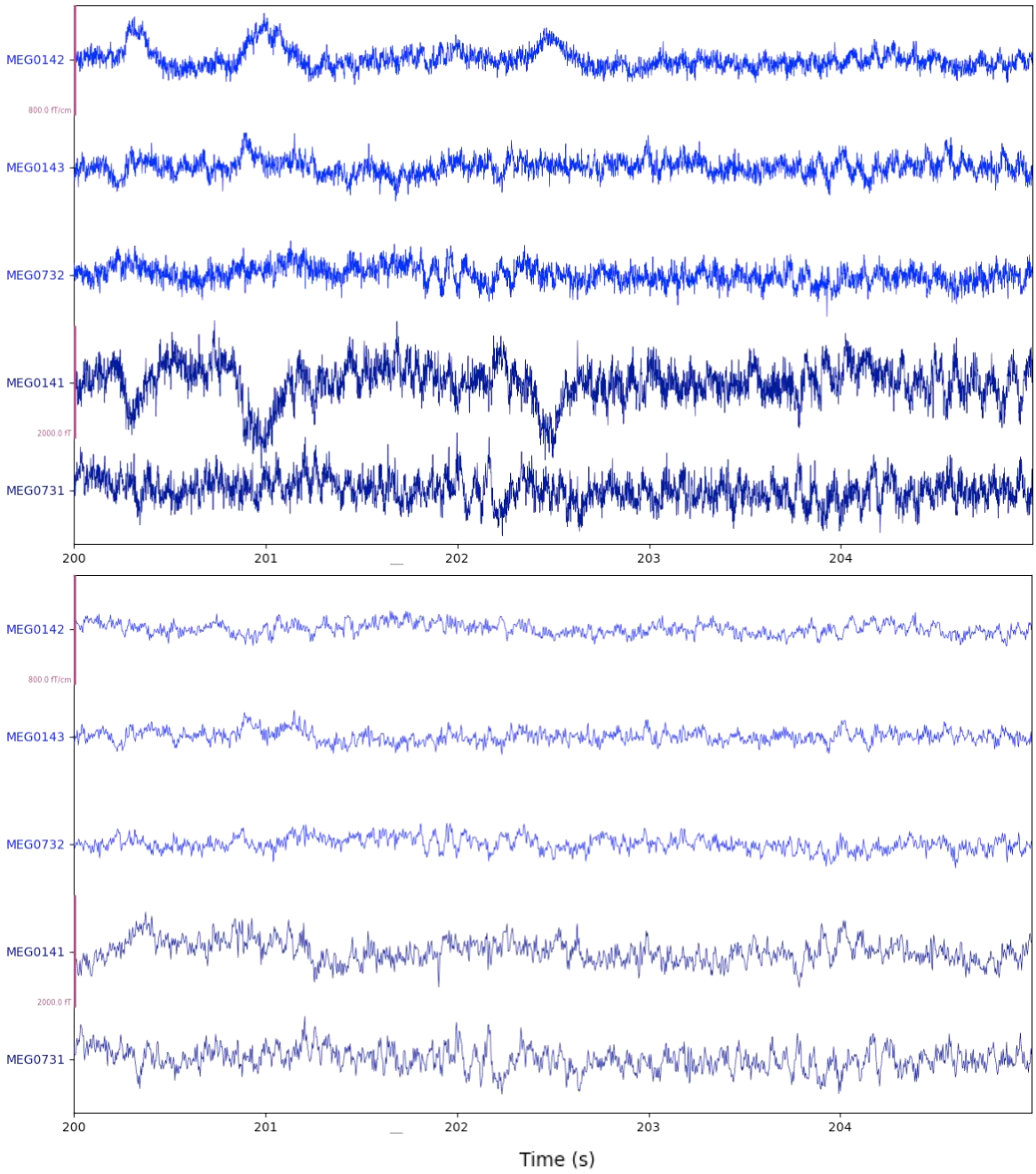

Figure 4.5. Example of 5 MEG channels before (top) and after (bottom) preprocessing. In particular, MEG0142 and MEG0143 are gradiometers placed in proximity of the left temporal lobe and MEG0732 is a gradiometer placed next to the central primary somatosensory area (BA3). MEG0141 and MEG0731 are magnetometers sensing areas respectively around left temporal lobe and central primary somatosensory area.

4.1.2 Filtering and signal space projections

Preprocessing pipeline principally involves filtering and projecting the signal in order to increase signal-noise ratio (SNR). As we already mentioned, noises can be both electromagnetic and biologically related, therefore different considerations about frequencies and characteristic shapes must be kept in mind.

Nowadays, filtering is quite always addressed by implementing digital filters using calculators, and a lot of Python libraries implement filter functions. In this project, MNE-Python filter has been used, calling the function mne.io.Raw.filter() and indicating the cutoff frequencies, the transition band for both low and high cutoff frequencies, the length of the FIR filter, the phase of the FIR filter and the window associated.

For the further analyses, I have used a filter with different cutoff frequencies but, since the signal to be processed was the same, the other parameters didn't vary. Low and high transition bandwidth was set to 'auto', which used respectively a multiple of low and high cutoff frequency, selecting the result of the following expression: min(max(cutoff_freq * 0.25, 2), cutoff_freq). To obtain the best result, all other parameters but the window were set to 'auto 'because the mne library has been developed focusing principally on MEG signals. The filter window chosen was the Hanning, which was tested to return good results.

Regarding Signal-Space Projections (SSPs), computing them as one of the first preprocessing steps is the most common approach for MEG signals. SSP aim to reject external disturbances, but unlike many other noise-cancellation approaches, it does not require external reference sensors to record disturbance fields. It is based on the idea that the signal can always be decomposed into 2 components, one related to the signal $b_s(t)$ and another one to the noise $b_n(t)$:

$$b(t) = b_s(t) + b_n(t)$$

Also, the noise $b_n(t)$ should be characterized by a well-known pattern that constitutes an orthonormal basis $b_1 \dots b_m$ and its angle with the signal vector $b_s(t)$ as close as possible to p/2. If these requirements are satisfied, then we can calculate a specific operator called signal-space projection operator $P_\perp$ so that:

$$P_\perp b_n(t) \approx 0,$$

and therefore

$$b_s(t) \approx P_\perp b(t).$$

MNE-Python provides functions to compute the SSP operator and then apply it to remove artifacts. In this dissertation, from the preprocessed data received from Dr. Seppo, the SSP related with eye movements and blinks have already been implemented and I just needed to apply it with the proper Python commands. First, I had to add the projections to the Raw object (containing the signal to be processed) writing raw.info['projs'] =+ projs_eog, where raw.info is the object's attribute and

projs_eog is the available EOG projectors, previously calculated by Dr. Seppo. Then, the artifaxts can be projected out by applying the SSP with the following instruction: mne.io.Raw.apply_proj(). However, ECG artifacts – even though we observed in the pre-inspection paragraph that they are not visible – are still needed to be removed. Hence, instead of reading the projectors, I applied the function compute_proj_ecg() and obtained both projector operators and ecg events as output. The function follows different steps: filter ECG data channel, find ECG R wave peaks, filter raw data, create epochs around R peaks and finally calculate SSP vectors around that data to capture the artifacts. Also, it will calculate one SSP operator per MEG sensor, which will result in 3 different operators (1 gradiometer and 2 planar magnetometers).
Projectors can be applied at any stage of the pipeline to the raw signal, but when it is divided in epochs the projectors are applied by default the they are present in the signal's 'info 'attribute.
We will talk more about the epoch stage in the following paragraph.

4.1.3 Epoching

In this paragraph, the process to isolate trials from the continuous signal will be examined. To represent and analyze equal-duration chunks, the MEG signal must be divided in epochs and that has been achieved by implementing a Python script. Epochs objects are data structures in which every event – indicated in the 'event 'file described in the previous paragraphs – allows to select a certain time window to cut the continuous signal with. Therefore, the main function to call is `mne.Epochs()`, after defining some useful parameters. Other than the signal itself and the event file, the Epochs() function requires the time before and after the event 'tmin 'and 'tmax', a dictionary listing all the possible types of events (in this case they were divided by delay length) called 'event_id', the baseline to consider when applying baseline correction (calculate baseline mean signal and subtract it to the entire epoch), and the criteria to satisfy in order to reject the epoch. These criteria are saved in a dictionary, are applied to every channel (gradiometer, magnetometer, eeg, eog, etc.), and if at least one of the channels exceeds the threshold the epoch will be rejected.
An example of division in epochs is shown in *Figure 4.6*.
Once the data are divided in epochs, we can separate the epochs basing on the delay length, task type, etc. and represent them in separate plots.

```
tmin, tmax = (-0.2, 3.5)  # from 200 ms before to 3500 ms after the event
event_dict = {'300': 300, '800': 800, '1300': 1300}
reject_criteria = dict(mag=3000e-15,  # 3000 fT
                       grad=3000e-13)  # 3000 fT/cm
baseline = (None, 0)  # baseline period from start of epoch (-200 ms) to time=0
events = mne.read_events(event_file)
epochs = mne.Epochs(raw_signal, events, event_dict, tmin, tmax, proj=True,
                    baseline=baseline, reject=reject_criteria, preload=True)
epochs.resample(330.)  # resampling to save memory
```

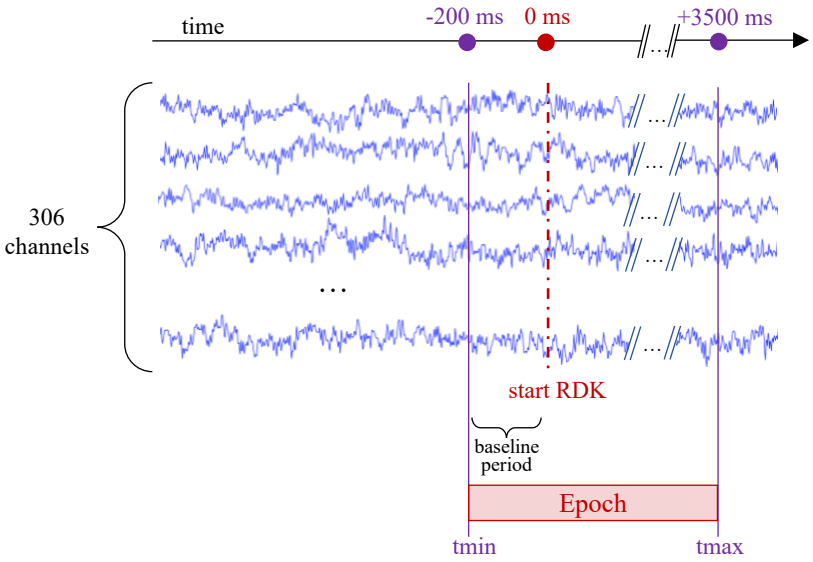

Figure 4.6. Example of Python code to create Epoch object.

4.2 BEHAVIORAL ANALYSIS

4.2.1 Reaction time and accuracy

Behavioral analysis of data is one of the first that are usually made in order to describe how subjects performed in terms of accuracy on a certain task. Once the procedure is described and the subjects are asked to undergo the experiment, it is important for the success of the current and further session to know whether the task was too hard for the subject – and therefore results are complex and confused – or too easy, which led to an unreliable and weak result. Hence, verifying the balance between correct and incorrect subjects' responses is fundamental to obtain meaningful results and maintain subjects' focus to the edge.

During data recording, a first accuracy inspection is made in real time from the output file generated by the experiment script, but afterwards a more complete and precise analysis is carried on the whole experimental data. Since it is a linear quantity, accuracy is computed by simply

counting the ratio between wrong trials and correct ones for each subject, express it in percentage, and then averaging all the results through the subjects. In *Figure 4.7* is shown the accuracy for every block of the experiment along every subject tested. Looking at these data closely, there is not a clear pattern either from subjects 'first and the second visit and also between different blocks in the same visit. Sometimes accuracy monotonically increases after each block (e.g. N_01) but most of the time decreases (e.g. N_02b, N_03b) or was not monotone (e.g. N_03, N_05b). The reason for the first behavior is thought to be a more solid training over the different blocks, but a decrease in accuracy can be explained with fatigability and lack of concentration.

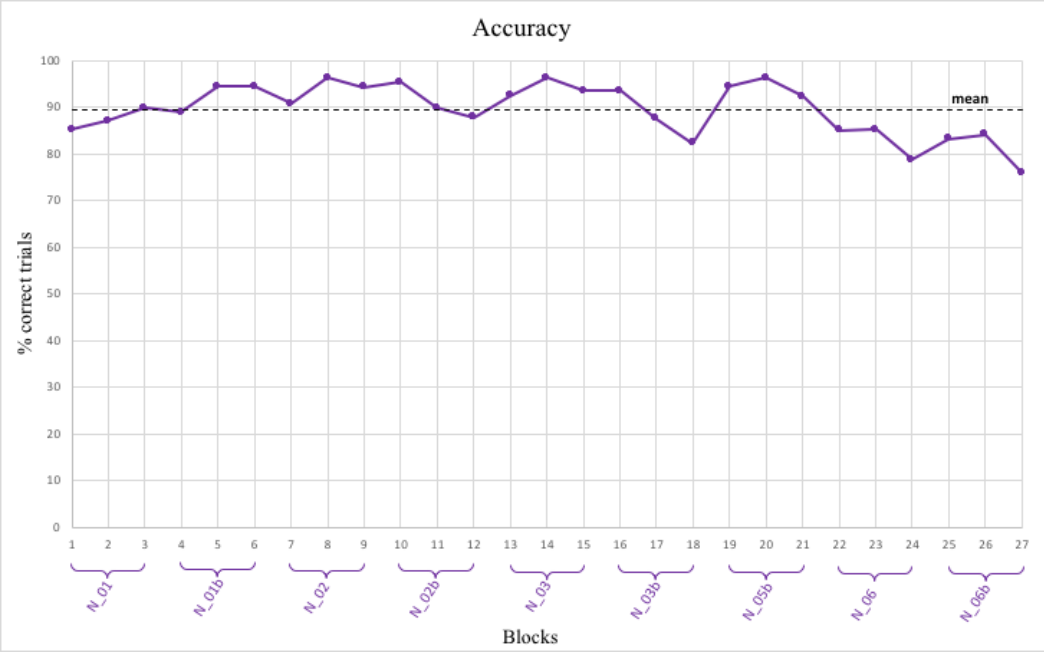

Figure 4.7. Accuracy variation over blocks (Mean= 89.413, SD= 5.569). Every subject performed three blocks (108 trials/block) during one visit, and their accuracy distribution is shown in the picture.

Considering the different types of trials inside each block – as described in Chapter 3 – one can compute further analyses, in order to retrieve meaningful behavioral results, by calculating the mean reaction time related to them. To address that, I considered the behavioral file produced by the experiment's Matlab script and retrieve the reaction time (RT) from it. Therefore, I decided to observe the variation of RT with respect to the delay duration – a.k.a. CTI –, the target of the trial – which could be either number or letter – and the classification between 'switch 'or 'repeat 'trial.

Let me first consider the delay effect on the RT. In the analysis pipeline, I read the behavioral Excel file as pandas.DataFrame, then selected only the interesting data, renamed the columns accordingly, select only the correct trials and finally iterate through the data frame rows retrieving the reaction time. Hence, in a Python script I wrote as follow:

```
# Read Excel file and convert into DataFrame.
df = pd.DataFrame(pd.read_excel('./dir/behavioral_file.xls'))
# Sub-select interesting data, renaming columns and index accordingly.
df.rename(columns=dict(zip(df.columns, df.iloc[161])),
          index=dict(zip(df.index, df.index + 2)),
          inplace=True)
# Select correct trials.
df = df[df["Evaluation"] == 1]
# Iterate through rows, retrieve RTs and save them in vectors basing on CTIs.
for idx,raw in df.iterrows():
    if raw['Delay Length (ms)'] == 300:
        RT_300ms.append(raw['React. Time (sec)']-(raw['Delay Length (ms)']+1000))
    elif raw['Delay Length (ms)'] == 800:
        RT_800ms.append(raw['React. Time (sec)']-(raw['Delay Length (ms)']+1000))
    elif raw['Delay Length (ms)'] == 1300:
        RT_1300ms.append(raw['React. Time (sec)']-(raw['Delay Length (ms)']+1000))
```

Obtaining three different vectors (RT_300ms, RT_800ms, RT_1300ms) containing the RTs associated with a particular CTI. The reaction time has been calculated by subtracting both the CTI and the radial motion interval from the time shown in the behavioral file. Proceeding in a similar way, RTs associated with different targets has been isolated. Although, for what concern the ‘switch ’or ‘repeat ’trials, a slightly different procedure has been used because the feeding of the RT array was controlled by several counters and flags to determine whether the subject underwent three trials with the same target in a row or not. If that was the case, the third trial – and the upcoming ones if the target remained the same – was labeled as ‘repeat’, whilst the first trial with a different target which was present after a ‘repeat ’trial was labeled as ‘switch’. Such paradigm was used in order to enhance the consistency of the selected trials, because – since participants didn’t know the target in advance – they could not predict the upcoming trial and therefore anticipating the task as described in Chapter 2. An example of the ‘switch/repeat selection ’is shown in *Figure 4.8*.

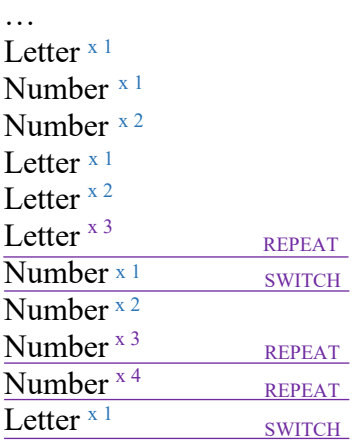

Figure 4.8. An example of the switch/repeat consistency paradigm.

4.2.2 Behavioral results

Although previous studies conducted by using a task-switching paradigm have shown the born of a switching cost, resulting in a higher reaction time during switching of tasks, our results are seen to differ. This behavior might have several explanations, which lay in the fact that the paradigm was based on a randomization of trials, without any predictable patterns. Experiment conducted with the purpose to demonstrate inhibition processes and switching costs rely on anticipation of task, performing a stronger and a weaker task, or unbalance the type of trials. On the contrary, dealing with balanced tasks presented in a random order, keep the subject self-aware that every time there could be an unpredictable switch of task, and therefore inhibition mechanisms related to task anticipation were compromised.

However, several studies showed that inhibition mechanisms are not present during tasks that involved a cue – a.k.a. "top-down" tasks – whereas they have been seen in "bottom-up" tasks, where the imperative stimulus itself indicates the task for the subject to perform.

Figure 4.9 shows the results obtained analyzing – with the consistency paradigm described in Chapter 3 – switching and repeating trials in terms of reaction time (a.k.a response time). Even though they seem to underlie a higher RT during repeat trials, the ANOVA computation have shown a p value >0.05 and therefore we can assert that there is no statistically significant evidence for this behavior.

However, we found interesting results focusing on the RTs associated exclusively with different CTIs, as shown in *Figure 4.10*. Indeed, even if from these data would be a too long shot to tell why, it is worth noticing that the higher the delay, the lower the reaction time. Also, the ANOVA verify the statistical significance of this result, with a P value <0.05. There is therefore a solid trend between the delay length and the reaction time of the subject, which will be discussed later on the dissertation, looking at the source estimate and the brain activation over time.

Finally, we wanted to verify whether there was a stronger and a weaker task, or if the subjects respond in the same amount of time. It happened to be very important also to because it is a possible explanation to the absence of switching cost during the test. *Figure 4.11* highlights that number and letter tasks have comparable reaction times for each CTI, and that reinforces the hypothesis of not observing any switching cost because of the equal effort throughout both tasks.

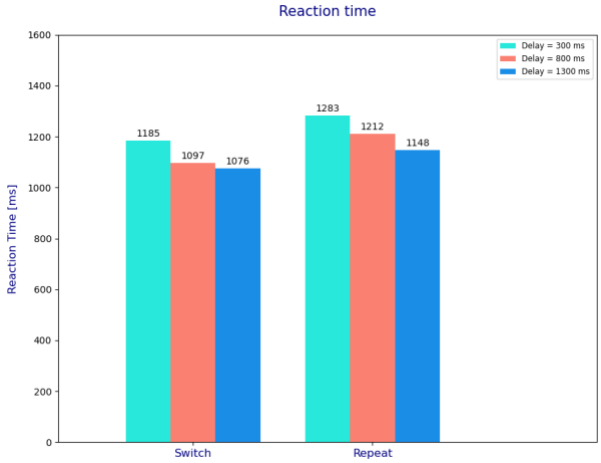

Figure 4.9. Reaction time between ‘switch ’and ‘repeat ’trials.

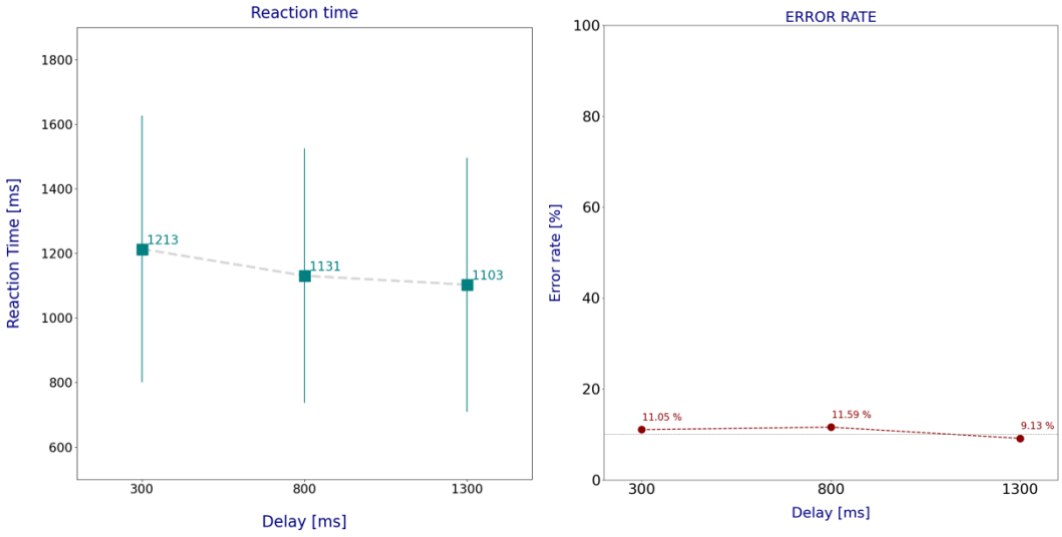

Figure 4.10. Reaction time and error rate throughout different cue-target intervals (CTI).

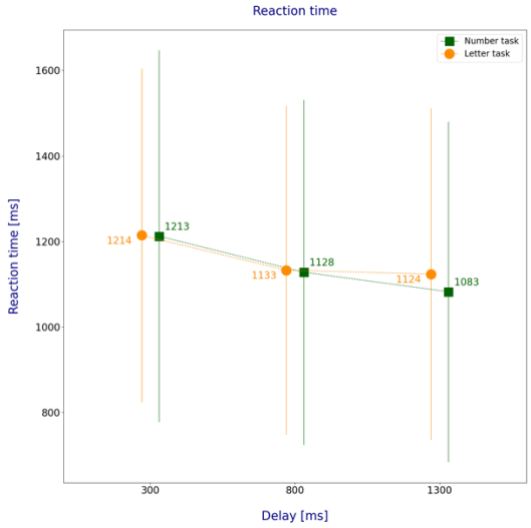

Figure 4.11. Reaction time over letter and number tasks.

4.3 BRAIN SOURCE ESTIMATES

In Chapter 1 we already mentioned the inverse and forward solutions necessary to address an accurate brain source estimate. Moreover, we introduced some of the MNE-Python functions able to manage .fif data structures and map the signal on the brain.

After preprocessing the data (see Chapter 3 – Preprocessing), the main steps are: reading the beamforming solution, load subject's source space – obtained from MRI scans –, computing the forward and inverse solutions, and finally apply the inverse solution to estimate the brain sources. An example is shown in *Figure 4.12*.

Specifically, `read_bem_solution()` simply read the prior calculated beamforming solution from the directory, then the function `setup_source_space()` creates a brain subspace to plot the signals in, and takes as inputs the name of the subject to analyze (e.g. 'LMV2016_N01') in order to retrive data generated by Freesurfer, the spacing (e.g. 'ico# 'for a recursively subdivided icosahedron, 'oct# 'for a recursively subdivided octahedron), indication about whether we want to add distance information to the source space, and the whole directory where to find the subject name.

Then, we calculate the forward solution with the function `make_forward_solution()`. It will require the signal information, the transformation file, the source space, the beamforming solution, and the indication about what signals to consider as sources (MEG, EEG, etc.). Also, since this processing requires a lot of computational power, we can specify the number of parallel processes the CPU has to run simultaneously.

After that, with the function `make_inverse_operator()` we use the forward solution to produce an inverse solution (a.k.a inverse operator), indicating the noise covariance matrix, and a series of parameter to weight differently the dipole component generated by tangential neurons ("loose" parameter) and the function to normalize the depth with ("depth" parameter).

Finally, we need to apply the inverse solution with the function `apply_inverse()`, specifying the epochs to take into considerations, the inverse solution itself, the regularization parameter (a.k.a. lambda2) and the inverse method to use between MNE (Minimum Norm Estimate), dSPM, sLORETA or eLORETA. Once we have the time source estimate variable, we can plot it and see a representation of the sources mapped in the 3D reconstruction of subject's brain.

```
bem = mne.read_bem_solution(bem_fname)
src = mne.setup_source_space(subject, spacing='ico5',
                             add_dist=False, subjects_dir=subjects_mri_dir)
fwd = mne.make_forward_solution(raw.info, trans=trans_file, src=src,
                                bem=bem, meg=True, eeg=False, n_jobs=-1)
inv = mne.minimum_norm.make_inverse_operator(raw.info, fwd, cov,
                                             loose=0.2, depth=0.8)
stc_300_mix = mne.minimum_norm.apply_inverse(epochs_mix['300'].average(),
                                             inv, lambda2, inv_method)
```

Figure 4.12. A trivial example of Python code for computing the brain source estimate.

4.3.1 TIME-FREQUENCY ANALYSIS

The frequency analysis was carried out by dividing the signal into 4 frequency bands: alpha band (8 – 13 Hz), beta band (16 – 30 Hz), low gamma band (30 – 55 Hz) and high gamma band (55 – 100 Hz). This has been obtained applying a simple digital filter in MNE Python, similarly as it has been done in the data preprocessing:

```
filtered_signal = raw.filter(l_freq,
                             h_frequ,
                             l_trans_bandwidth = 'auto',
                             h_trans_bandwidth = 'auto',
                             filter_length = 'auto',
                             phase = 'zero',
                             fir_window = 'hann')
```

We studied the different pathways of cortical activation to understand the mechanisms and their timing during the task. As already mentioned in Chapter 2, experiments based on a task-switching paradigm generate signals going either forward and backward.

Looking at the power spectral density of the data (see *Figure 4.2*), it is noticeable that alpha band around 12 Hz carries the highest signal magnitude. Therefore, visualizing the data in broad frequencies – without dividing them into separate bands –, will sometimes result in an alpha activity that hides other frequencies.

In the following analysis I will focus on different frequency bands, in order to underlie interesting activations related to a specific time or interval during the trials. The data have been obtained meaning all subjects but the “N_01b”, because its data were off-scale and has been considered not reliable for the source estimate analysis.

4.3.1.1 Activation during RDK

In the following analysis we will discuss how motion perception is recognized by participants, looking at separate bandwidth contributes. RDK is one of the most famous cues in neuroscience experiments, and it has been seen that a subject can tell whether is an expansion or a contraction in less than 300 ms. Since in our paradigm the RDK is 1000 ms long, it is likely to think that in the last 700 ms the subjects were forming the rule associated with the motion.

In particular, during RDK period there are different behaviors associated with each frequency band.

In the first 300 ms of motion, the signal is found to be – as expected – in the occipital lobe, but interestingly only below 60 Hz. In high-gamma band we don't find any signal centered in the occipital lobe. Also, as it is noticeable in the figures below, occipital lobe is involved only in the first 300 ms for both alpha and low-gamma rhythms, then the areas involved in the rule association become more significantly activated. Instead, beta rhythm maintains a significant occipital activation during the whole RDK and decrease in magnitude only in the last 400 ms, which may underline a specific visual awareness mechanism. Such mechanism is thought and seen to be accomplished by maintaining an occipital baseline activity on beta frequencies during the whole dot motion period, while it disappear when - in the following periods - displays in the screen change (see paragraph 4.3.1.2).

After the first 300 ms of motion, the brain activity is supposed to move from occipital to parietal and frontal lobes, where the high-level processes are achieved. However, throughout different frequency bands it has been seen to spread otherwise and not following the same pattern. Specifically, alpha rhythm – which is the strongest one – follows the dorsal pathway reaching the parietal lobe in the precuneus (PrCun) and near subparietal sulcus (SbPS), while both low- and high-gamma rhythms cover the most cortical frontal areas, in the superior frontal gyrus (F1).

One of the possible explanations of the distribution of alpha activity relies on the particular role of precuneus, which is known to be involved in switching attention between moving objects, but most importantly in working memory processes. Precuneus, considered also the medial part of P1, plays a fundamental role in visuospatial functions as it is suggested to achieve motor imagery and motor coordination while shifting between different targets. Considering both visuospatial and memory characteristics of precuneus, it is likely to assume that the subject during the last 600 ms of RDK is already visualizing the upcoming finger movement as well as remembering the rule associated with the radial direction of dot motion.

Furthermore, in the interval between 300 and 600 ms, alpha rhythm in dorsal posterior cingulate (DPC) area shows an increasing activity. Several studies demonstrated a sustained DPC activity in patient suffering from dyslexia (e.g. Stoitsis et al., 2008) but - from our perspective - none of the patients were affected by dyslexia and besides there were no letters involved yet. However,

being one of the most connected areas in the brain, the posterior cingulate cortex is widely known as a central node in the default mode network (DMN). The default mode network quickly deactivate during externally-directed tasks but it is active when attention is internally-directed (episodic memory retrieval, planning, etc.). Indeed - as previously mentioned - persons with impairment in the DMN have poor cognitive functions and attention.

Hence, since alpha band do not highlight any major frontal activity, it is likely to believe that the main processes are linked with motion perception and imagery, planning, locating objects in space and motion coordination rather than goal-oriented processes.

Indeed, frontal activity is noticeable at high frequency, both in low and high gamma band with a slight difference between the two. In the lower band of gamma rhythm, the activation is majorly located in the occipital lobe during the first hundred milliseconds of RDK. However, above 30 Hz the results underline a sustained frontal activity in similar spots, which is thought to be related with high-level processing.

The signal is spread through middle and - mostly - superior frontal gyrus (F1 and F2), and transverse frontopolar cortex. Although these regions are wide in human brain, their specific functions are poorly understood and changes throughout different experiments and tasks. One of the principal functions of the FP-PFC in higher cognition is monitoring and managing subgoals while maintaining information in working memory (Braver & Bongiolatti, 2002). In particular, Koechlin et al. (1999), concluded that monitoring of internally generated information requires both maintenance in working memory (i.e. creating a “mental scratchpad” to hold the information produced internally) and a subgoal (i.e. holding the task and the information themselves).

As an extension to this view, a research carried on by Christoff and Gabrieli (2000) suggested that the FP-PFC may subserve the monitoring of internally generated information, while DL-PFC is involved when externally generated information is evaluated.

Though, according to our results it is important to underline that in alpha and beta bands the frontal activity is tiny with respect to the occipital and parietal ones, and it is noticeable a major frontal activity only at high frequencies (>30 Hz).

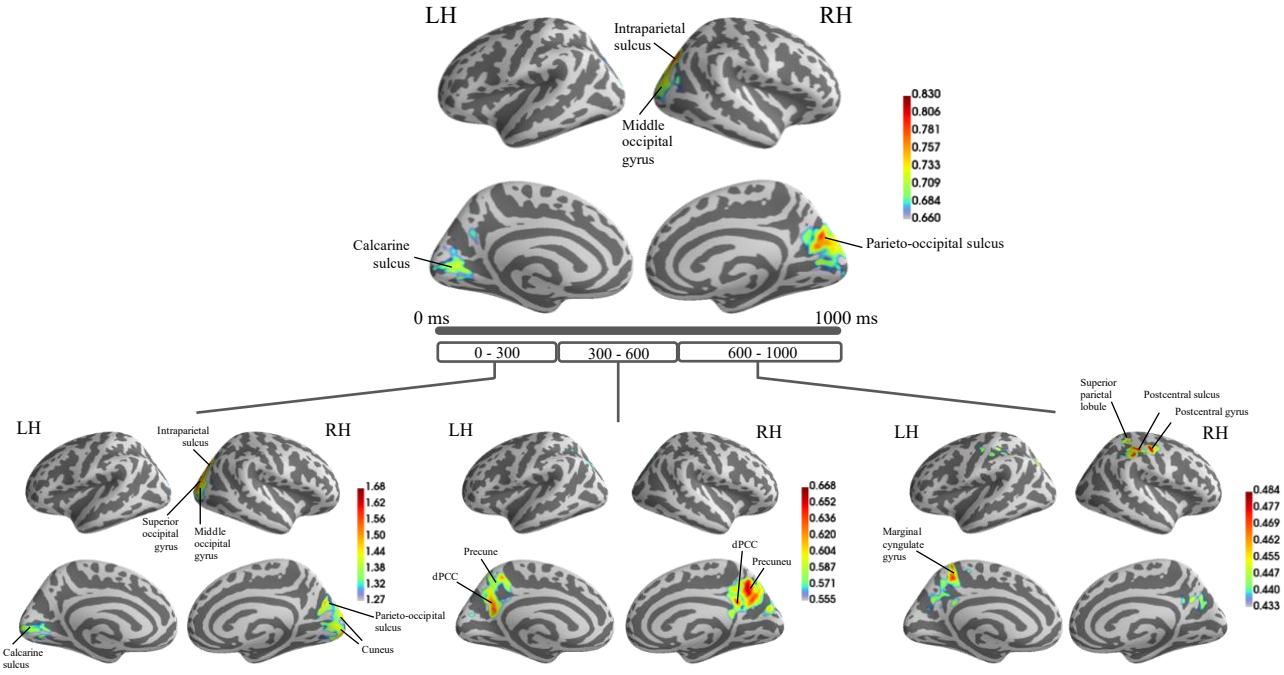

Figure 4.13. Alpha band (8-13 Hz) brain source estimations during RDK.

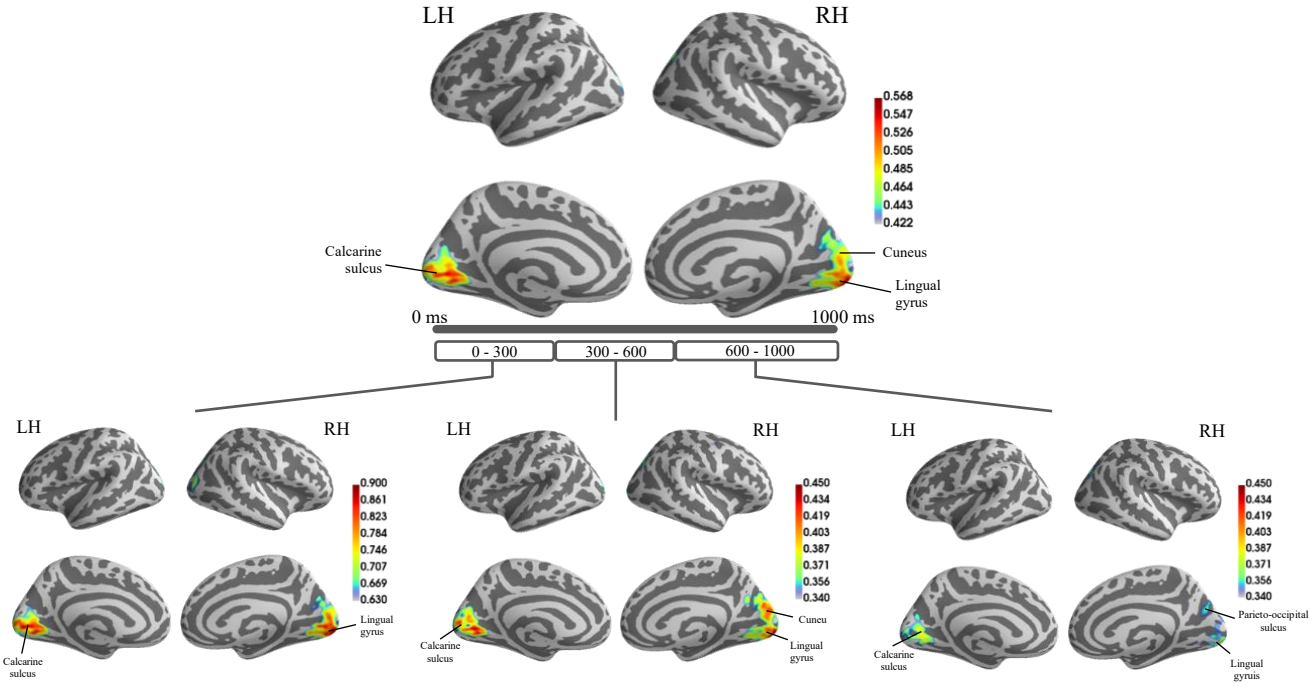

Figure 4.14. Beta band (16-30 Hz) brain source estimations during RDK

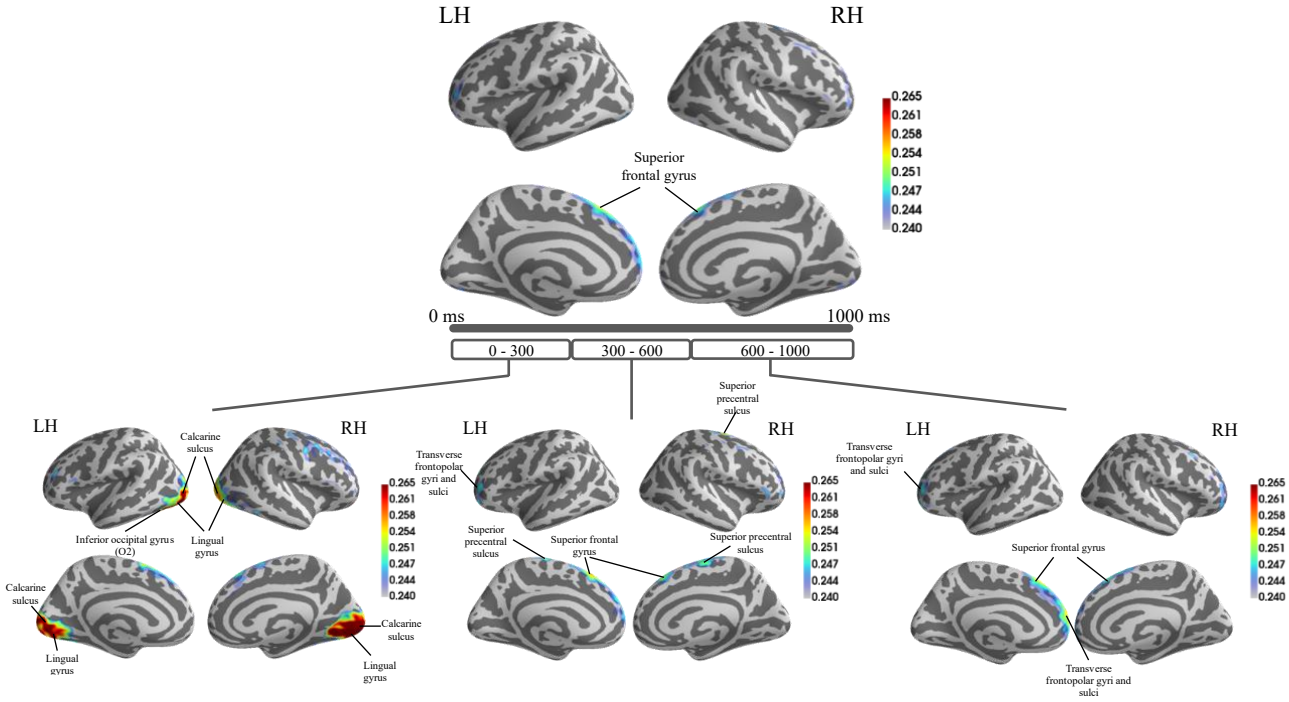

Figure 4.15. Low-gamma band (30-55 Hz) brain source estimations during RDK

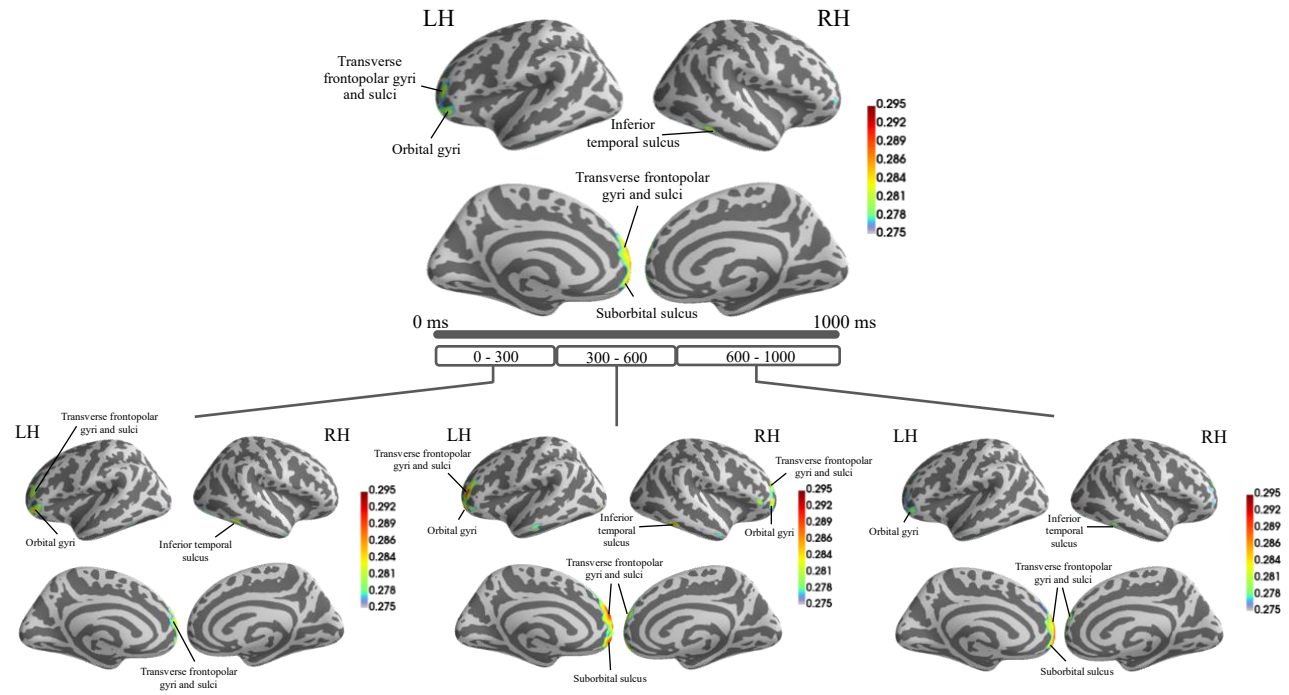

Figure 4.16. High-gamma band (55-100 Hz) brain source estimations during RDK

4.3.1.2 Activation during CTI

Cue-target interval (CTI) represents one of the main periods of interest because it underlies different brain mechanisms interacting together. Indeed, even though the main goal of the task is achieved through working memory, brain source estimates are seen to underline several other processes. Interestingly, these processes – represented by the activation of specific brain areas – seem to be somehow coded in frequency. Frequencies below 30 Hz are involved in vision and low-level computations, whereas above 30 Hz goal-oriented processes become primary. It is important to notice that the magnitude across the frequencies vary, thus what is showed in the following figures is referred to the main activation, but other areas can be involved if we had lowered the threshold. For example, *Figure 4.17* represent the source estimate of brain activation relative to alpha band in the range [0.5 ; 0.65], but it does not mean that there would not be any activity localized in other regions. However, range constraint has been required to obtain a proper visualization of the data.

Considering alpha band activity (*Figure 4.17*) no significant activity emerges that remains constant. Indeed, looking at the first 300 milliseconds of each epoch type, it appears a heterogeneous brain activity which cannot lead to any conclusion but the fact that right after the RDK the activity in alpha band is unclear. However, by looking separately at the different brain images obtained by filtering the signal in alpha band, we can notice that in the epoch with 300 milliseconds of CTI there is a weak occipital activation and a spike in the angular gyrus (Brodmann area 39), which is thought to be associated with body image and therefore can be interpreted in this case as the voluntary willingness to press the button, by thinking about the position of the fingers and which one to move.

On the contrary, in the epochs with higher CTI, the occipital lobe activation in V1 and V2 becomes more relevant, reaching parietooccipital and parietal regions in the last hundreds of milliseconds.

Regarding beta rhythm, as anticipated in the previous paragraph, it seems to encode an ‘attention mechanism’ because – after the first 300 ms –, since the display is all black during CTI and the subject does not see anything, beta activity fades in the occipital lobe. Although, that is not the only important region that encode information in beta band. Indeed, a constant activity holds in the postcentral gyrus area, which is the primary motor cortex for voluntary movement. It is difficult to say why such area maintains its activation in beta band during the whole cue-target interval, but the answer may lay in the fact that the subjects are “preparing” themselves to move the fingers and complete the task.

During cue-target interval – as well as in the previous paragraph –, high-level computations are achieved in prefrontal cortex, and they are modulated by frequencies above 30 Hz. In *Figure 4.19* and *Figure 4.20* both low and high gamma rhythms are represented during CTI. In *Figure 4.19*, we can notice that the activity in completely localized in frontal lobe, and it flows backwards

from BA10 to BA9 – through the superior frontal gyrus (F1). This behavior is particularly visible in the medial view of the brain during epochs with 1300 milliseconds of delay.

Even though prefrontal cortex is an extensive region of the human brain, it is still poorly understood. In 2007, Koechlin and Hyafil proposed a theory according to which Brodmann area 10 is involved in defining the hierarchy of the ongoing task with respect to the upcoming one, and in maintain some tasks on hold while performing others. Instead, Brodmann area 9 is proven to be involved in a lot of functions, such as short term memory and attention. However, functions in this area seem to differ between left and right hemisphere. Processing of empathy and emotions are achieved in the left hemisphere, whereas working memory and attention involves right hemisphere. Indeed, looking at *Figure 4.19* for higher CTIs, the most involved hemisphere considering frontal activity is the right one.

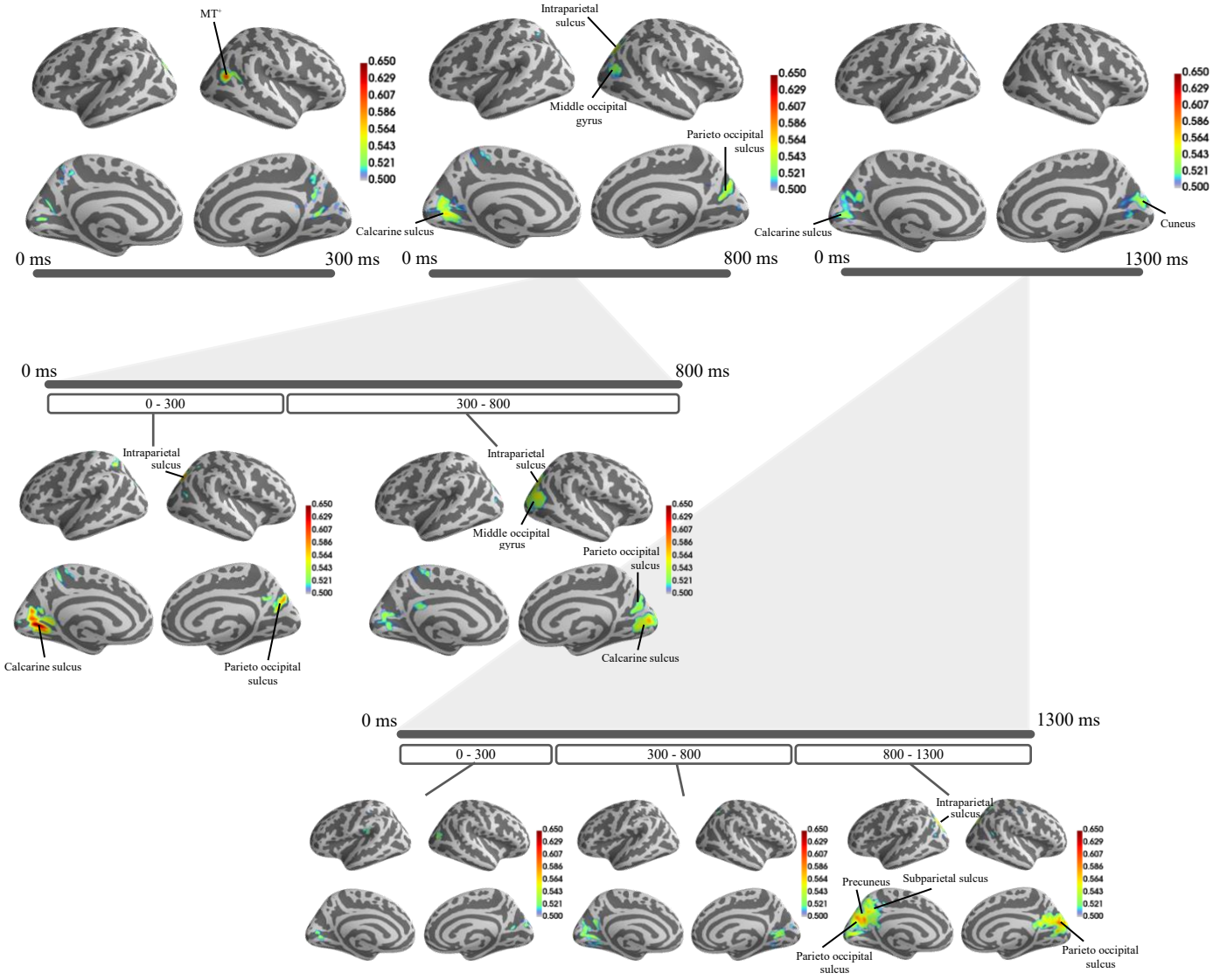

Figure 4.17. Brain source estimations in alpha band (8 – 13 Hz) during CTIs.

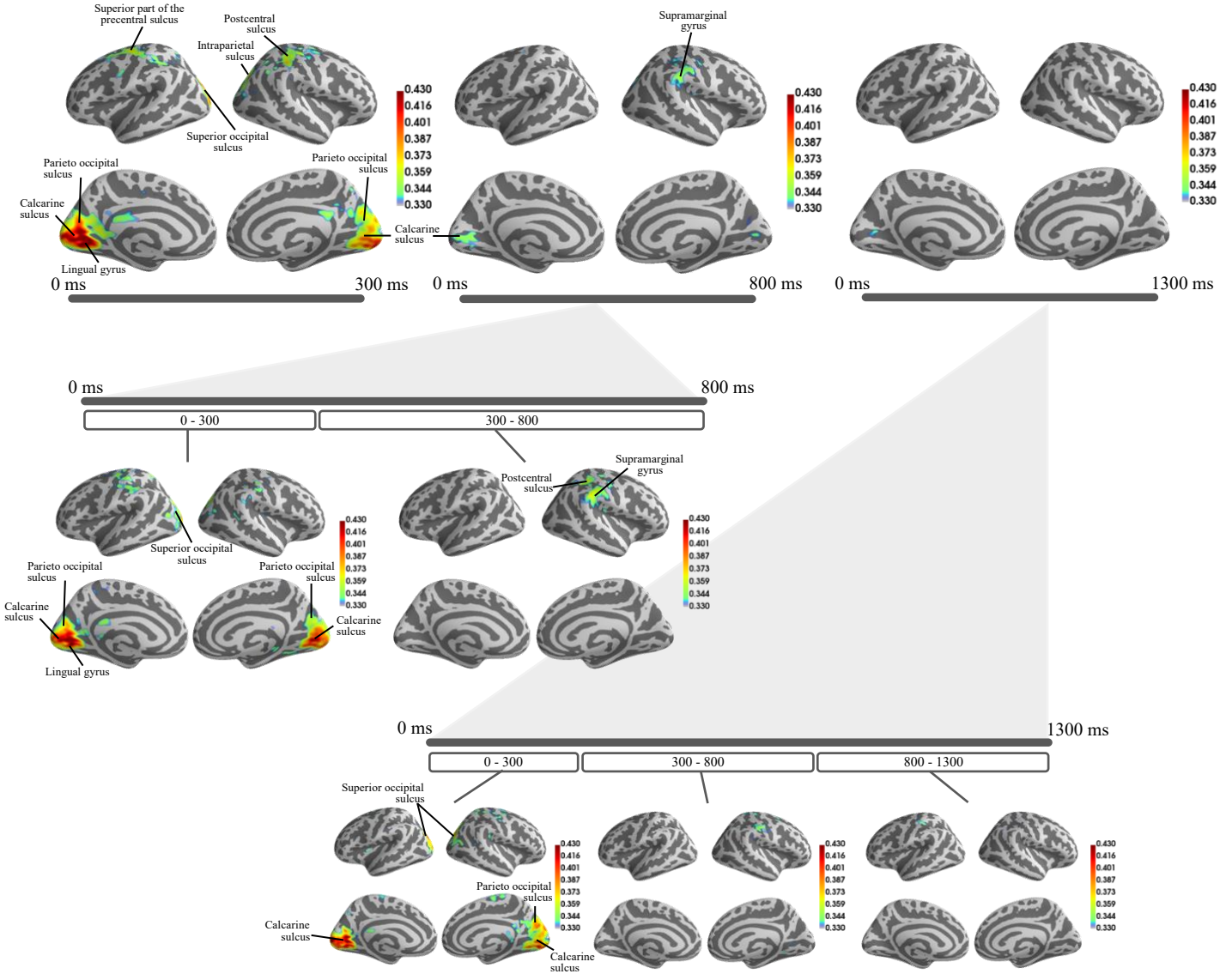

Figure 4.18. Brain source estimations in beta band (16 – 30 Hz) during CTIs.

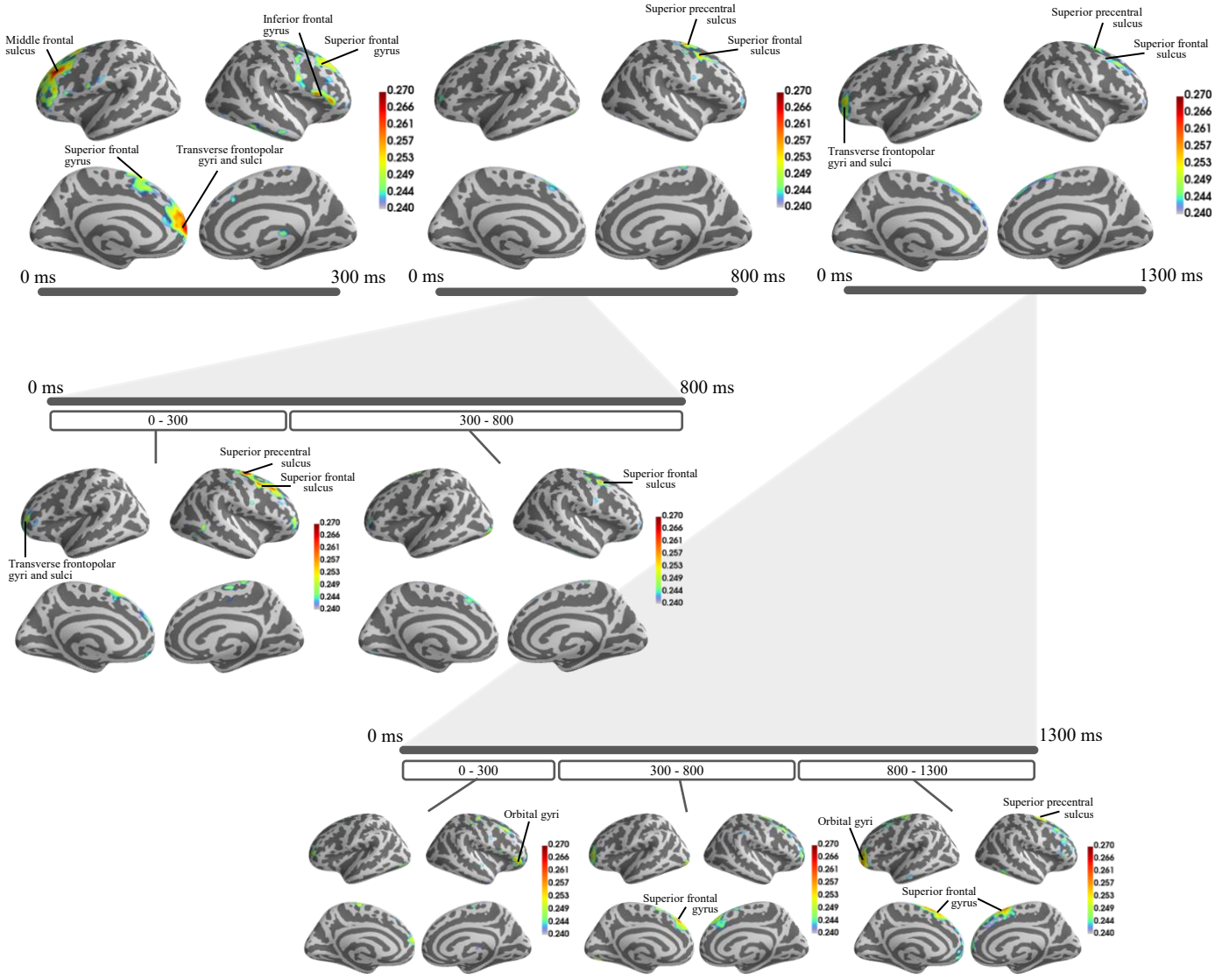

Figure 4.19. Brain source estimations in low-gamma band (30 – 55 Hz) during CTIs.

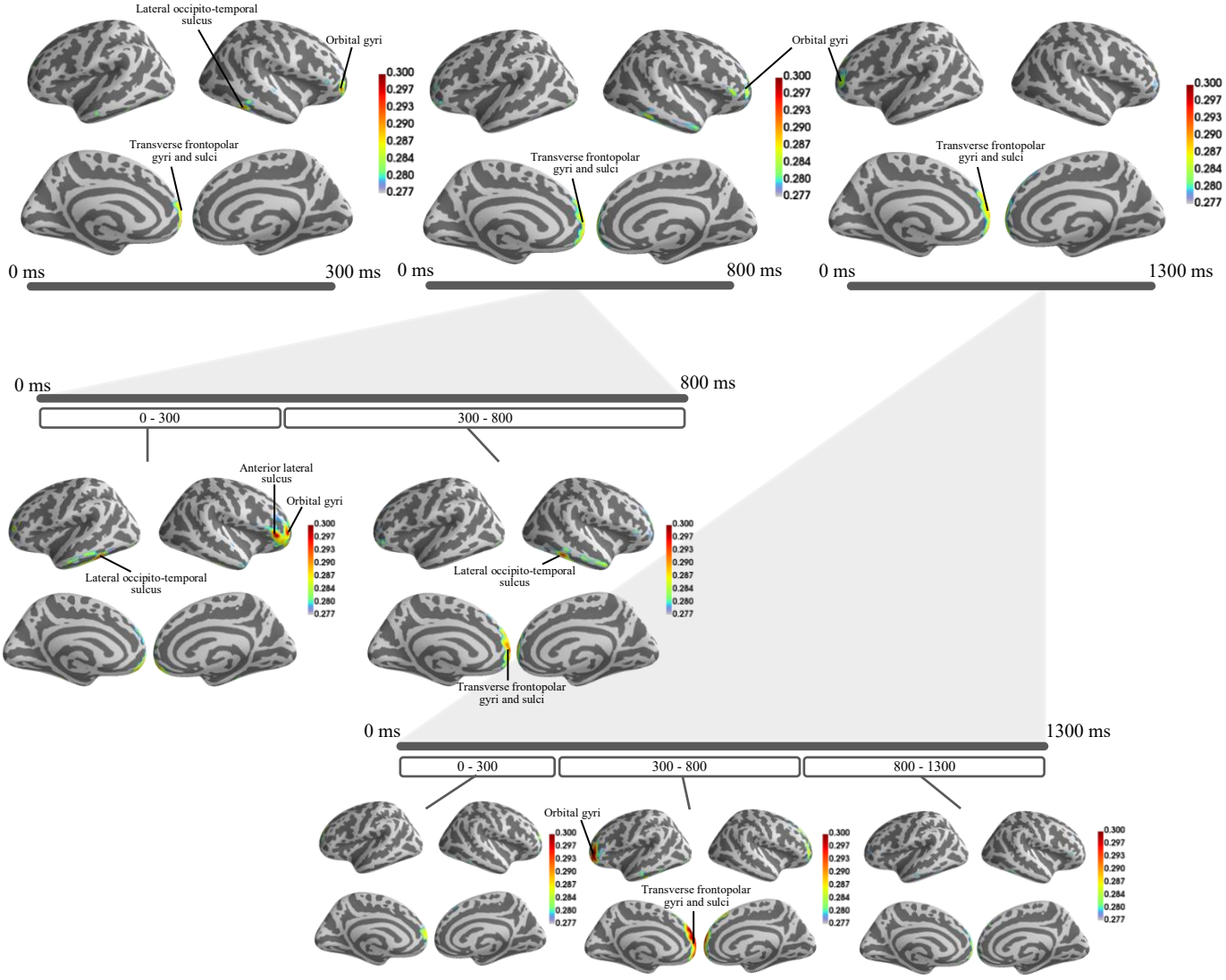

Figure 4.20. Brain source estimations in high-gamma band (55 – 100 Hz) during CTIs.

4.3.2 ACTIVITY BEFORE USER'S RESPONSE

In this paragraph, I am going to briefly discuss the brain activity in the 500 milliseconds before the subjects' responses. This analysis is therefore carried out by looking at the response times in the behavioral files (Excel files) for every trial and cut each epoch 500 ms before its respective RT. Afterward, the resulting signals have been divided into three groups based on CTIs.

Figure 4.21 shows the brain activity throughout different delays. For every delay length, as we explained in Chapter 3, all the trials were balanced and therefore this will not introduce any randomization bias. The obtained results highlight a brain activity that is very similar for every CTI, which might lead us to the conclusion that delay time does not affect brain activity before the subject's response. However, considering that the subjects could answer whenever they wanted, trying although to be as fast and precise as they could, this result is understandable and not surprising. Moreover, looking at the active regions themselves, we can notice that the parieto-occipital sulcus area – right below the precuneus – is strongly active and that might represent a key for the succeeding of the button press. In fact, we know that this region serves as a point of convergence between vision and proprioception. Hence, in our experiment – since the subjects are asked to press a certain button – this activation is likely to indicate that the subjects are picturing the buttons and the fingers in their heads, perceiving the position of the fingers with respect to the buttons, and pressing them to answer the task.

Also, a significant activity can be found in the superior part of the precentral sulcus for every delay. Due to the position of this region – just rostral to the primary motor cortex – it is believed to play a key role in planning complex and coordinated movements.

For a general view of the brain activation in the time window considered, *Appendix I* shows it divided by intervals of 100 ms.

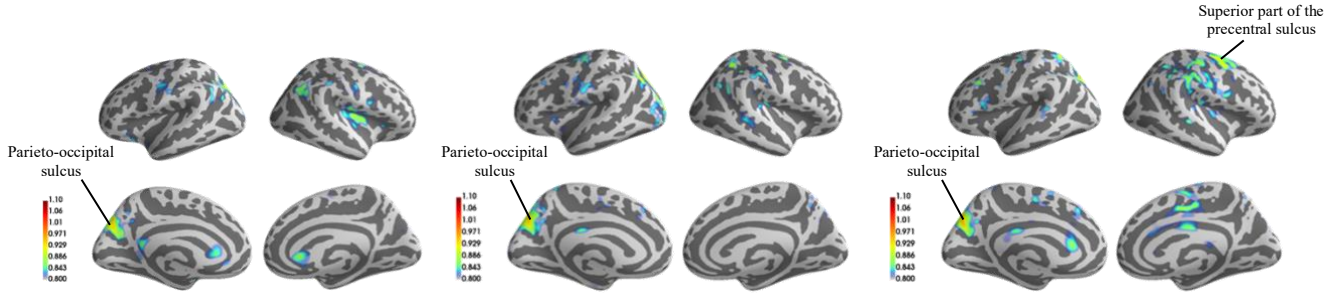

Figure 4.21. Brain activity during the 500 ms before the subjects' responses, considering epochs with 300 ms (left), 800 ms (middle) and 1300 ms (right) of CTI.

4.3.3 SWITCH-REPEAT SOURCE ESTIMATES

In this paragraph, a discussion about switch and repeat evidence in brain activation is carried out. First, it is important to point out that the analysis has been made using the random dot kinematogram (RDK) as the time interval because it was in that period that the subjects recognize the switching or the repeating of the task. However, as previously mentioned during the description of the experimental paradigm, subjects didn't know in advance if the cue was about to indicate the 'number task' or the 'letter task'. Therefore, theoretically, they couldn't prepare in advance for the upcoming task, and it wouldn't matter that much which one they performed in the previous trial. For that reason – in this analysis, in order to obtain more solid and reliable results – we applied the so-called 'switch/repeat consistency paradigm' (paragraph 4.2.1), which considers as 'repeat' trials only the ones that come after three or more same cues.

Analyses on switch and repeat trials have been led – during RDK – in two different ways. On the one hand, the range of signal's magnitudes has been fixed and the different brain activities compared to each other every 100 milliseconds. Thus, putting this constraint required choosing a tradeoff between the signal we wanted to see in the repeat and switch trials. Since they are significantly different, that might have concealed or spread some brain activations. *Figure 4.22* shows the results obtained by fixing the magnitude range, for some time intervals during RDK. On the other hand, this analysis has been carried out considering for every 100-milliseconds interval its own optimal magnitude. It will allow us to focus on the most active brain areas, without considering the difference of magnitude. This last analysis has not been described in this thesis.

Some observations can be made looking at the brain activity showed in *Figure 4.22* in detail. One of the most noticeable aspects is that for repeating trials the magnitude of the signals is on average higher than the one during switching trials. That, in my opinion, could probably underline an inertia mechanism that originates adaptation in the subject. Indeed, after 2 times in a row with the same cue, the subjects feel more secure and inclined to stick with the previous task, and – when the cue confirms the same task again (repeating trial) – they tend to concentrate more on the actual random dot motion despite thinking more about the rule. This behavior may be confirmed in the last 300 milliseconds of RDK where, in fact, there is no noticeable prefrontal activity during the repeating trials but there is during the switching trials instead. Also, in these intervals, two other things are important to point out: there is higher activity in the right hemisphere during the repeating epochs which is not present in the switching ones, and a sustained and steady occipital activity also during the last hundreds of milliseconds only during the repeating epochs.

Moreover, from the beginning of RDK and for the following 200 ms, the estimated signal is seen to be located in the middle temporal visual area (MT+) for both types of epochs analyzed.

Although, in switching trials, it is localized on the left hemisphere and decreases rapidly, while during repeating epochs it is seen to be in the right hemisphere and decreases slowly.

Finally, considering two of the intervals in the middle of RDK (see *Figure 4.22*), brain activity during switching trials is restrained only in the occipital lobe, while for the repeating task – perhaps because of a lower concentration required – the brain activity is seen also in other regions. For example, in the parietal lobe, the signal is seen to activate during the 300-400 ms interval, but then it fades away afterward.

In *Appendix II* the brain activity is showed in detail.

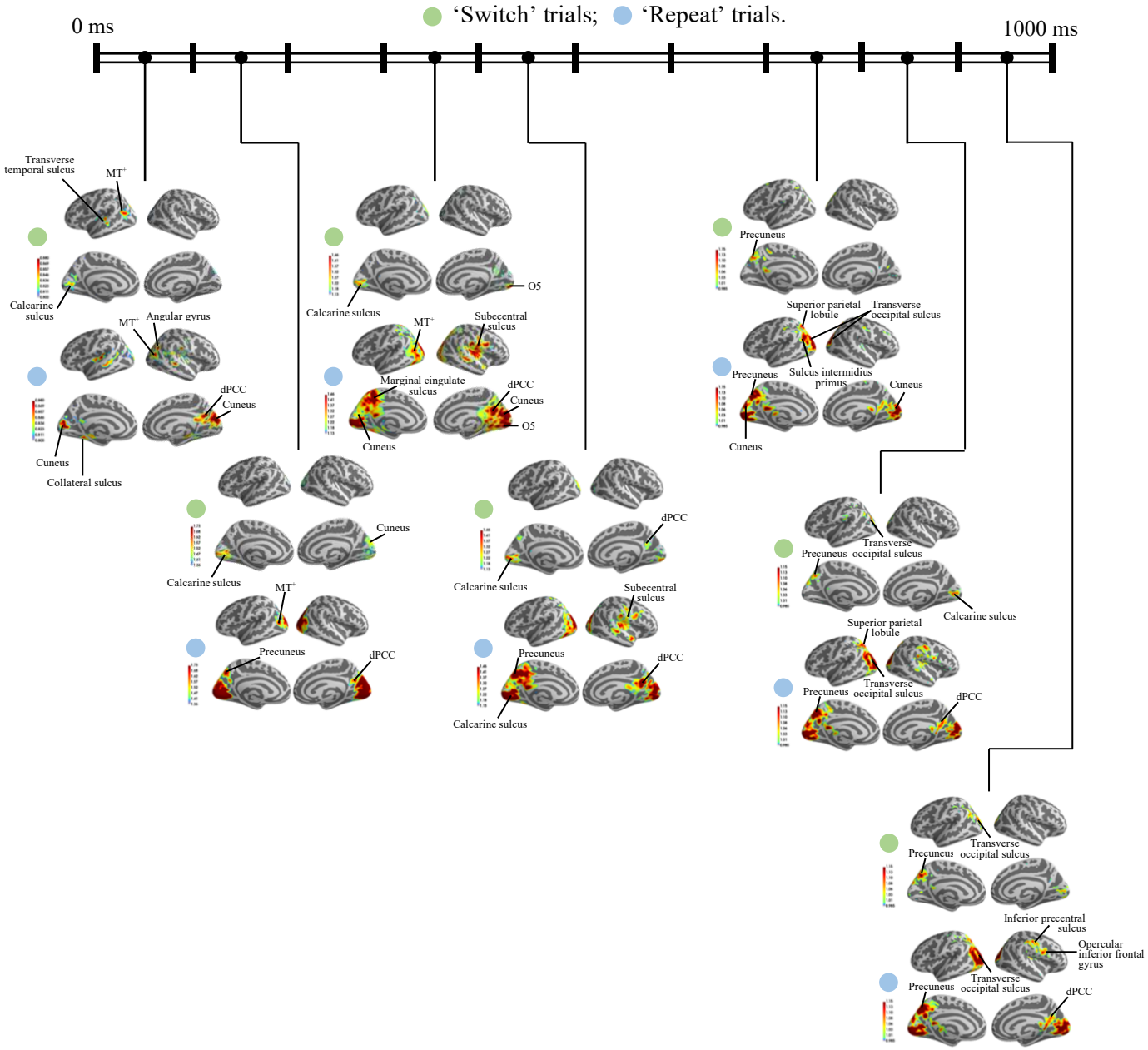

Figure 4.22. Comparison between ‘Switch’ and ‘Repeat’ trials in several intervals during random dot kinematogram.

4.3.4 VISUAL FIELD SOURCES

In this paragraph we will focus on the occipital activation of the brain during the ongoing experiment. The main goal of this analysis is to better understand the reaction time of the subjects when the image was displayed. Therefore, we are not going to discuss the dynamics of the brain and its networks, but only the occipital response to the presentation of the cue and after the CTI. The visual source analysis will be carried on by looking at the signal over time, grouping the epochs by the length of the delay (CTI).

In particular, four main occipital regions – derived from Desikian segmentation – have been taken into considerations for this study: pericalcarine, lingual, lateral-occipital and cuneus. The four areas are highlighted in *Figure 4.23*.

The preprocessing the data underwent was the same described in paragraph 4.1, with the only difference that this time – in order to show the regions separately – we had to upload the Desikian region's labels in the Python script. They have been added to the Raw object (signal object) to call and isolate only the channel we are interested in. It has been plotted in 2D, having the epoch time (ms) in the x-axis and the source amplitude (DN) in the y-axis.

During the processing of the data, first we computed an inspection to determine whether there was a similar occipital activity across the subjects, or it was reasonably different, and therefore likely to be considered inconsistent. After, we looked at the signals separately for each subject and each occipital subregion, finding out that the subjects N_01 and N_01b were off scale and hard to reconstruct confidently. Therefore, we didn't consider both 'N_01' and 'N_01b' recordings.

An example of the graphs we looked at is shown in *Figure 4.24*, where the signal is stable throughout all the trials, and it results in a consistent and meaningful average. Furthermore, for each occipital subregions, we merged the data retrieved from every subject into a single chart, comparing the magnitude and the shape of all subjects' averaged signals. We did that for each occipital subregion and an example is shown in *Figure 4.25*, where it is noticeable a similar activation. Finally, an average of all subjects' activations has been computed (*Figure 4.26*) for each region.

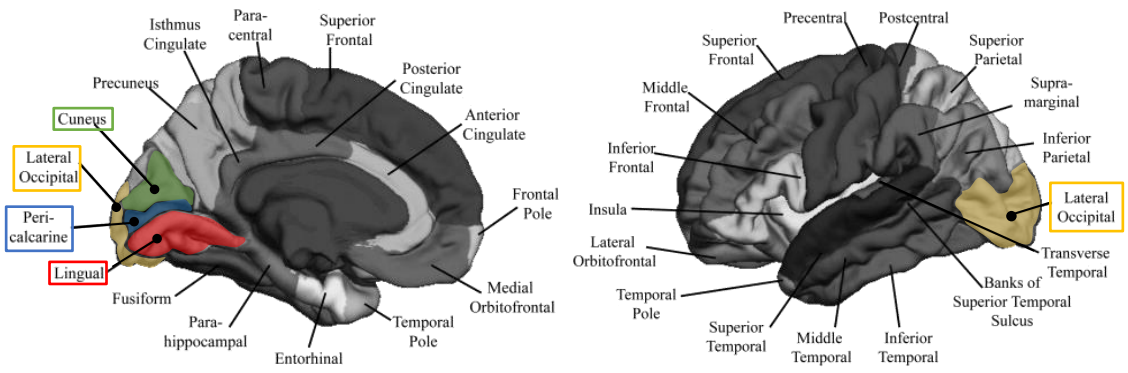

Figure 4.23. Desikian brain segmentation highlighting occipital areas (left hemisphere).

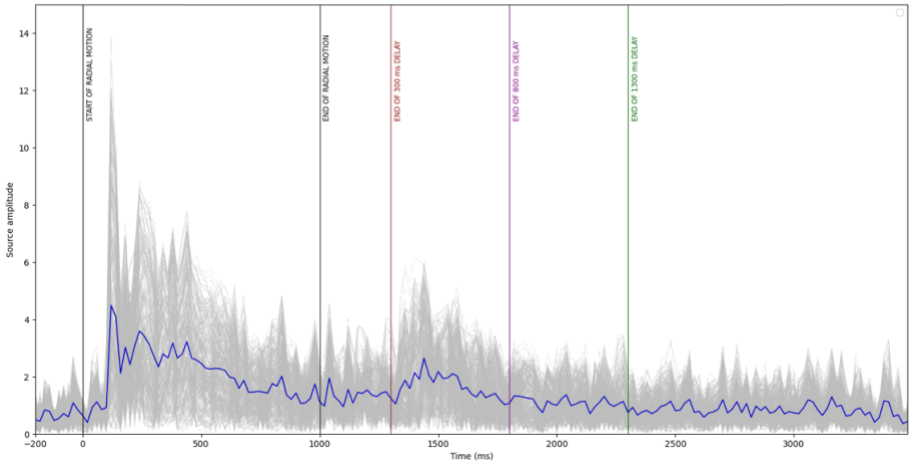

Figure 2.24. Representation of the signals in the lingual region (left hemisphere) for the subject 'N_03'. The graph shows in grey the overlapped signals from all epochs and the averaged signal in blue. Data have been retrieved from epochs with 300 ms of CTI.

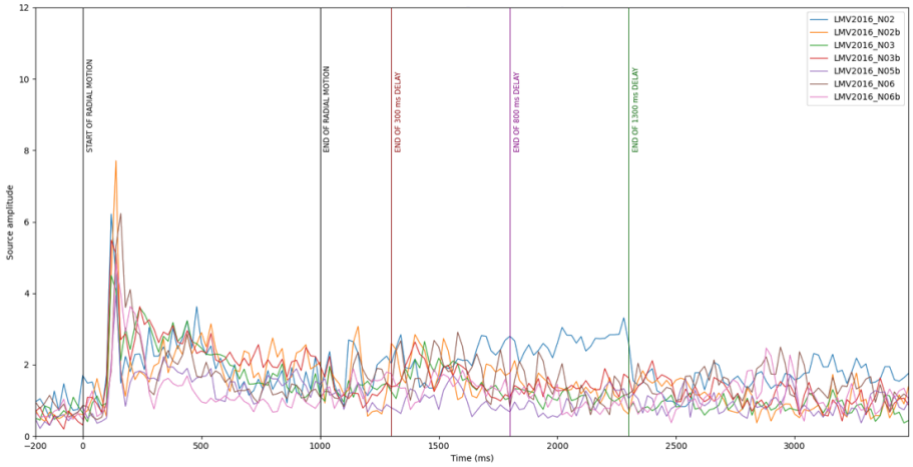

Figure 4.25. Representation of the mean lingual activation (left hemisphere) during an epoch. All valid subjects have been considered and plotted.

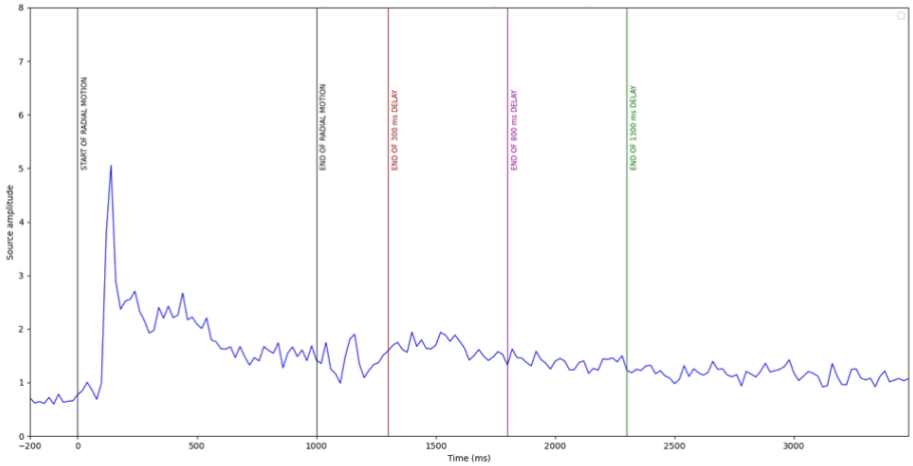

Figure 4.26. Representation of the mean lingual activation (left hemisphere) during one epoch.

Considering the epochs where the CTI was equal to 300 ms, the graphs has a peak about 150 ms after the cue start and another one about 150 ms after the ending of it. This behavior is consistent with the biology of visual system, because the transmission time of the image from the eye to the brain is known to be around 100-150 ms. Also, a lower peak after the radial motion is understandable, considering that very few areas activates during the blank period. Although, there is a sharp peak because the human visual system detects a change in the display.

Proceeding as previously described for every occipital subregion, an estimate of the main involved areas can be drawn (*Figure 4.27* and *Figure 4.28*, respectively for left and right hemisphere).

Observing the results showed in *Figure 4.27* and *Figure 4.28*, it is noticeable a similar trend for both hemispheres. However, even though the signal associated with each region is seen to maintain the peaks roughly at the same time for both hemispheres, in the right hemisphere the peaks are sharper and higher. That allows also to notice an activation of all occipital regions about 850 ms after the peak associated with the display of number and letters (after CTI).

As we already mentioned in the previous paragraphs, the bandwidth responsible for this peculiar behavior is the beta band, which is centered in the occipital lobe and sense a changing in the screen displayed.

However, considering that the subjects' response time is usually higher than 1 second, seeing a sudden activity only 850 ms after the first peak is unusual. If we consider for simplicity 1200 ms as a typical response time after CTI, because the screen changes only after the subject's response, we were expecting to observe a peak about 1350 ms after the end of the CTI. More analyses need to be done to assess the nature of this behavior, but that exceeds the purposes of this dissertation.

Another interesting outcome is that – with the only exception of the peak mentioned above – the interval between the change of the scene on the screen and the occipital activation is constant, no matter what is displayed. Though, the baseline activity and the amplitude of the peaks vary depending on the activity required and the scene projected.

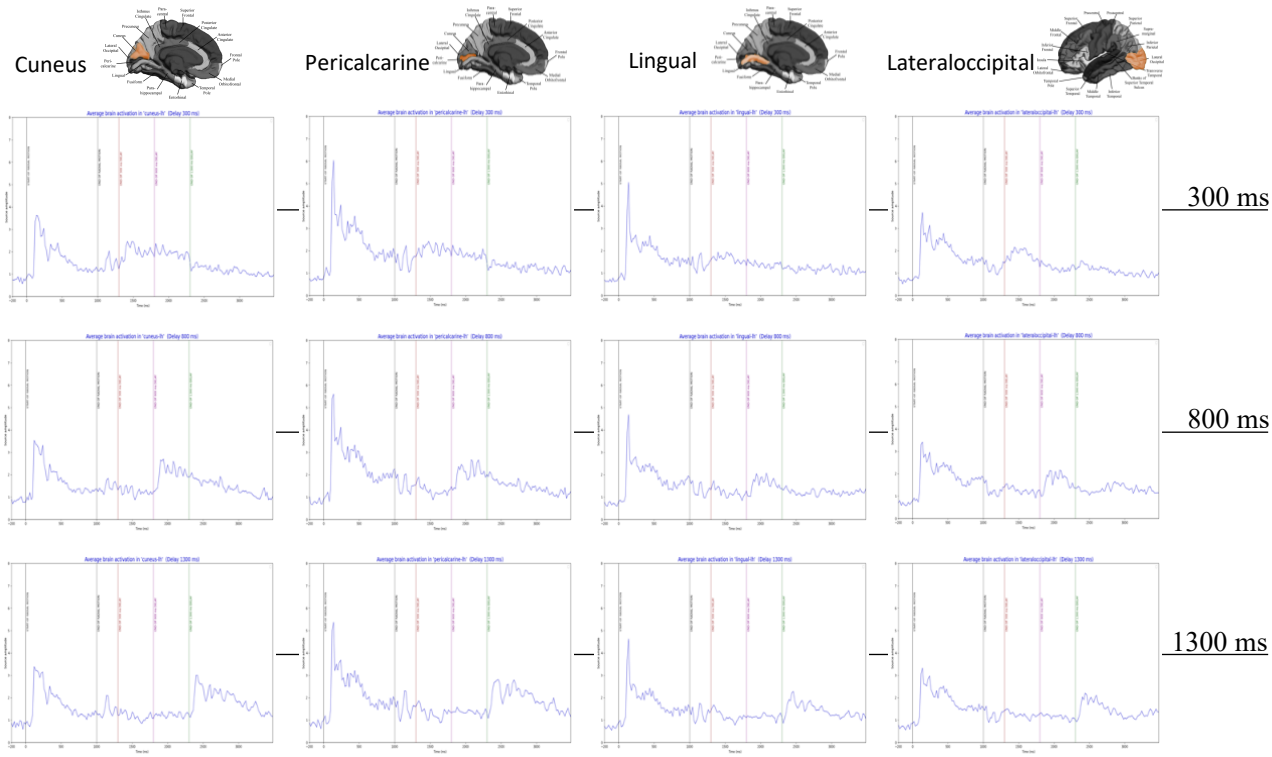

Figure 4.27 Mean brain activity in occipital lobe (left hemisphere) during the epoch interval.

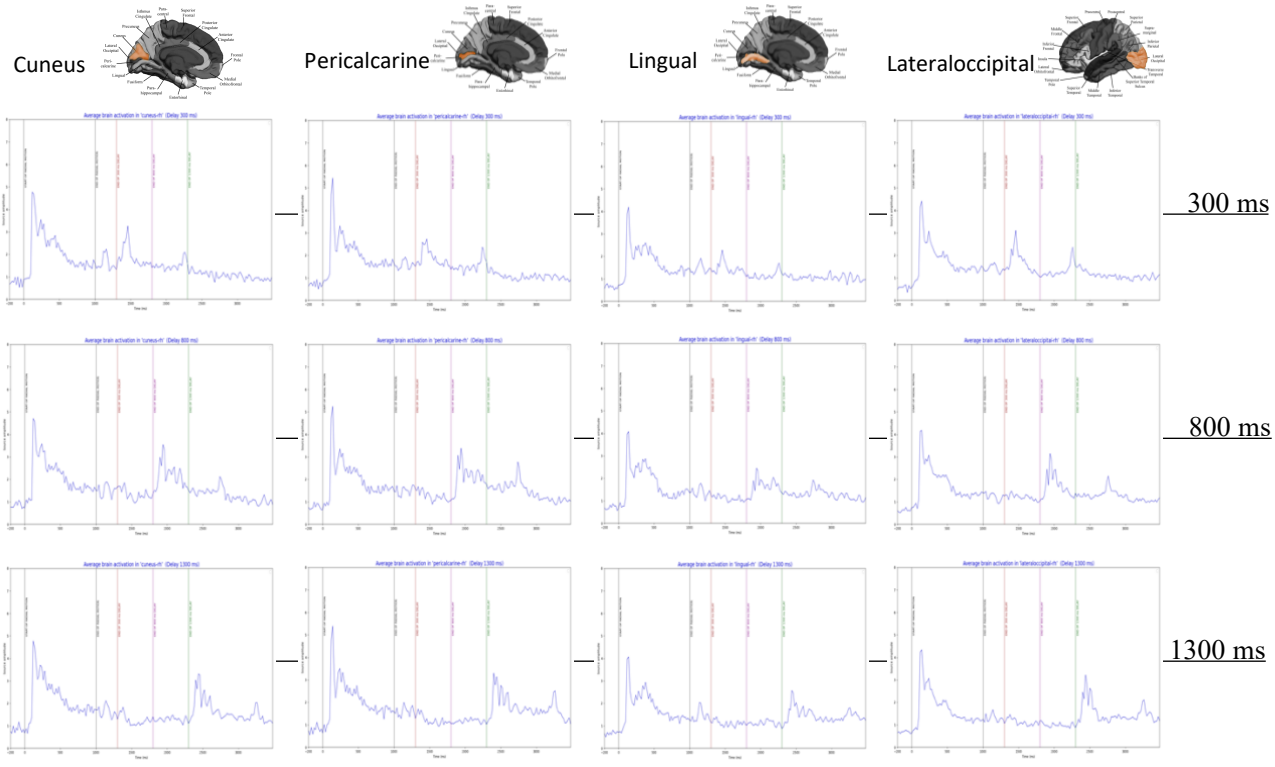

Figure 4.28 Mean brain activity in occipital lobe (right hemisphere) during the epoch interval.

4.4 MACHINE LEARNING ANALYSIS

In this analysis, the aim was to understand the behavior of the most common linear classifiers to establish whether they can automatically detect a reasonable difference in brain activation during letter or number tasks. Moreover, we will identify particular times where these differences become relevant. The analysis has been performed during the random dot kinematogram (RDK) because in this interval the subject was asked to understand the goal of the upcoming imperative stimulus and remember the rule associated with the task. Hence, the brain activity should be different and the classifiers able to detect them.

Afterward, the classifiers have been tested to verify their capability to differentiate between epochs with different delays, relying only on the MEG data and the source estimate. The comparison has been made between trials with 300/800/1300 milliseconds of CTI, with all their permutations. It resulted in three different comparisons because the classifiers could only separate between two classes.

Finally, classifiers have been tested on their ability to classify between epochs with different delays, though this time considering not the whole epoch time but only 500 ms before the subject's response.

The results of these analyses are shown in the following paragraphs.

This analysis – as well as most of the others – has been implemented in Python language, using 'mne' package. Because mne-python relies on scikit-learn (machine learning library for Python developers), we could use many different classifiers by simply calling them and setting some parameters. In particular, we applied multi-voxel pattern analysis (MVPA) – which is a well-known technique in neuroimaging community to compare the distributed pattern of activity – using 5 different linear classifiers: logistic regression, linear discriminative analysis (LDA), linear support vector machine, Ridge classifier, and SGD classifier.

These have been called in Python as follow:

```
Logistic Regression
clf_01 = make_pipeline(StandardScaler(),
                       LinearModel(LogisticRegression(solver='lbfgs')))
Linear Discriminative Analysis
clf_02 = make_pipeline(StandardScaler(),
                       LinearModel(LinearDiscriminantAnalysis(solver='svd')))
Linear Support Vector Machine
clf_03 = make_pipeline(StandardScaler(),
                       LinearModel(LinearSVC(loss='squared_hinge')))
Ridge Classifier
clf_04 = make_pipeline(StandardScaler(),
                       LinearModel(RidgeClassifier(solver='auto')))
SGD Classifier
clf_05 = make_pipeline(StandardScaler(),
                       LinearModel(SGDClassifier(loss='hinge',
                                                 learning_rate='optimal')))
```

The algorithms used for solvers have been chosen considering the type of data we were dealing with and its respective classifiers. For example, with LDA classifier we selected a single value decomposition (SVD) solver because it is considered the best when there are high features data. However, sometimes the default solver has been used to speed up the computation.
Once we have defined the structure and logic behind the classifiers, we applied it to the source estimate retrieved from MEG data by calling a slide estimator with the function:

```
estim = SlidingEstimator(clf_01,
                         n_jobs=-1,
                         scoring='roc_auc',
                         verbose=True)
```

Finally, we applied 5-fold cross validation to evaluate the performance of the classifier, by implementing the following function:

```
scores = cross_val_multiscore(estim,
                              X_data,
                              Y_labels,
                              cv=5,
                              n_jobs=-1)
```

At the end of the pipeline, a moving average with a 3-samples window length has been applied to smooth out the graph and make it more readable (*Figure 4.29*).

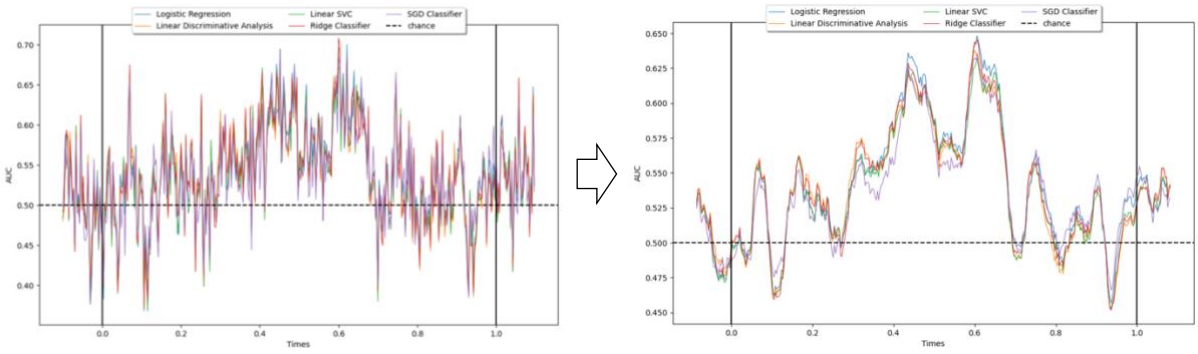

Figure 4.29. 3-Samples moving average applied on classification scores graph.

4.4.1 MVPA during RDK

As previously mentioned, during random dot kinematogram the subjects were asked to understand whether they had to perform a 'number task' or a 'letter task'. During the cue, even though the areas involved in recognizing the dot motion are supposed to activate in the same way for both types of tasks, the activity on other areas can be different for one task with respect to the other one. Indeed, *Figure 4.30* shows an ascending trend from 200 ms to around 700 ms, which can explain two different brain activations during the display of an expansion or a contraction dot motion. After 700 milliseconds, the score decreases again probably because the subject is activating similar brain areas involved in goal-oriented processes. This result is biologically relevant, because it may highlight separate brain pathways for 'number tasks' and 'letter tasks', that become similar again at the end of the random dot kinematogram. In the last hundreds of milliseconds, the subjects seem to have already understood the direction of the dot motion and they are processing the task. From an empirical test conducted at the Brain and Vision Laboratory (Boston, MA), we know that 300 milliseconds are enough to understand if the motion is an expansion or a contraction. Therefore, the ascending trend in *Figure 4.32* may indicate some other high-level processes rather than only the understanding about expansion or contraction dot movement.

Also, looking at the graph from a computational point of view, *Figure 4.30* shows that the performances of the classifiers seem to be very similar, with the only exception of the SGD classifier.

Focusing on the most interesting points of the graph in *Figure 4.30*, *Figures 31-A* and *31-B* show the different brain patterns derived from 'Logistic regression classifier' and 'Linear support vector classifier (SVC)', for both types of sensors.

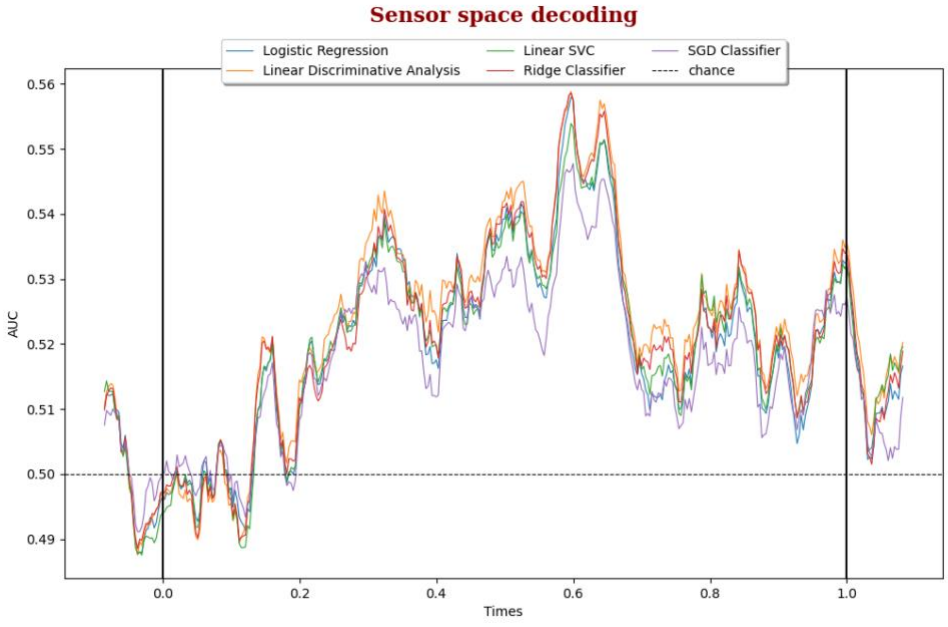

Figure 4.30. Classification scores (5-fold cross validation) for different classifiers during RDK.

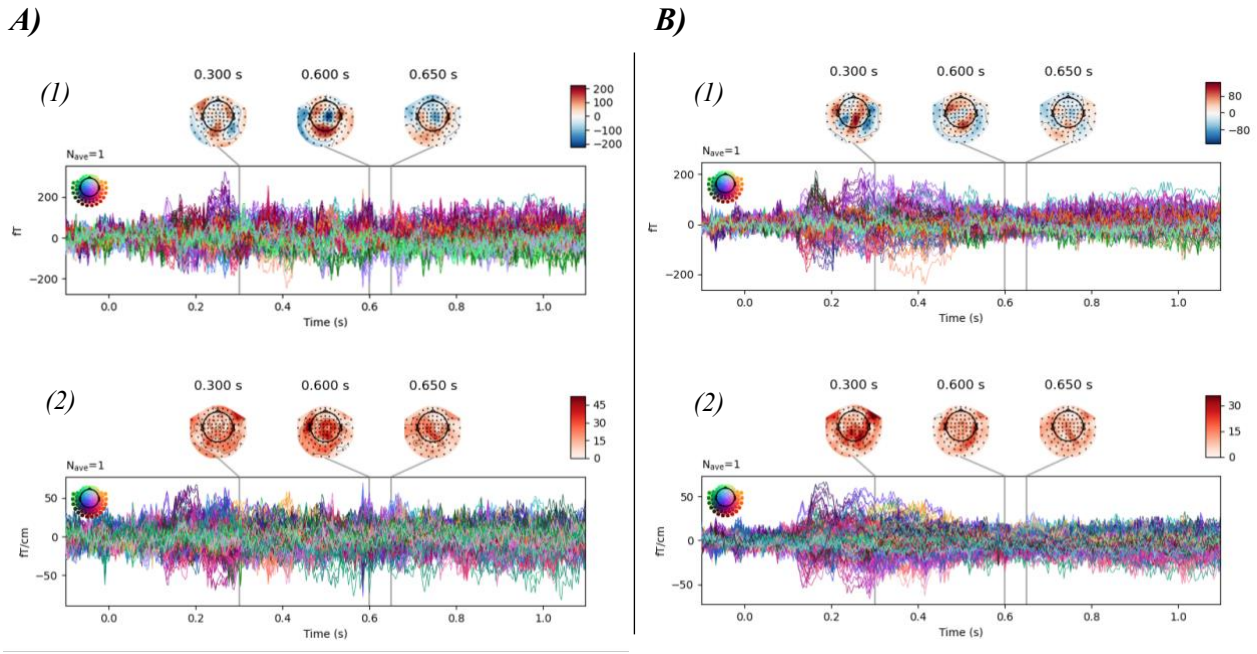

Figure 4.31. A) Brain activation patterns decoded with 'logistic regression classifier' for magnetometers (1) and gradiometers (2). B) Brain activation patterns decoded with 'Linear support vector classifier' for magnetometers (1) and gradiometers (2).

4.4.2 MVPA across different CTIs

Multi-voxel pattern analysis has been applied also to compare the activity across epochs with certain cue-target intervals (CTIs). Because this analysis is thought to be applied only with two classes, we applied it firstly between epochs with 300 ms and 800 ms of delay, then 800 ms and 1300 ms and finally 800 ms, and 1300 ms of delay. That resulted in the graphs showed in *Figure 4.32*.

Although MVPA worked neatly during RDK – as described in the previous paragraph –, in this case it showed some flaws and inconsistencies. Particularly, during the interval where both epochs show the black screen, we were expecting random classifiers because the subject was seeing the same scene, although all graphs in *Figure 4.32* indicate a high classification score. On the contrary, when the delay for one epoch finishes while the other continues, we were expecting to see a sharp increase in the score.

This is true for *Figure 4.32-A* where, after the 300 ms CTI, the score increases because the other epochs have a 500 ms blank period left, thus the displayed scene is significatively different. When the 800 ms delay finishes, the brain activity becomes more similar for both epochs, and hence the classification score decreases.

Figure 4.32-B and *Figure 4.32-C* are significantly hard to interpret linking the score to the biological brain activity, therefore we cannot draw any other conclusion but the fact that the classifiers were not able to fit and manage the data properly.

4.4.3 MVPA 500 ms before subject's response

Another question we set out to answer was to observe whether there was a different brain activation during the 500 milliseconds preceding the subject's response and if a classifier would be able to discriminate two responses considering that they derived from two different delays. As described in the previous paragraph, we applied multi-voxel pattern analysis separately: first comparing epochs with 300 and 800 milliseconds of delay, then 800 and 1300 ms, and finally 300 and 1300 ms. Results are presented in *Figure 4.33*.

Considering that – from the behavioral analysis (see section 4.2) – we found a correlation between the CTI length and the response time, it was trivial to assume that this behavior would somehow be confirmed by a different activation pattern that result in a faster or slower response. Although, as we can notice by looking at *Figure 4.33*, the classifiers exhibit random behavior. That can underline either a similar brain activity throughout epochs with different delays or simply a slightly diverse pattern between all epochs which results in an impossibility to automatically determine whether the CTI was 300, 800, or 1300 milliseconds.

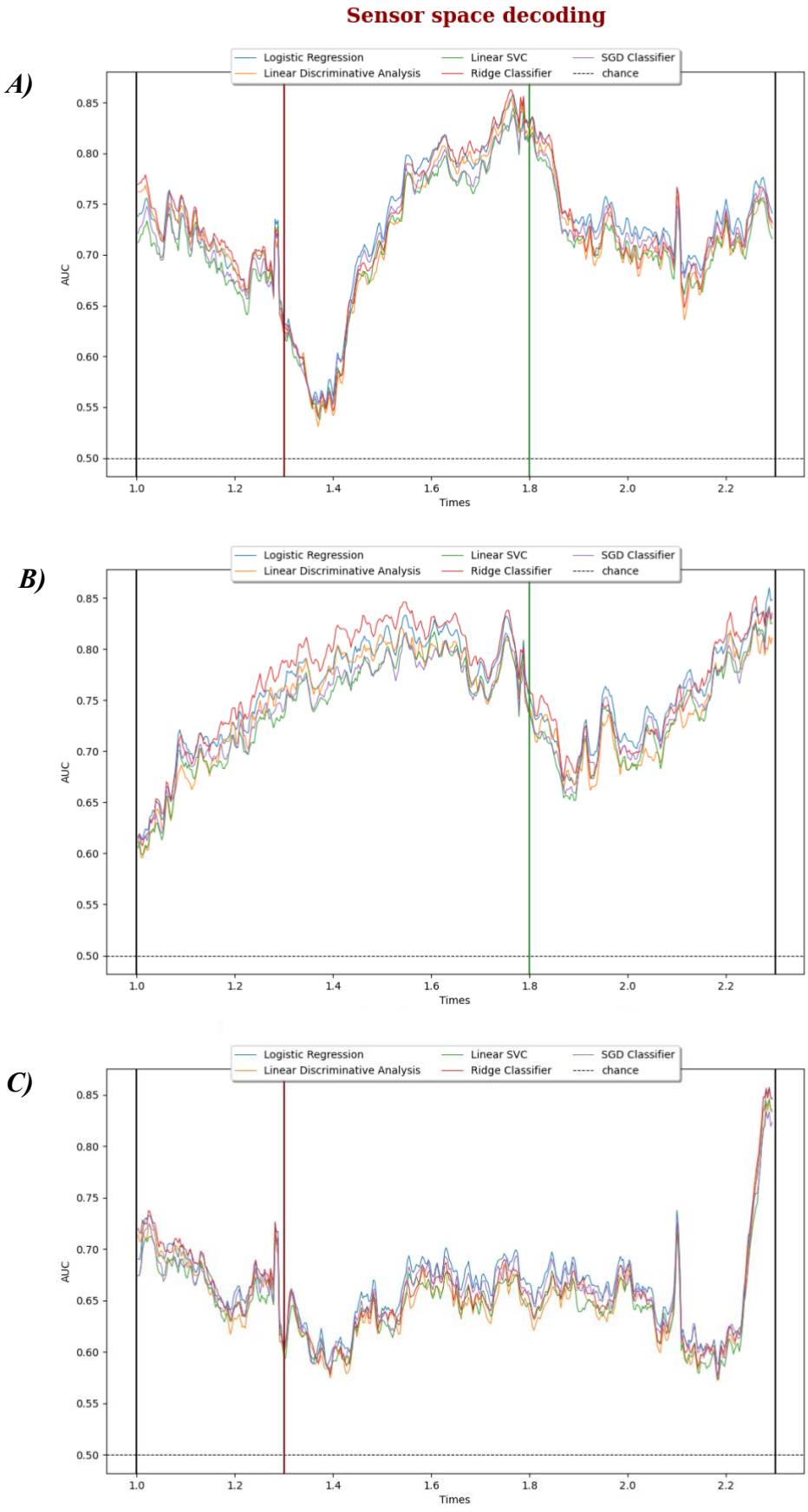

Figure 4.32. Classification scores (5-fold cross validation) for different classifiers across the three cue-target intervals. A) Comparison between epochs with 300 ms and 800 ms delay. B) Comparison between epochs with 800 ms and 1300 ms delay. C) Comparison between epochs with 300 ms and 1300 ms delay.

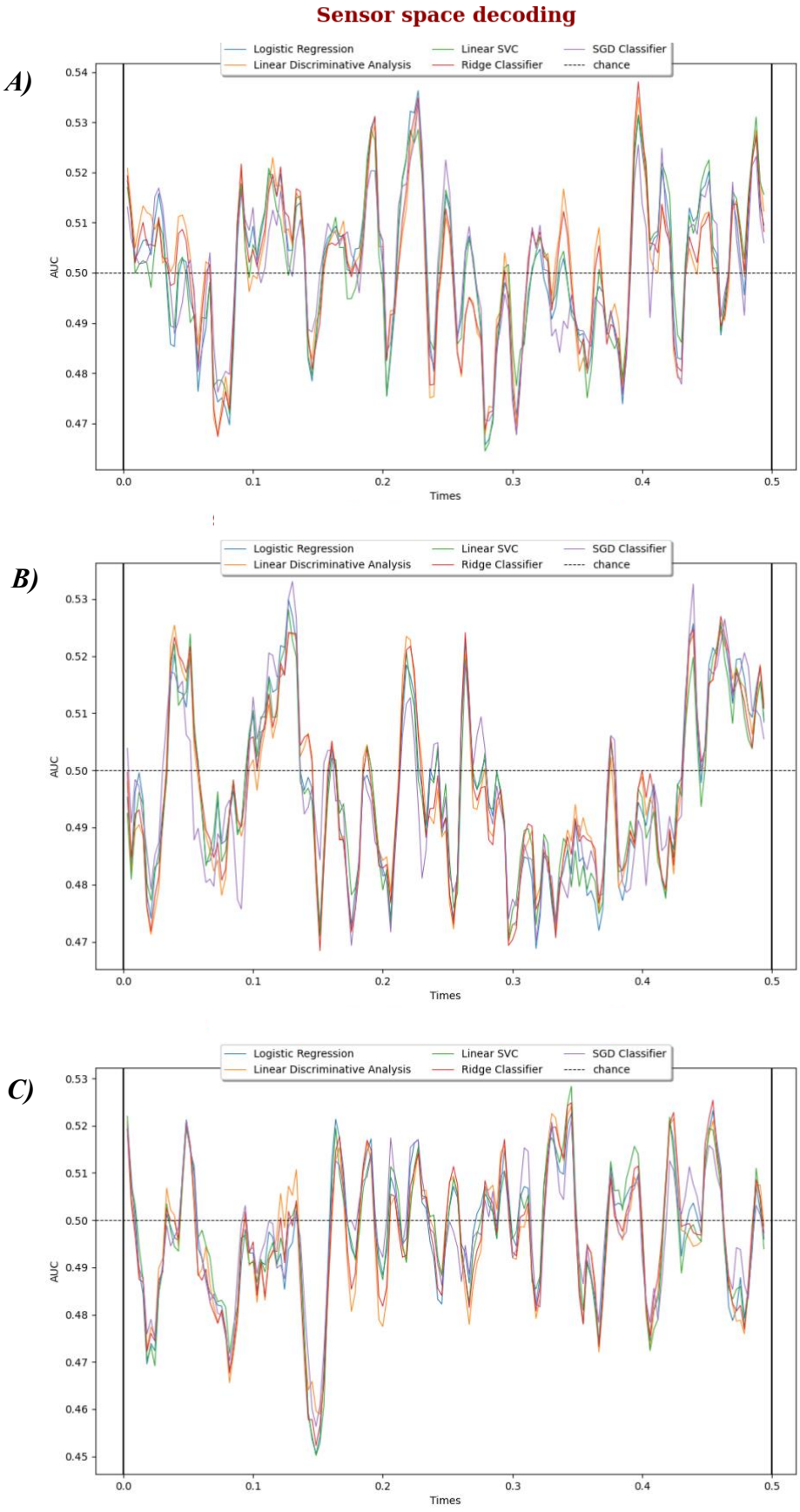

Figure 4.33 Classification scores (5-fold cross validation) for different classifiers considering 500 ms before the subjects' response. A) Comparison between epochs with 300 ms and 800 ms delay. B) Comparison between epochs with 800 ms and 1300 ms delay. C) Comparison between epochs with 300 ms and 1300 ms delay.

References

Braver, T. S., Bongiolatti, S. R. The role of frontopolar cortex in subgoal processing during working memory. *NeuroImage* 15, 523-536 (2002).

Koechlin, E., Basso, G., Pietrini, P., Panzer, S., and Grafman, J. The role of the anterior prefrontal cortex in human cognition. *Nature* 399: 148–151 (1999).

Christoff, K., Gabrieli, J. D. E. The frontopolar cortex and human cognition: Evidence for a rostrocaudal hierarchical organization within the human prefrontal cortex. *Psychobiology* 28: 168 – 186 (2000).

Stoitsis, J., Giannakakis, G., Papageorgiou, C., Nikita, K., Rabavilas, A., Anagnostopoulos, D. Evidence of a posterior cingulate involvement (Brodmann area 31) in dyslexia: A study based on source localization algorithm of event-related potentials. *Progress in neuro-psychopharmacology & biological psychiatry* 32: 733-8 (2008).

Koechlin, E., Hyafil, A. Anterior prefrontal function and the limits of human-decision making. Science 318, 594–598 (2007).

Chapter 5

CONCLUSIONS AND IMPLICATIONS

Neuroscientific research over the last decades strongly relied on the advantage ensured by the growing computational power and complexity of algorithms to analyze and reconstruct recorded brain signals. Nowadays, hundreds of signals can be processed with way more refined techniques than in the past.

It is not only about the rising of artificial intelligence, but whole informatics and electronic infrastructure that has been built to carry on a new way of doing research. A new era made of big data and complex models handled with brute force ensured by faster electronic components. In neuroscience, which has always been a tremendously complex research field due to the nature of the brain signal itself, better analyze capabilities along with high computational power could lead to discoveries considered unthinkable years ago. Magnetoencephalography is one of the techniques that – as precise and yet noisy as it is – takes all the advantages derived from better algorithms and technical innovations. Indeed, in my opinion, it is not wrong to think that MEG – as well as fMRI – might lead neuroscience research as one of the main imaging techniques in the next years.

In this dissertation, we widely discussed the main aspects of MEG imaging and the processing of the measured signals to obtain interpretable results. However, more and more analyses could be carried out and more algorithms could be applied with different parameters, focusing on other frequencies, regions, or time intervals. Perhaps, each of them would have been led to other results and outcomes as well. Considering the nature of our experiment, we decided to search for shred of evidence during random-dot kinematogram (RDK) and cue-target interval (CTI), because in these periods the subjects recognize whether there was a switch or a repeating trial and they were forced to hold on the associated rule for an unknown and varying amount of time. The brain regions that have been found to be more active confirmed some of the theories described in Chapter 2 concerning working memory and high-level processing. Though, once the source

estimate is computed and plotted over the brain surface, they still need to be interpreted knowing in advance what the subject was doing in a specific interval. Without any human support – based on neuroscientific knowledge – data would still be not directly usable for an automatic system. Indeed, performing a machine learning analysis (Chapter 4) to detect automatically pattern differences between variations of the task, we noticed that the results were not promising with the models and parameters used. Even though multiple classifiers with their own optimizers and solvers have been tested, all the results are seen to show some flaws in the model. Hence, the problem to overcome could be either the machine learning algorithms or the data we fed them with. Since these algorithms have already shown promising results in neuroscience, it is very likely to assume that the weaknesses in our analysis are represented mainly by the recorded data and – probably – wrong processing for this type of analysis. Focusing only on specific brain areas and not on the MEG recordings from all the sensors, as well as apply some fancier filtering and cleaning techniques, might have helped the machine learning model to differentiate between epochs.

The importance of knowing the performances of these algorithms is essential nowadays, because of the flourishing AI market and the possible application of new techniques. Having a computational model to automatically detect and interpret specific brain activity is still a utopia, however further promising results in neuroscience might lead to a better understanding of brain communications and hence to apply this knowledge in robotics, brain-computer interfaces, and brain-inspired technological systems.

As previously mentioned, results have been interpreted knowing in advance how the experiment was structured and what brain activity to expect. For example, occipital activation was expected – and found – right after images were displayed. However, in order to prove or make a hypothesis on the behavior of the brain in specific situations, other tests with varying experiments must be run. For instance, if we find an area that is particularly active, it would be a long shot to deduce that in every situation similar to the one we studied, the brain activity would be the same. Indeed, in few hundreds of milliseconds, the activity has been seen to rapidly change in every frequency band. Hence, one of the main weaknesses of this study – which although can be the beginning of a better understanding of brain processes related to task switching and working memory capabilities – is represented by the enormous quantity of information that we can retrieve. That had led us to make some assumptions and define arbitrary constraints, such as where to analyze brain activity, at what frequency, magnitude, or interval, and also fix the parameters of the functions used to compute the processing of the forward and inverse problems.

Despite that, in the time-frequency analysis, we observed neat results: low frequencies were most involved in primary processes – like vision and attention – while high frequencies have been seen in the prefrontal cortex and are thought to be associated with cognitive processes such as working memory and goal-oriented mechanisms.

Appendix I

Brain source estimations: 500 ms before subjects' response.

Cue-Target Interval			
	300 ms	800 ms	1300 ms
0–50 ms	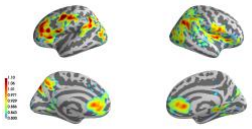	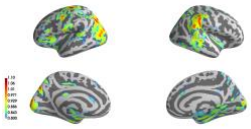	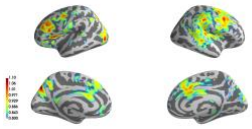
50–100 ms	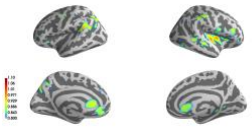	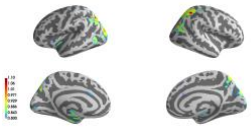	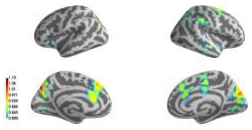
100–150 ms	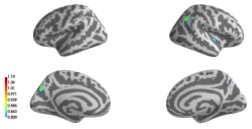	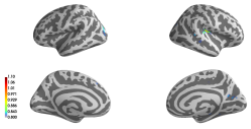	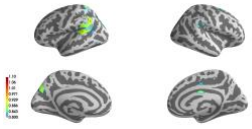
150–200 ms	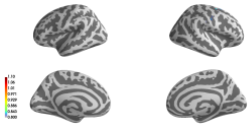	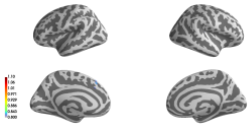	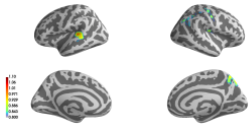
200–250 ms	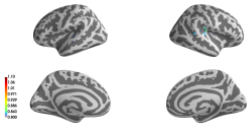	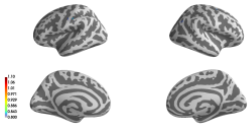	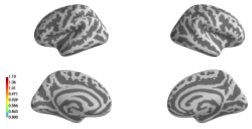
250–300 ms	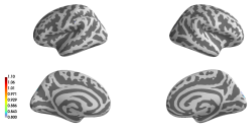	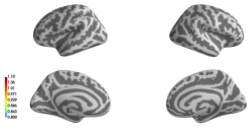	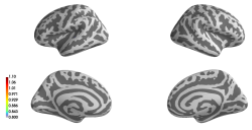
300–350 ms	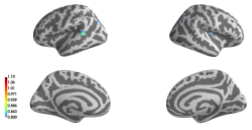	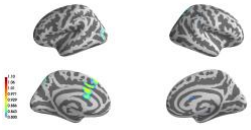	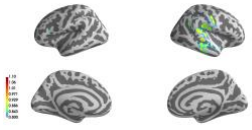
350–400 ms	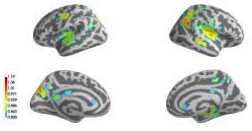	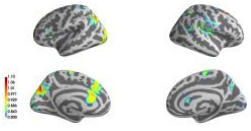	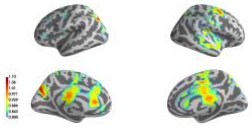
400–450 ms	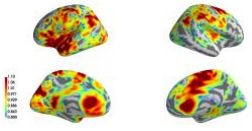	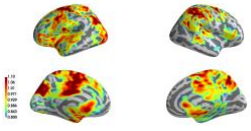	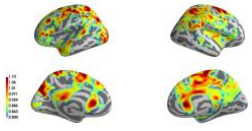
450–500 ms	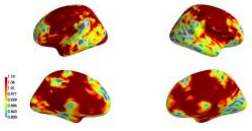	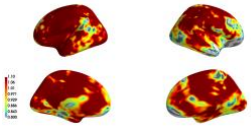	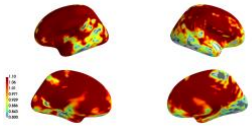
SUBJECTS' RESPONSE			

Appendix II

Brain source estimations: ‘Switch’ and ‘Repeat’ during RDK.

Trial type		
	Repeat	Switch
0–100 ms	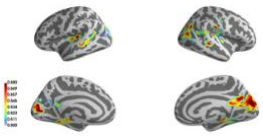	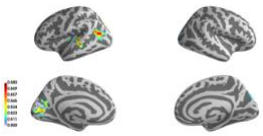
100–200 ms	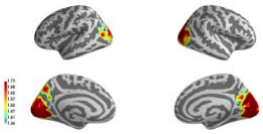	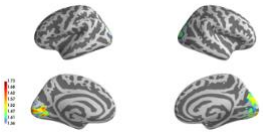
200–300 ms	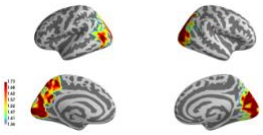	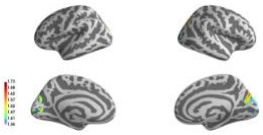
300–400 ms	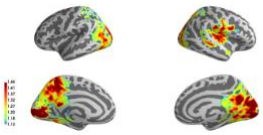	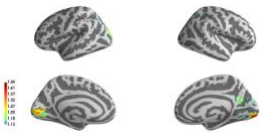
400–500 ms	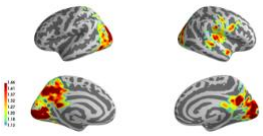	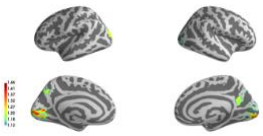
500–600 ms	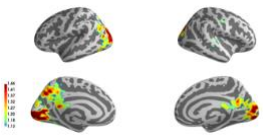	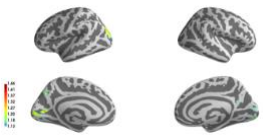
600–700 ms	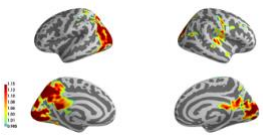	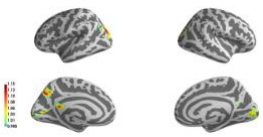
700–800 ms	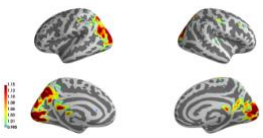	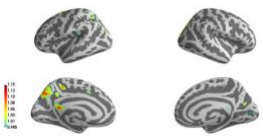
800–900 ms	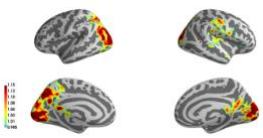	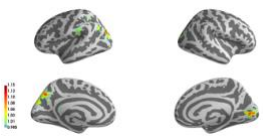
900–1000 ms